FLUORESCENT POLYCYTOSINE-ENCAPSULATED SILVER NANOCLUSTERS

A Dissertation
Presented to
The Academic Faculty

By

Yasuko Antoku

In Partial Fulfillment
Of the Requirements for the Degree
Doctor of Philosophy in Chemistry

Georgia Institute of Technology

May 2007

FLUORESCENT POLYCYTOSINE-ENCAPSULATED SILVER NANOCLUSTERS

Approved by:

Professor Robert M. Dickson, Chairman
School of Chemistry and Biochemistry
Biochemistry
Georgia Institute of Technology

Professor Bridgette Barry
School of Chemistry and

Georgia Institute of Technology

Professor Christoph J. Fahrni
School of Chemistry and Biochemistry
Biochemistry
Georgia Institute of Technology

Professor Facundo M. Fernandez
School of Chemistry and

Georgia Institute of Technology

Professor Mohan Srinivasarao
School of Polymer, Textile & Fiber
Engineering
Georgia Institute of Technology

Date Approved: January 17, 2007

ACKNOWLEDGEMENTS

I thank my adviser, Professor Robert Dickson for passion and support in my research project. I also thank my thesis committee and Professor Jeffrey Petty for his help and support. I would like to thank our group members, Tom Vosch, Chris Richards, Sandeep Patel, Dulal Senapati, Jung-Cheng Hsiang, Junhua Yu, Sungmoon Choi, Rusty Nicovich, Wonsang Koh, Soonkyo Jung, Kewei Xu, Jose Gonzalez and Tae-Hee Lee for their help.

I thank my parents Tsuyoshi Antoku and Kazumi Antoku, brothers Tsutomu and Susumu, sister, Keiko, brother-in law Christakis Papageorgiou**,** nieces Celine and Sofia, my lovely pets, Barney and Honey Bunny for their love and support.

TABLE OF CONTENTS

LIST OF TABLES

LIST OF FIGURES

SUMMARY

Small silver nanoclusters are synthesized using polycytosines as matrices. Different size silver nanoclusters ranging from Ag_1 to Ag_7 exhibit bright emission maxima at blue (480nm), green (525nm), red (650nm), and IR (720nm) wavelengths with varying the excitation wavelengths. With electrophoresis, correlation of emission with mass spectra, the Ag cluster sizes are identified with blue emitters as Ag_5, green emitters as Ag_4, red emitters as Ag_3, and IR emitters as Ag_2. Ag_4 and Ag_5 appear to be partially oxidized while Ag_2 and Ag_3 are likely fully reduced.

Silver cluster stability and their dynamics are observed from silver clusters encapsulated by polycytosine (C_m:Ag_n). From length study of polycytosine, the longer the polycytosine is, the more stable the larger clusters such as Ag_5 are. In time-dependent optical measurements, isosbestic points are observed from C_m:Ag_n by converting red and IR species into blue and green species, while in the case of temperature-dependent optical properties, with increasing temperature, the blue (oxidized Ag_5) and green (oxidized Ag_4) emitters convert into the red (Ag_3) and IR (Ag_2) emitters. NaCl-dependent optical measurements support the assignments of oxidized and fully reduced silver emitters. Circular dichroism (CD) is used to investigate conformational changes in C_m and C_m:Ag_n with varying conditions (time, temperature and NaCl) and the studies indicate that no conformational changes in C_m:Ag_n are observed from the time and temperature, while the conformational changes in C_m:Ag_n are observed from the NaCl studies. From pH-

dependent emission study of C_m:Ag_n, the silver nanocluster dynamics slow down at high pH.

Using confocal microscopy technique, single molecules on IR species, C_{12}:Ag_2 are investigated and demonstrate that C_{12}:Ag_2 is brighter and more photostable than Cy5 which is known to be one of the best IR dyes. With low excitation power, molecules can be monitored for hours, giving bright blinking free, stable fluorescence. The photophysics of this new dye make it a promising candidate for single molecule studies in biological applications.

1 INTRODUCTION

1.1 Motivation.

Noble metals exhibit a variety of behaviors from bulk to clusters. At the bulk level, they are good conductors since they are devoid of a band gap.(1) When sufficiently small to preclude the continuous density of states of the bulk, silver nanoclusters exhibit strong fluorescence from discrete energy levels.(2-6) Molecular silver nanoclusters (Ag_2 to Ag_8) and their charged counterparts have been reported to strongly fluoresce in the visible spectrum within rare gas matrices, on silver oxide surfaces, as well as in aqueous solutions.(7-13) These small silver nanoclusters show molecular behavior with well-defined electronic structures identified by both experiments and calculations.(2, 8, 10-12, 14-18) While mass selection and soft landing methods enable control and study of few atom Ag nanocluster properties,(19-22) such size control in aqueous solutions is greatly complicated by aggregation and reactivity. Some success has been reported by using poly(amidoamine) dendrimers (PAMAM) as matrices to create several atom silver clusters in aqueous solutions.(23) PAMAMs have been shown to stabilize Ag nanoclusters while the surrounding polymeric matrix at least partially protects the nanoclusters from aggregation. Biological macromolecules such as peptides have also served as templates to synthesize silver nanoclusters.(24, 25) The amine functional groups of peptides assemble silver cations and then protect the growing nanoparticle against aggregation after reduction of the cations.(24, 25) Our attention has been directed to another biological system, DNA. Since the 1960s, it has been well known that metal

cations selectively interact with DNA bases.(26-32) With the high affinity of DNA bases toward metal cations, silver ions can be localized and then reduced to form silver nanoclusters.(33-38)

A reason to control the size of metal nanoclusters is to understand and manipulate the size-dependent electronic and optical properties.(39-45) Small (2-8 atoms) Ag nanoclusters are of particular interest since they exhibit very strong absorption and emission.(3, 13, 46, 47) Thus, small silver nanoclusters may serve as ideal fluorophores for single molecule spectroscopy and biological labels.

This thesis is devoted to create few-atom or molecular-scale silver nanoclusters utilizing DNA as a template. Polycytosines were found to be good matrices to tune and narrow the distribution of silver nanocluster sizes in aqueous solutions. Their bright photostable emission in bulk and on the single molecule level may serve as a new class of emitters for biological labeling.

1.2 Electronic structure of metal clusters.

As bulk metals reduce in size to the nanometer scale (nanoclusters), the transition from metal to molecule occurs. Instead of forming continuous densities of states and behaving as conductors, few-atom metal nanoclusters maintain discrete energy levels. In 1937 Frohlich discovered the discreteness of electronic energy levels from small metal particles and in 1962 Kubo proposed that the discrete electronic energy level caused the small metal particles to behave abnormally at low temperature.(48, 49) Considering the continuous states of bulk metal described by band theory, Frohlich and Kubo suggested that as the size of the metallic particle decreases, the electronic energy levels become discrete and the energy level spacing of the small metal particles δ is given by(50)

$$\delta = \frac{E_F}{N}, \tag{1.1}$$

where E_F is the Fermi energy of the bulk metal and N is the number of atoms in the particle. DiCenzo and Wertheim(51) proposed that the energy level spacing for the bulk metal is equal to or less than thermal energy, kT, thereby enabling the electrons to freely flow at room temperature. Thus, for discrete levels to be observed, the equation 1.1 above must satisfy(50)

$$\delta = \frac{E_F}{N} \geq kT, \tag{1.2}$$

However, as the size of the metal particle becomes smaller, the energy spacing for the smaller metal particles becomes larger than kT. Thus, thermal energy is no longer sufficient to excite the electrons to higher states. This is schematized in Figure 1.(1)

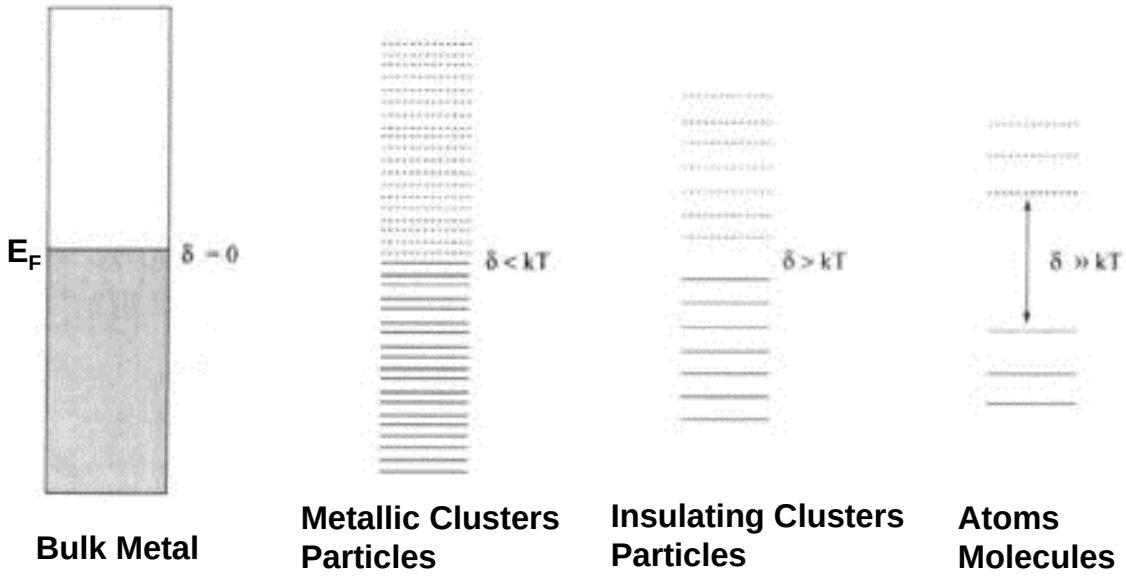

Figure 1. Transitions of electronic structures of metal from bulk metal (right) to small nanoclusters. Reproduced from reference (1).

1.3 Jellium Model

In the early 1980's, a periodic pattern of intense peaks in the mass spectra of alkali metal clusters Na_N was observed by Knight and co-workers.(52) The Na clusters with N=2,8,18,20,40,58, which are called magic numbers, have greater stability than do others.(52) This magic pattern in stability can be explained by a model called the jellium model.(52) Due to a strong electron shielding effect, valence electrons of noble metal atoms are considered to move freely after neglecting electron-electron and electron-ion interactions. In this model, the cluster is considered to be a uniformly positively charged sphere with electrons that can move freely in this sphere. This model can be used in the case the valence electrons are weakly bound like for alkali and noble metals such as silver and gold.(1) The jellium model is a simple quantum mechanical system with quantized electron energy levels rising resulting from the boundary conditions imposed by a 3-D harmonic potential. The Schrodinger equation is solved for a one-electron particle confined within a sphere by an attractive central potential due to the nuclei cores and yields electronic energy level spacing δ as the following equation.(52)

$$\delta = \frac{E_F}{N^{1/3}} \tag{1.3}$$

where E_F is the Fermi energy of the bulk metal and N is the number of atoms (assuming one free electron per atom) in the particle. This equation describes how the electronic structures of alkali clusters changes with the number of free electrons.

The jellium model describes not only electronic structures of Na clusters but also other metals electronic structures.(1) Rademann and coworkers reported that ionization

energies of Hg_n decrease with increasing number of atoms per cluster and approximately follow $N^{-1/3}$. (53) Knight et al. observed $N^{-1/3}$ size-dependence in the ionization potential of potassium clusters K_N (N <100). (54) The Skala group also found that the binding energy of Li clusters has $N^{-1/3}$ size-dependency.(55) This set of studies clearly demonstrated that electronic structures of simple metal clusters were described by the spherical jellium model.

1.4 Silver cluster formation in the gas phase.

While high conductivity is observed from bulk metals, non-metal-like discrete energy levels are observed in molecular-scale metal particles.(1) This molecule-like behavior of metal clusters fascinated researchers to investigate noble metals in different size domains in order to understand and manipulate the size-dependent properties. Figure 2 shows a schematic illustration of productions of clusters, size selection, and deposition.

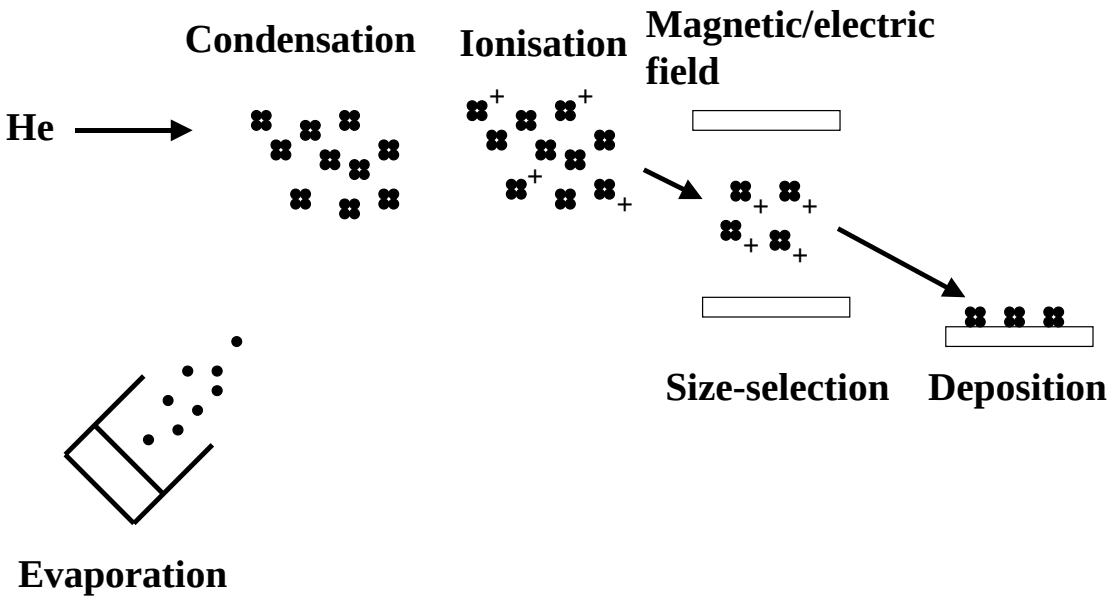

Figure 2. Schematic illustration of productions of clusters, size selection and deposition. Adapted from reference (56).

Historically, in order to create metal clusters, inert gas ions or pulsed lasers are used to target a rod of material of interest.(56) After the atoms or molecules are produced in the gas phase, nucleation occurs where the atoms or molecules are cooled down to form a cluster nucleus.(56) One way to remove the excess energy is that dimers form and a third atom collides with the dimer, taking extra energy away from the dimer as kinetic energy (e. g. $A + A + A\ (KE_1) \rightarrow A_2 + A\ (KE_2 > KE_1)$).(56) Inert gases can similarly cool the clusters through collision and deactivation. After nucleation, clusters grow from the nucleation site. Those clusters formed in the previous step can also remove excess energy by evaporation. The cooling through evaporation occurs by losing one or more atoms with bond breaking. The deattached atom or atoms carry the excess energy as kinetic energy. This is depicted in the following: $A_N\ (T_1) \rightarrow A_{N-1}\ (T_2 < T_1) + A\ (KE)$.(56) After the clusters are formed, they must be separated according to their size, usually performed via ionization and deflection in either a magnetic or electric field according to their mass to charge ratio. The ionized clusters are produced by methods of electron impact ionization or photoionization.(56) By the method of electron impact ionization, thermal electrons or a focused electron beam is used to knock off electrons. With the method of photoionization, a laser is used to generate cationic clusters by tuning excitation energy to a cluster absorption resonance. After size selection using mass spectrometry, clusters can be deposited on an inert substrate (such as graphite, silicon and oxides) for investigation, or trapped with rare gas matrices (10, 11, 57-61).

Molecular scale silver nanoclusters have been created by a variety of methods (58-63), but primarily mass selection and soft-landing methods (10, 11, 60) after cooling with an inert gas. Depending on the creation conditions, various optical properties were

reported. Meyer et al. reported on depositing Ag_2 and Ag_3 on cooled sapphire or CaF_2.(20) In this experiment, Kr^+ was used to create cationic silvers and a Bessel Box(22) was used to filter the energy of the clusters, then a quadrupole mass filter was used for mass selection. Before depositing on the substrate, the Kr gas was used to dissipate the energy of the cationic silvers that were subsequently neutralized by low energy electrons. By dissipating energy to the inert gas, the neutralized silver clusters can be deposited on the substrate softly (soft landing) to minimize fragmentation and interaction on the surface. With soft landing, interaction with the substrate causes the electronic structure of the clusters to be minimally perturbed.(1) In the case of dimer, excitations at 275 and 390 nm were observed,(20) while the trimer has absorptions at 331, 364, 402, 421, 458 and 514 nm and emissions at 381, 560 and 626 nm.(20) Kern et al. further investigated soft-landing methods for nondestructive cluster deposition.(22) Similar methods were used for production of the cationic silver clusters, control of kinetic energy and their mass selection.(22) The silver clusters were deposited onto a Pt substrate at 80 K or 90 K or into a preadsorbed Ar layer at 26 K.(22) The Ar layer was preadsorbed on the substrate to dissipate the kinetic energy of the clusters. The clusters were characterized using variable-temperature STM.(22) Kern was able to illustrate control of soft-landing nanoclusters using a rare-gas layer by comparing the clusters formed by hard landing with the clusters deposition by soft-landing.(22) Buttet et al. reported on optical properties of Ag_8 in argon matrix and argon droplets.(64) The silver clusters (Ag_8) in an argon matrix were created using the same method as Meyer.(20) A pick-up method was used to produce Ag_8 in argon droplets.(19, 65) A beam of argon passed through silver vapor and picked up silver atoms that aggregate in the argon matrix to form clusters.(65)

The deposition of Ag_8 occurred at low temperature (below 25 K).(64) An emission peak at 321 nm with a 312 nm excitation was observed from Ag_8 in Ar matrix,(66) while 320 nm emission peak excited with white light was observed from Ag_8 in Ar droplets.(19) The excitation spectrum of Ag_8 in Ar matrix was recorded to compare it with the excitation of Ag_8 in helium droplets.(19, 67) The excitation spectrum with 312 nm maximum of Ag_8 in Ar matrix was in excellent agreement with the excitation of Ag_8 in helium droplets.(66) Fedrigo et al. reported the optical properties of Ag_2 and Ag_3 in argon matrices deposited on a cooled CaF_2.(68) Ag_2 shows absorption at 237, 262 and 273 nm, giving rise to 278 nm and 479 nm emissions from the 237 nm absorption, 286 nm and 479 nm emissions from the 262 nm absorption and 298 nm and 479 nm emissions from the 273 nm absorption. On the other hand, the absorption at 242.5, 255, 384 and 441 nm of Ag_2 gave rise to an emission at 476 nm. In the case of trimer (Ag_3), the excitations at 321, 331 and 350 nm resulted in an emission at 374 nm, while the excitations at 386, 402, 423, 444 and 492 nm resulted in the emissions at 616 and 705 nm. Fluorescence and absorption spectra of Ag_4 codeposited on a cold sapphire plate with an argon matrix were reported by Felix et al.(9) Ag_4 gives rise to an emission band centered at 458 nm from multiple absorption bands at 235, 251, 258, 262, 268, 273, 299, 387 and 405 nm. In 2004, Schulze reproduced the fluorescence spectra of dimers and trimers deposited in Ar matrix.(11, 12, 69) The maximum fluorescence intensities are observed at 478 and 620 nm, while lower fluorescence intensities were observed at 699 and 954 nm.(69) They assigned the fluorescence at 478 nm and 620 nm to Ag_2 and Ag_3 emission and the fluorescence at 699 nm to Ag_3 only emission. It is unknown which silver clusters give rise to 954 nm emission.(69)

Not only optical properties but also stability of silver nanoclusters were reported. For example, Alameddin et al. recorded the mass spectra from ionized silver clusters and the discontinuities of ion abundances were observed.(70) The ionization potentials for different cluster size are determined and even numbers of silver clusters such as 8, 20, 34, 40 and 48 have high ionization potentials. Figure 3 shows the ionization potentials for Ag clusters. These stable clusters and even-odd alternation is consistent with spherical jellium models.(1)

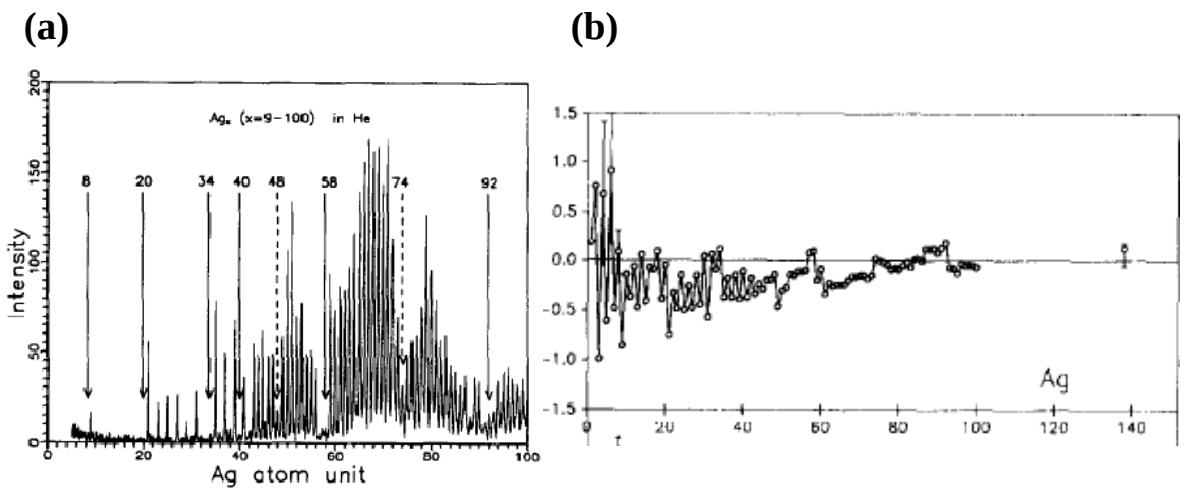

Figure 3. (a) Mass spectra obtained from ionized silver clusters (b) ionization potentials for Ag clusters. Reproduced from reference (70).

Taylor et al. reported that electron affinities of silver clusters (Ag_{1-60}) followed an even-odd alternation pattern.(71) The even-odd alternation patterns of silver nanoclusters are also observed by Ho et al.,(72) Handschuh et al.(73), Katasuke et al.(74) and Zhao et al.(75)

Silver and silver nanoclusters have well known catalytic properties.(76, 77) It is used for example in the production of formaldehyde from methanol and in the production of ethylene oxide from ethylene.(76-78) By creating nanoclusters of silver, this can greatly increase the active area of the catalyst and reducing the amount of catalyst that is needed. The silver cluster might also show additional catalytical properties that may be different from bulk silver.(79, 80)

1.5 Silver cluster formation in aqueous solutions.

Henglein et al. investigated optical properties of silver clusters in aqueous solutions.(81-85) Creating silver clusters in aqueous solutions is challenging due to aggregation issues.(1) In his work, polyphosphate was used as matrix to protect the silver clusters from aggregation. The silver cluster solutions were made by mixing silver nitrate ($AgNO_3$) and sodium polyphosphate ($Na_2O(NaPO_3)_n$) with alcohol. The mixtures were deaerated and exposed to γ-rays for reduction of the silver clusters. The alcohol was used to scavenge hydroxyl radicals. The following reduction process was elucidated in the formation of silver clusters.(82) At first, water was broken down to a hydrogen atom (H) and a hydroxyl radical (•OH) using γ-rays. The hydroxyl radical subsequently reacts with alcohol (CH_3OH) to form organic radicals ($•CH_2OH$).

$$•OH(H•) + CH_3OH \rightarrow H_2O(H_2) + •CH_2OH \qquad (1.4.1)$$

The next step is that the organic radicals react with silver ions to reduce the silver ions.

$$\bullet CH_2OH + Ag_n^{x+} \rightarrow CH_2O + Ag_n^{(x-1)} + H^+ \quad (1.4.2)$$

The radicals are considered to be strong reducing agents.(86) After the silver clusters are formed in solution, the absorption of the silver clusters was measured. The absorbance bands at 360 nm, at 310 nm, and at 275 nm are from Ag, Ag_2^+ and Ag_4^{2+}, respectively. It is reported that Ag_4^{2+} species are stable for hours in the presence of air.(81, 84, 85, 87) Henglein suggested several mechanisms to form Ag, Ag_2^+ and Ag_4^{2+}.(82, 85) The first mechanism is described in the following reaction. Ag^+ is reduced by hydrated electrons produced from γ-rays.(82)

$$Ag^+ + e_{aq}^- \rightarrow Ag^0 \quad (1.4.3)$$

The Ag^0 rapidly complexes with Ag^+.(82)

$$Ag^0 + Ag^+ \rightarrow Ag_2^+ \quad (1.4.4)$$

Subsequently, Ag_2^+ dimerize. (82)

$$2Ag_2^+ \rightarrow Ag_4^{2+} \quad (1.4.4)$$

Another mechanism is described using the standard potentials of the silver electrode as a function of agglomeration number of silvers.(82) The standard potentials of silver atom, silver dimer and silver trimers were calculated using the thermodynamic properties of the clusters in gas phase(88) and the free enthalpy of sublimation of silver.(89) Figure 4(85) shows the standard potentials of the silver electrode as a function of agglomeration number of silvers. Since the thermodynamic properties above Ag_3 are not known, the dashed lines after Ag_3 to Ag_{15} are estimated values. As shown in Figure 4, as the number of the silver atoms increase to infinity (bulk), the potentials become more positive and approach to +0.799 V. This is the conventional value for the silver electrode. In contrast, the standard potential of the Ag atom is –1.8 V. This means that an Ag atom

can be a reducing agent to many inorganic and organic compounds. For silver dimer, the potential is close to 0 V, while the potential of the trimer is close to –1.0 V. This suggests that the Ag_3 is more likely to lose an electron than is Ag_2: (82)

$$Ag_3 \rightarrow Ag_2 + Ag^+ + e^- \qquad (1.4.5)$$

The dimer might interact with silver ions to form Ag_4^{2+}: (82)

$$Ag_2 + 2Ag^+ \rightarrow Ag_4^{2+} \qquad (1.4.6)$$

The potential for this reaction is even more positive, thereby indication that Ag_4^{2+} is an extremely stable species compared to other silver species formed in his study.

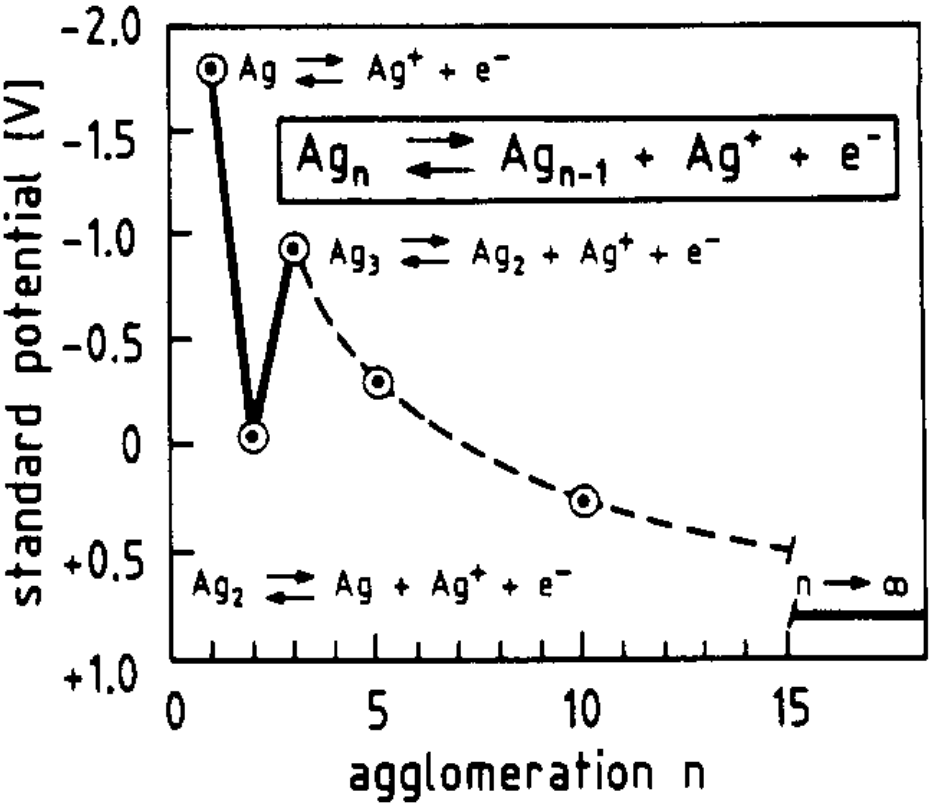

Figure 4. The electrochemical standard potential of the silver microelectrode vs the agglomeration number of the silver atoms. Reproduced from reference (82).

More recently, another method of making silver clusters in aqueous solutions was reported by using dendrimers as scaffold.(3, 13) The preparation for creating silver clusters is very simple. The dendrimer (PAMAM) and silver nitrate were mixed and the silver ions were photoreduced. The dendrimer is a good matrix to at least partially protect the silver clusters from aggregation and is water-soluble. Droplets of the solution were placed on a cover slide and by using blue excitation (maximum at 480 nm) from a Hg lamp, fluorescence of the silver clusters encapsulated in the dendrimer was recorded on a CCD camera.(13) A typical fluorescence image of the silver clusters is shown in Figure 5(b). (13)

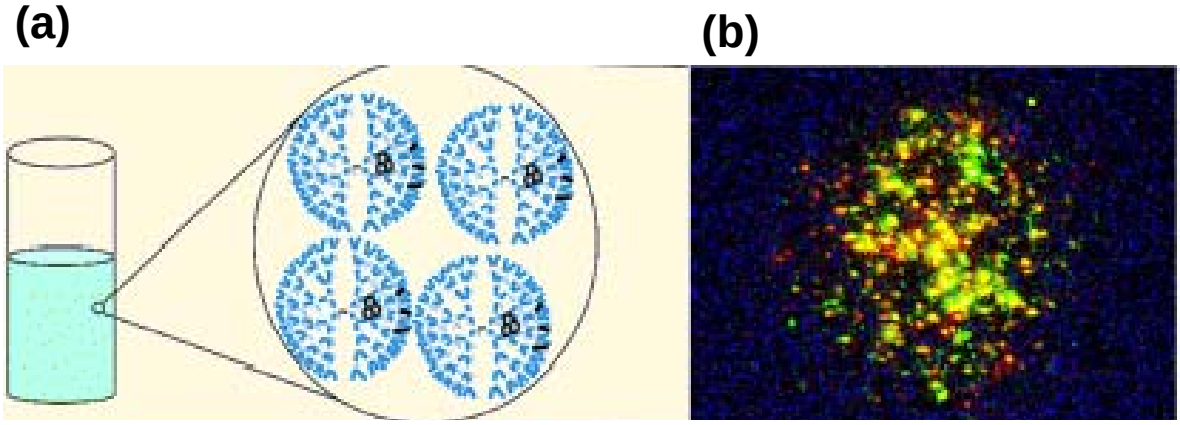

Figure 5 (a) cartoon of the silver clusters encapsulated in the dendrimer (b) Fluorescence image of the silver clusters encapsulated in the dendrimer. Reproduced from reference (13).

The fluorescence image shown in Figure 5(b) is presumably multicolored due to the formation of differently sized silver clusters.(13) Although some progress in creating silver clusters in aqueous solutions was made with dendritic scaffolds, there is a difficulty to create them in high concentration without aggregation.

One promising solution has been to utilize biological macromolecules such as peptides to encapsulate and stabilize the silver nanoclusters.(25) Yu et al. reported fluorescence from silver nanoclusters encapsulated by short peptides, HDCNKDKHDCNKDKHDCN, in aqueous solutions. Lysine (K), Aspartic acid (D) and Cysteine (C)-rich strands were chosen since silver ions are known to have higher affinity for K, D and C.(25) The silver clusters encapsulated by the peptides were able to enter live cells, which are shown in Figure 6.(25)

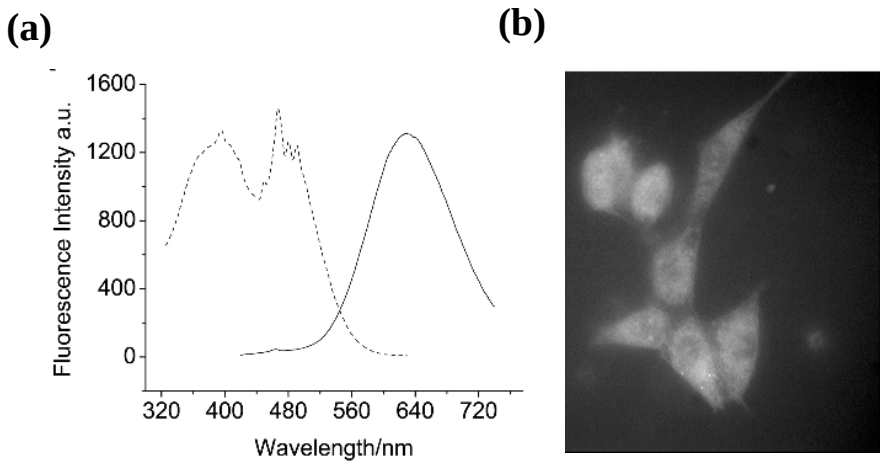

Figure 6. (a) the excitation (monitoring at 630 nm emission) and emission spectra excited at 400 nm of silver nanoclusters encapsulated by a short peptide, HDCNKDKHDCNKDKHDCN. (b) Fluorescence image of a cell loaded with the peptide-encapsulated silver nanoclusters. Reproduced from reference (25).

In this work, we have used another biological system, DNA, which is known for high affinities to bind to silver ions.(90-93)

1.6 Silver Ion-DNA Interaction.

In 1962 Yamane and Davidson reported a strong interaction between DNA and Ag^+.(92) Using calf-thymus DNA, absorption of the DNA was monitored before and after addition of Ag^+. With addition of Ag^+ the absorption of the DNA (at 260 nm) was shifted, thus they suggested that the electronic structure of DNA was perturbed. Since the absorption of DNA results from heterocyclic bases (pyrimidine and purine) but not from sugar-phosphate backbones, they concluded that Ag^+ was likely binding to the bases (not the negatively charged sugar-phosphate backbone). They also changed the ratio (r) of silver ions to bases and investigated the change in absorbance according to the different ratio (r) of Ag^+ to bases. They reported that for $0 < r < 0.2$, one complex was observed, having a characteristic absorbance and strong binding to Ag^+. On the other hand, another complex was observed for $0.2 < r < 0.5$, having different absorbance and weaker binding towards Ag^+. In 1967, Eichhorn et al. further studied interactions of individual bases, adenosine (A), cytidine (C) and guanosine (G) (except thymidine (T)) to Ag^+ in different pH (4, 6 and 9).(90) The structures of the bases are shown in Figure 7.

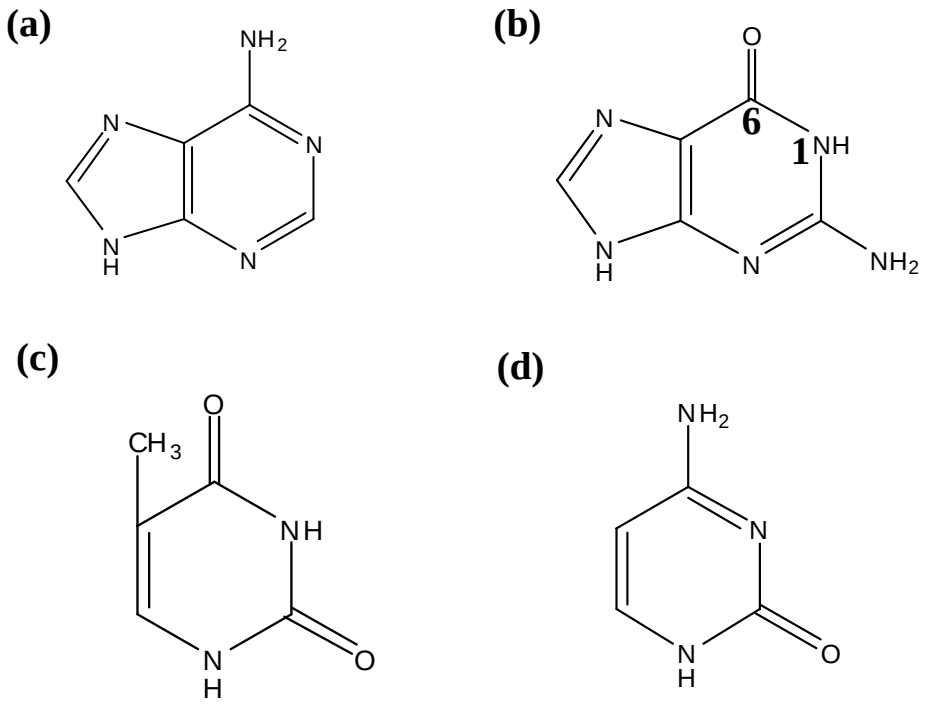

Figure 7. Structures of (a) Adenine, (b) Guanine, (c) Thymine and (d) Cytosine.

For A and C, a significant absorbance change was observed between pH 6 and 9 with the addition of Ag^+, while the absorbance change for G occurred between pH 4 and 6. Besides the absorption study, the solutions of Ag^+-A, Ag^+-C and Ag^+-G were titrated with 0.01 N NaOH. They concluded that the silver ions replaced a proton from the amino group from A and C, while the silver ions bond at the N_1 position or oxygen on C_6 for G. They extended the studies to polyadenine (poly A) and polycytosine (poly C). Similar results (absorption and titration) as the nucleoside were observed from the polynucleotide silver complexes. Arya and Yang investigated silver polynucleotide complexes using circular dichroism (CD).(91) (CD is described in detail in the experimental section.) The CD spectra of poly C/Ag complexes between 200 and 250 nm were remarkably different from the spectra of the uncomplexed poly C. Furthermore, the CD spectra of the poly C/Ag complexes stopped changing when the ratio of Ag^+ to bases reached 0.5. In contrast, no change in the CD spectra for poly A and poly G was observed after the ratio of Ag^+ to bases reached 1. At last, they suggested that single-stranded polynucleotides cross-linked to form a duplex mediated by silver ions. From all evidence shown above, silver ions prefer to bind with nucleotides, thereby changing the electronic configuration of the bases.(90-92, 94) By taking advantage of strong affinities of silver ions toward bases, the silver ions can be reduced to form small silver particles.

1.7 Limitations of Current Dyes for Biological Imaging at The Single Molecule Level.

Although there are numerous dyes exhibiting different photophysical properties,(95, 96) organic dye-based single molecule and even bulk in vivo imaging dynamics studies suffer from poor photophysical properties of the organic dyes. For example, imaging intracellular dynamics with organic dyes is limited by low probe

brightness, (97, 98) poor photostability (99, 100) and oxygen sensitivity. (101) These problems become especially severe in single molecule studies. Advances in nanotechnology have led researchers to use quantum dots as alternative imaging agents. Compared with organic dyes, quantum dots are brighter, resistant to photobleaching, readily excitable with low intensity sources and have large two-photon cross sections. (102, 103) However, toxicity, (100, 104) power-law blinking, (105-108) and large probe size (109, 110) cause problems when utilized for tracking or imaging studies.(104) Derfus et al. reported that CdSe-core quantum dots were toxic to live cells. For specificity in cells, quantum dots are typically functionalized by attaching primary and biotinylated secondary antibodies to streptavidin-conjugated quantum dots. (100, 111-113) Thus, the large ~20 nm diameter functionalized quantum dots affect cellular uptake and have limited accessibility in live cells.

Although optical imaging expands the opportunities to study biological systems, there is a major drawback using UV and visible light. Biomolecules in cells have higher absorption and scattering in this range of wavelengths, thereby reducing light penetration through tissue. Additionally, many intracellular species exhibit weak fluorescence when illuminated at these wavelengths, thereby increasing background. However, there is low biomolecular and water absorption in the near infrared (NIR) region. Hence, creation of bright near-infrared fluorophores is an important goal for tracking or imaging studies. The problem with NIR dyes is that they generally have a low quantum yield because of the low energy difference between the excited and ground states. This increases the rate of nonradiative relaxation so that it becomes competitive with radiative decay (fluorescence).

In comparison with other NIR fluorescent dyes (e.g. polymethine(114), diphenylmethane(115, 116), quinone(117) , azo dyes(118)) Cy5 is brighter and has a good quantum yield (20 % in phosphate buffer saline (PBS)) (119). These properties allow it to be used for imaging studies. However, it shows strong blinking. Blinking occurs when a molecule temporally undergoes transition from emissive state (on state) to non-emissive state (off state).(120) For organic dyes, blinking is often caused by a triplet state. Figure 8 shows a three-state level to describe a blinking process.

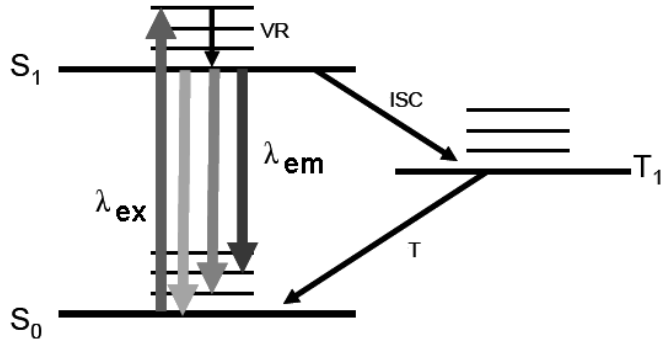

Figure 8. Diagram of three-state level. λ_{ex} and λ_{em} is an excitation and emission wavelength, respectively. VR, ISC and T stand for vibronic relaxation, intersystem crossing and phosphorescence, respectively.

As a single molecule is excited to a singlet state (S_1), it can relax to a ground state (S_0) by emitting light after staying at S_1 for certain time (ps to ns) or it can go to a triplet state (T_1) without emitting. When the molecule stays in the triplet state (μs-ms regime generally), no light can be emitted. Then, the molecule relaxes from the triplet state to the ground state either non-radiatively or by phosphorescence. In the case of Cy5, blinking is caused partially by cis-trans isomerization and partially by the triplet state.(121) Blinking is a major drawback of these materials as single molecules for tracking or imaging because no fluorescence information can be obtained. Consequently, for both in vitro and in vivo single molecule studies, fluorophores with high emission rates and excellent photostability must be identified that are completely devoid of blinking on all relevant timescales.

2 EXPERIMENTAL SECTION

2.1 Optical characterization.

The size distribution of silver nanoclusters in aqueous solutions was controlled by using polycytosine as a template. The optical properties of polycytosine-Ag complexes were studied by using a Photon Technology International (PTI) fluorometer, a Shimadzu UV-2401 PC spectrophotometer, and a Jasco J-710 spectropolarimeter (Circular Dichroism). The optical properties of individual polycytosine-Ag molecules were also characterized for application as fluorescent dye and biological labeling on the single molecule level.

2.2 Synthesis of C_m:Ag_n solutions.

Silver nitrate (Sigma-Aldrich, 99.9999%) and sodium borohydride (Aldrich, 98%) were used without further purification. Oligonucleotides (Integrated DNA Technologies) were desalted by the manufacturer and peptide nucleic acid (PNA) was synthesized and HPLC-purified by PANAGENE Inc. Oligonucleotides with lengths of 8, 12 and 24 bases of cytosine and PNA, 5'-$(C)_m$-3' (m = the number of bases), were received as solids and dissolved in deionized water. The oligonucleotides and $AgNO_3$ solutions (1 Ag^+/2 bases) were mixed and cooled to 0°C with ice.(91, 122, 123) After 10 minutes, the solutions were reduced with $NaBH_4$ and shaken intensively to form silver nanoclusters (C_m:Ag_n). The $NaBH_4$ was dissolved in deionized water and added within 30 seconds. PNA solutions were made using the same procedure as the oligonucleotides. The solvents for all solutions were deionized water unless otherwise mentioned.

2.3 Electrospray Ionization Mass Spectrometry.

Electrospray Ionization (ESI) is a useful technique to analyze and determine the molecular mass of large non-volatile biomolecules, with very low fragmentation due to its gentle ionization process. The mass spectrometer consists of three basic parts; ion source, mass analyzer and detector.(56) A Quattro LC ESI mass spectrometer was used to measure masses of the silver nanoclusters in various oligocytosines. Fifty μL of aqueous C_m:Ag_n solution were injected into the ESI capillary needle. At the tip of the capillary, a 2.5 kV voltage was applied in order to form charge droplets. The solvent evaporated from the droplets by using a warm counter flow of N_2, thereby causing the droplets to shrink in size. Droplets are exploded due to the surface tension being overcome by the charge density. Eventually, the ions desorb from the charged droplets and pass through a small aperture into different pumping steps and finally the analyzer. ESI mass spectra present multiply charged ions $(M - zH)^{Z-}$. The software (MassLynx 3.4) converts the multiply charged ions into the real mass of the analyte. As an example, Figure 9.a and b show the deprotonated raw data (multiple charged ions) and the deconverted data of C_6:Ag_n.

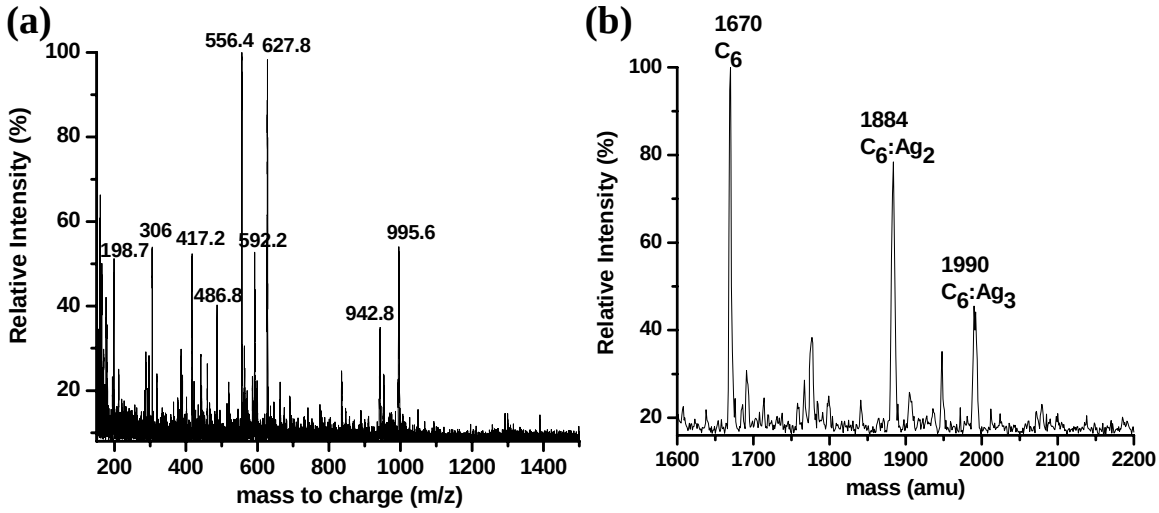

Figure 9. (a) Raw data and (b) converted data for C_6:Ag_n with [C_6] = 100 μM, [Ag^+] = 300 μM, and [BH_4^-] = 300 μM. Mass spectra were obtained by using a Micromass Quattro LC operated in negative ion mode with 2.5 kV needle and 40 V cone voltage. Experimental conditions: (18 M Ω deionized water, air saturated, measurement within a day after reduction, stored at room temperature under room light, etc).

2.4 Circular Dichroism.

Circular Dichroism (CD) is widely used to study conformation changes in macromolecules such as proteins and nucleic acids caused by environment, ionic strength, pH and temperature changes and also caused by interaction with small molecules.(124) CD uses circularly polarized light shown in Figure 10 to study chiral molecules which interact differently with left and right circularly polarized light, depending on chiral arrangement of dipoles in space. The definition of CD is the absorption (A) difference between left (l) and right (r) circularly polarized light: $CD = A_l - A_r$. With CD, oligocytosines-silver nanocluster interaction can be studied.

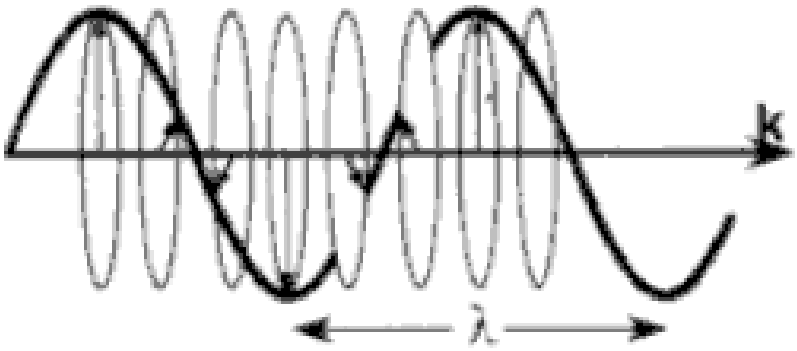

Figure 10. Circular polarized electromagnetic radiation.(124) Arrows indicate electric field vector.

2.5 Gel Electrophoresis.

Gel Electrophoresis is a useful technique to separate biological molecules such as proteins and DNA according to charge, hydrodynamic radius, and arrangement of molecules.(125) An electric field is used to separate charged macromolecules as they migrate electrophoretically through entangled gel. DNA is negatively charged due to the phosphate backbone. Thus, an electric field will cause DNA to migrate. Different gels such as polyacrylamide and agrose have different size pores through which macromolecules migrate with different rates. Polyacrylamide gels of varied concentration were used for electrophoresis. The gels contained 20 mL of acrylamide 40 % stock (Acrylamide:Bis-acrylamide (29:1) and Fisher scientific), 1.25 mL of 80 % glycerol (Fisher scientific), 500 μL of 10 % ammonium persulfate (Fisher scientific), 50 μL of TEMED (N,N,N',N'-Tetramethylenediamine, Fisher scientific), 4 mL of 5X TBE [Tris/Borate/EDTA(ethylenediaminetetraacetic acid)] and 14.25 mL of deionized water. Ammonium persulfate and TEMED were used for polymerization of acrylamide. The dimensions of the gels were 20 cm in length and height, 1.5 mm in thickness. The buffer, 0.5X TBE was used to run the gels. The gels were placed in a cold room to minimize band diffusion and its temperature was constant at 4°C. Before the samples were loaded, the gel was run for 30 minutes in order to remove acrylamide monomers. 50 μL of C_m:Ag_n samples ([C_m] = 250 μM and [Ag_n] depends on the length of polycytosines) and 10 μL of 2 M sucrose (Fisher scientific) were mixed in order to prevent the samples from dissolving into the 5X TBE buffer (running buffer) and loaded in each lane of the gel. The dye, bromophenol blue mixed with 2 M of sucrose was placed in one of the lanes in

the gel to determine when the run needed to be stopped. The gel was run for 24 hours at 80 V under constant voltage mode. After the run was stopped, a fluorescence gel scanner was used to image the C_m:Ag_n in the gel. This image is taken by using 635 nm excitation and 650 nm long pass filters. After the fluorescence bands were cut with a razor blade, they were suspended in deionized water so that the sample diffused out of the gel into the water. The sample solution was centrifuged for an hour to remove sediments (sucrose used to dissolve the sample). After the supernatants were extracted, they were poured into a filter attached to a centrifuge tube. In this case, the 3kDa cut-off filter was used since the mass of C_{12} is 3407Da. They were centrifuged for 100 minutes with 14000g and about 50 μL of C_{12}:Ag_n solution remained in the filter was sent to mass spectroscopy facility for analysis.

2.6 Fluorescence Imaging of C_m:Ag_n.

Single molecules of silver nanoclusters (C_m:Ag_n) were imaged on a cover slip after immobilization in poly(vinyl alcohol) (PVA) thin films. With the right ratio of concentrations of molecules to PVA, the single molecules can be imaged and are shown in the insert of Figure 11. The cover slides were cleaned by sonicating them in 1M NaOH for 30 minutes, followed by rinsing the cover slides with deionized water, drying them with nitrogen gas and putting them in the ozonator for 2 hours. The samples, C_7:Ag_n in the inset were prepared by diluting 1 μL of C_7:Ag_n solution in 999 μL of a saturated aqueous PVA (poly(vinyl alcohol), 5mg/mL (Acros Organics, 98% hydrolyzed, 16,000MW) solution. This mixture was then spun coated on a cleaned glass cover slide, spinning at 1500 RPM for 1 minute. The samples were then put on an inverted

microscope (Olympus, either IX-70 or IX-71) and imaged with a charged-coupled device (CCD) camera as shown in Figure 11. A laser or Hg lamp can be used as excitation sources. In this case, a Hg lamp was used. The excitation light passes through a band pass filter (3) that blocks all wavelengths except the excitation wavelength (510-550 nm). After the light is reflected by a dichroic mirror (2), it is focused by an oil-immersion objective (Olympus, 100X, 1.4 NA) (1) on the sample. The dichroic mirror is used to reflect the excitation wavelength and pass through the emission wavelengths of fluorescence emitted by the excited molecules in the sample. The emission light passes through an emission filter (5) and is then guided to a CCD camera (Roper Scientific, Micromax or Andor, Ixon) by a mirror (4).

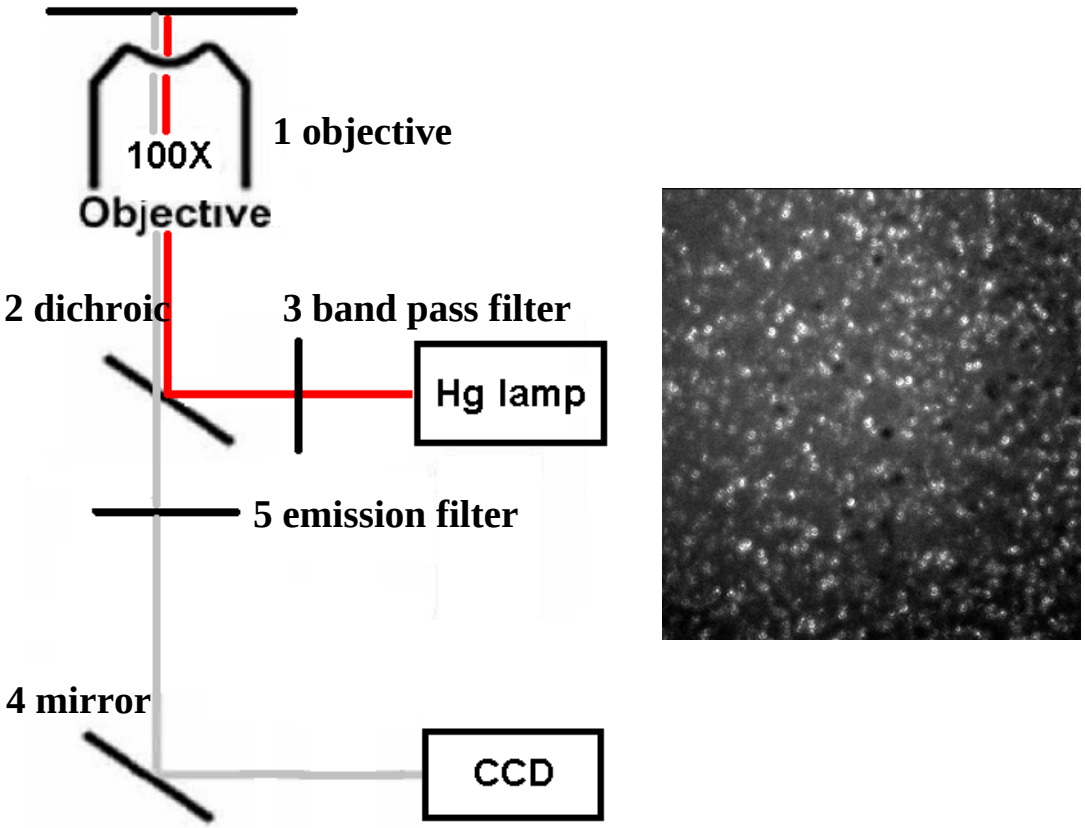

Figure 11. Schematic set-up for imaging of C_m:Ag_n taken by CCD camera using Hg lamp excitation. The insert is the image of C_7:Ag_n on PVA film taken by CCD camera, using green Hg lamp excitation (510-550 nm). Initial solution conditions: [C_7] = 100 μM, [Ag^+] = 350 μM and [BH_4^-] = 350 μM.

2.7 Confocal Detection of Single Molecules on PVA film.

Confocal microscopy enables high signal to noise detection of the fluorescence emitted by a single molecule. This technique is used to investigate the single molecule properties of C_m:Ag_n molecules in the PVA film discussed in the previous section. The C_m:Ag_n molecules in the PVA film (the sample preparation was the same as the previous section) are placed on a scanning stage (MS2000; Applied Scientific Instruments) (1) in order to position the molecules accurately to where the detector is aligned. To align the detector, the attenuated laser is aligned into the microscope and focused on the cover slide and then into the fiber. After the fiber is connected to the avalanched photo diode (APD), the x-y axis of fiber coupler is adjusted in order to obtain maximum counts from the APD. A continuous wave (CW) or pulsed laser can be used as excitation source. In this case, a 647 nm CW (Melles Griot, Air cooled Krypton Argon laser) was used. The excitation light passes through an excitation filter (4) that blocks all wavelengths except the excitation wavelength. After the light is reflected by a dichroic mirror (3), it is focused by an oil-immersion objective (Olympus, 100X, 1.4 NA) (2) on the sample. After, the emission light is passed through an emission filter (5), the emission light is directed to either a CCD camera (Roper Scientific, Micromax or Andor, Ixon) (7) or to one or two avalanche photodiodes (APD) (Perkin Elmer SPAQ) (9) with the path selector (6). The emission light was focused onto two APDs using a fused fiber splitter (8) used as a pinhole and a 50/50 beam splitter.

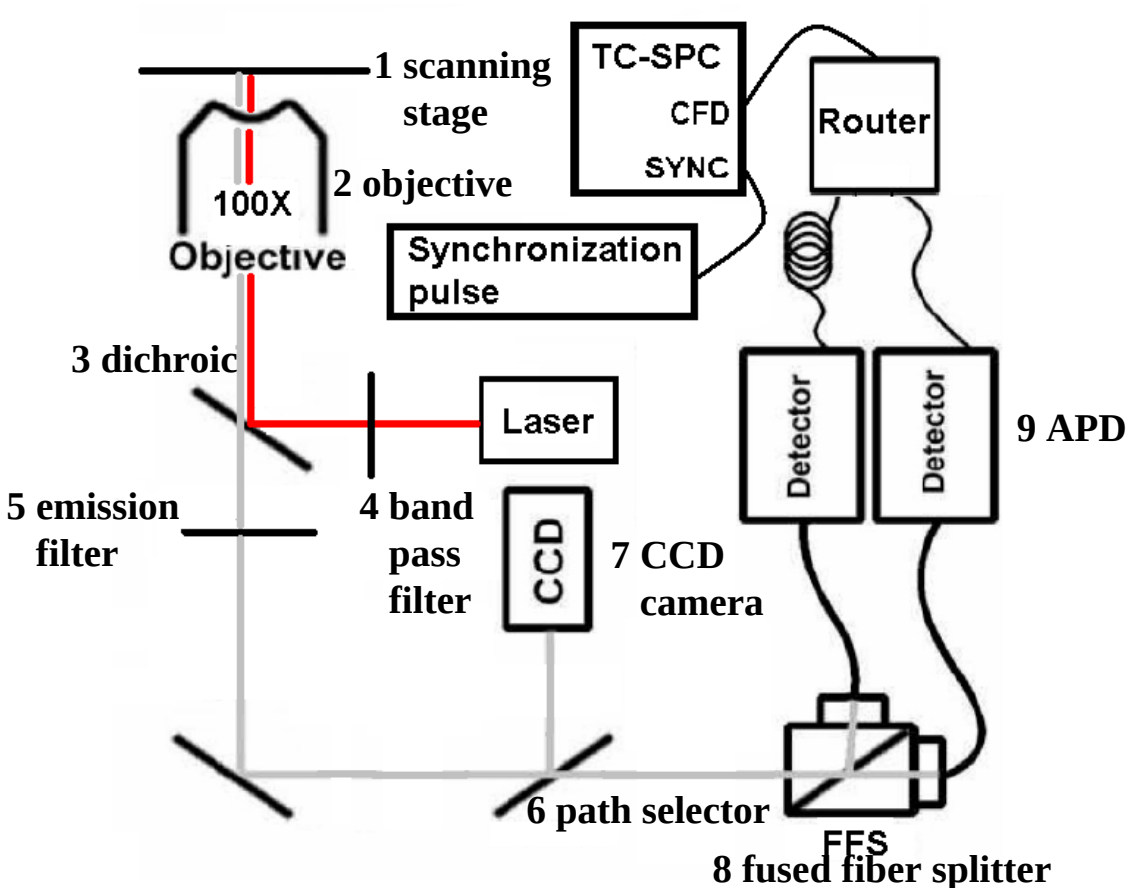

Figure 12. Schematic confocal arrangement for experiments of single molecule detection.

The detected single photon counting signals from the APD are digital (TTL) positive pulses. Since the single photon counting board (Becker & Hickl SPC-630) can only accept a negative pulses and the amplitude of the pulse must be less than 1V, the signals out of the APD need to be inverted and attenuated. The board consists of two inputs, SYNC and CFD. The synchronization pulses are sent to the SYNC. The APD signals are sent to the CFD. In this case, more than one detector was used, thus the signals from several detectors were sent to a router (HRT41 Becker & Hickl GmbH) and then to the CFD of the board. The signal from one of the two APDs was delayed by at least 200 ns using a digital delay (DG535 Stanford Research Systems) to circumvent detector and board dead times. Within the BH SPC-630, the CFD and SYNC inputs are sent to time-to-amplitude converter (TAC). The APD signals are recorded by the board and stored as micro and macro time. The micro time represents the time difference between a detected photon and the next arriving synchronization pulse, starting with the beginning of the experiment. When the CFD pulse (detected photon) sends a signal to the TAC, the voltage starts to increase linearly until the SYNC pulse (synchronization pulse) sends a signal to the TAC. This is shown in Figure 13. Logically, it is easier to understand that SYNC (synchronization pulse) is a start input to increase the voltage for the TAC and the CFD (fluorophore signal) is a stop input for the TAC. However, this would start the TAC every synchronization pulse and is a high burden on the electronics. Therefore, the CFD (fluorophore signal) is the start input and SYNC (excitation pulse) is the stop input.

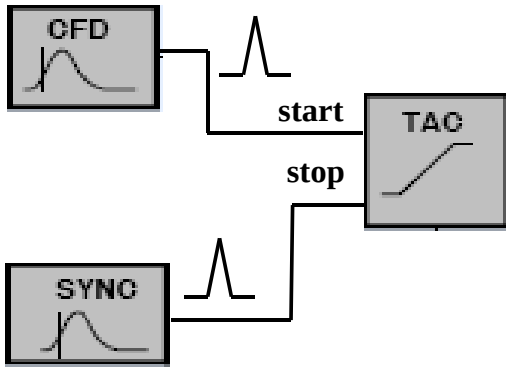

Figure 13. Diagram of time-to-amplitude converter (TAC).(126)

The range of the micro times is defined by the size of the TAC window and determined by the delay between two individual synchronization pulses (sync channels). The resolution of the micro time depends on either 256 or 4096 channels of the TAC window and is calculated by (the micro time range)/ (the number of the channels). By using the micro times, the fluorescence decay curve can be obtained.

On the other hand, the macro time represents the time difference between a detected photon and the start of the experiment. As the start button is clicked (start of the experiment), the clock starts to tick. When the detected photon from the APD is sent to CFD (there's another clock which is independent of micro time clock), the board registers the time of the photon with respect to the time of the start of the experiment and also registers which APDs the photon is detected from (channel number). The macro time (clock) has a time resolution of 50 ns. Using the macro time, a fluorescence intensity trajectory can be constructed by binning the macro time trace. Also, the autocorrelation function can be calculated with the macro times. This is very useful for Fluorescence Correlation Spectroscopy, which will be discussed later.

In order to construct an absolute time, the macro time (50 ns resolution) needs to be combined with the micro time (25 ps resolution with gain 1). Since the macro time has 50 ns resolution, the micro time is necessary to obtain higher time resolution.

For this we expanded on the approach by Weston et al.(127) to use the macro timer as a poor stopwatch to determine the number of sync cycles that have passed between two photon detection events and replace this value with the more precise value of a multiple of the measured sync period. From this value we subtract the micro time to get the

absolute time when a photon was detected. After the absolute times for the detector 1 and 2 are constructed, cross correlation is performed to observe fluorescence antibunching.(128)

2.8 Confocal Detection of Single Molecules in Solution.

Fluorescence Correlation Spectroscopy (FCS) is a powerful technique to study the fluorescence of single molecules in solution. With extremely low concentrations of molecules (a few molecules in the detection volume), the molecules diffuse in and out of the detection volume and that gives rise to fluorescence fluctuations. An FCS set-up is shown in Figure 14(a). A continuous wave (CW) or pulsed laser can be used as excitation sources. In this case, a 594 nm CW (JDS uniphase, HeNe laser) and a pulsed laser with 647 nm maximum (PicoQuant, diode laser) were used. The excitation light passes through an excitation filter (3) that blocks all wavelengths except the excitation wavelength. After the light is reflected by a dichroic mirror (2), it is focused by a water-immersion objective (Olympus, 60X, 1.2 NA) (1) into the sample solution. The emission light is passed through an emission filter (4) and focused into a fused fiber splitter (5) which acts as a pinhole in order to block the emission light not originating from the focal region. Although only one detector was necessary for this FCS measurement, two detectors were used to remove the peak resulted from the afterpulsing of the detector, thereby yielding faster time dynamics.(129) The emission light was focused onto two avalanche photodiodes (6) (APD) (Perkin Elmer SPAQ) through the fused fiber splitter. After the signals out from the APD were inverted and attenuated, they were sent to the board. The APD signals from fluorophores are sent to the CFD. In this case, more than one detector was used, thus the

signals from several detectors were sent to router (HRT41 Becker & Hickl GmbH) and then to the CFD of the board. The signal from one of the two APDs was delayed by at least 1.2 μs using a digital delay (DG535 Stanford Research Systems) due to the dead time of the board. Both CFD and SYNC inputs are sent to time-to-amplitude converter (TAC). The APD signals are recorded by the board and stored as micro and macro time. The fluorescence time trace of C_m:Ag_n sample on each detector was obtained from the macro time and the crosscorrelation is performed using both fluorescence time traces.

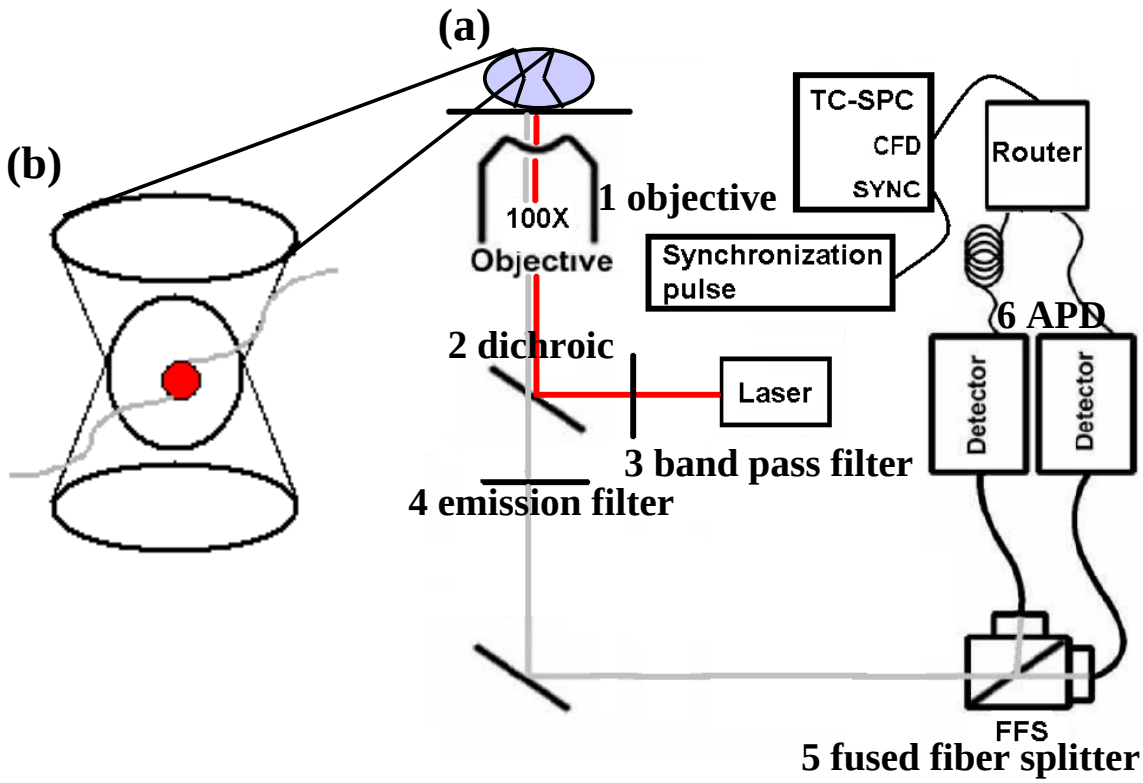

Figure 14. (a) Schematic arrangement for FCS experiments. (b) Close up of laser beam exciting the sample in solution. The molecule (red with two gray tails) diffuses into the laser beam.

3 FLUORESCENCE AND IDENTIFICATION OF C_m:Ag_n

When sufficiently small to preclude the continuous density of states of the bulk, silver nanoclusters can exhibit strong fluorescence from discrete energy levels.(2, 3, 5, 6, 46) While mass selection and soft landing methods enable control and study few atom Ag nanocluster properties,(11, 19-22) such size control in aqueous solutions is greatly complicated by aggregation and reactivity. Some success has been reported by using poly(amidoamine) dendrimers (PAMAM) and peptides as matrices to create several atom silver clusters in aqueous solutions, but only at low concentrations.(13, 23) Since 1960's it has been known that silver ions have strong affinities towards DNA.(90-93) Petty et al. demonstrated that the silver ions encapsulated by the 12-base oligonucleotide 5'-AGGTCGCCGCCC-3' were reduced by sodium borohydride ($NaBH_4$) to form silver nanoclusters and the distribution of the silver cluster size was narrow.(130) This particular oligonucleotide was used since it exhibits no intra- or inter-molecular interactions. NMR data showed that cytosine (C) has the strongest affinity towards silver ions of all the bases (adenine (A), thymine (T) and guanine (G)). It is this primary interaction between cytosine and Ag^+, the size control and optical properties of the resulting encapsulated nanoclusters that are extensively detailed in this thesis.

3.1 Identification of the different emitting cluster species in C_{12}:Ag_n.

At first, optical properties for 12 bases of cytosine (single-stranded C_{12}:Ag_n) are investigated. Reduced solutions of C_{12}:Ag_n show distinctive emission peaks at 480 nm (blue), 525 nm (green), 650 nm (red), and 720 nm (IR) when varying the excitation wavelength. Figure 15 shows the excitation and emission spectra of C_{12}:Ag_n at different

excitation and emission wavelengths. Figure 15a shows emission spectra excited at 340 nm and excitation spectra monitored at 480 nm emission for C_{12}:Ag_n. C_{12}:Ag_n shows a peak in the excitation spectrum at 340 nm. For the emission spectra excited at 340 nm, C_{12}:Ag_n shows an emission peak at 480 nm. Red emission is observed for fresh solutions but for equilibrated solutions (after a few days) no red emission can be observed. The reason for this is the kinetics involved in the cluster formation process. This will be discussed in a later section. In Figure 15b, the emission spectrum when exciting the sample at 440 nm is given. An emission maximum at 525 nm for C_{12}:Ag_n can be seen. For the corresponding excitation spectrum of C_{12}:Ag_n monitoring at 540 nm emission, two peaks at 340 nm and 440 nm were observed. The excitation peak for 340 nm is from the tail of the blue emission that also has a substantial contribution at 540 nm. In Figure 15c, the excitation peak for the red C_{12}:Ag_n emission is observed at 580 nm and the emission maximum is observed at 650 nm. IR emission excited at 640 nm for C_{12}:Ag_n has a maximum at 705 nm as shown in Figure 15d. The excitation spectra show a maximum at 660 nm for C_{12}:Ag_n. To summarize this, C_{12}:Ag_n shows distinctive emission peaks, blue (480nm), green (525nm), red (650nm), and IR (700nm). As shown later, distinctive silver nanoclusters give rise to these specific emission spectra.

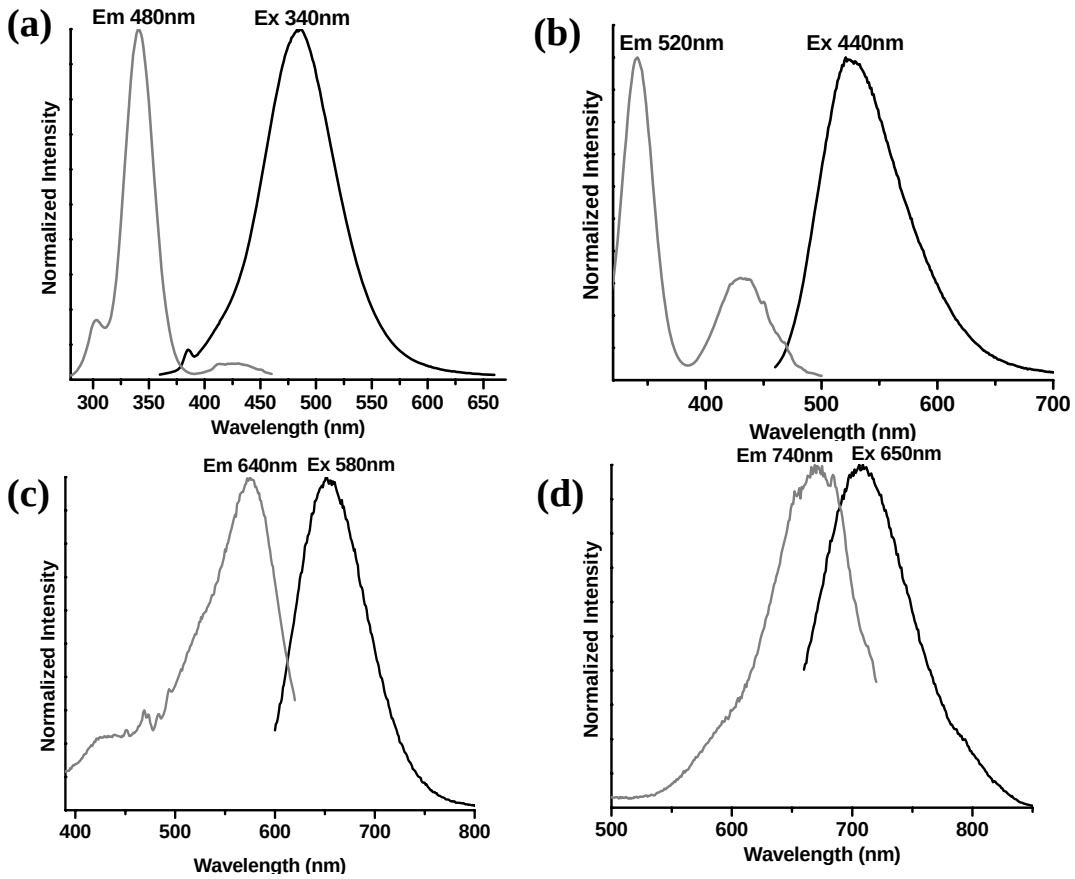

Figure 15. Emission and excitation spectra for C_{12}:Ag_n. Gray lines are excitation spectra of (a) 480nm (b) 520nm (c) 650nm (d) 700nm emission for C_{12}:Ag_n with [C_{12}] = 60 μM, [Ag^+] = 360 μM, and [BH_4^-] = 360 μM. Black lines are emission spectra excited at (a) 340 nm (b) 440nm (c) 580 nm (d) 650nm for C_{12}:Ag_n. Experimental conditions: (18 M Ω deionized water, air saturated, measurement 3 days after reduction, stored at room temperature under room light, etc).

Electrospray Ionization (ESI) is a useful technique to determine the molecular mass of large non-volatile biomolecules.(56) It is used to determine the molecular mass of biomolecules. Ionization is gentle enough to yield low overall fragmentation charged droplets are formed at the tip of a capillary, and the solvent evaporates to form gas phase ions.(56) In order to confirm interaction of Ag with C_{12} and to determine silver nanocluster size distributions, electrospray ionization mass spectra of C_{12}:Ag_n are heavily relied upon. Figure 16 shows a typical mass spectrum for C_{12}:Ag_n. The peaks that appear at 3516, 3621, 3728, 3834, 3940, and 4047 amu correspond to C_{12}:Ag_1, C_{12}:Ag_2, C_{12}:Ag_3, C_{12}:Ag_4, C_{12}:Ag_5, C_{12}:Ag_6 and C_{12}:Ag_7, respectively. The most abundant species in C_{12}:Ag_n is C_{12}:Ag_4. The peaks observed next to each C_{12}:Ag_n (23 amu off) are Na-DNA:Ag_n adducts. This mass spectrum clearly indicates that silver nanoclusters are bound to C_{12}. Although the mass spectra cannot distinguish if single Ag clusters or multiple Ag clusters are bound to C_{12}, the distribution of silver nanocluster size models as poisson distribution and ranges from Ag_1 to Ag_7. Since the distinctive emission peaks, blue (480nm), green (525nm), red (650nm), and IR (700nm) for C_{12}:Ag_n are characterized and the distribution of silver nanocluster size for C_{12}:Ag_n is determined, each silver nanocluster size can be correlated with different emission peaks.

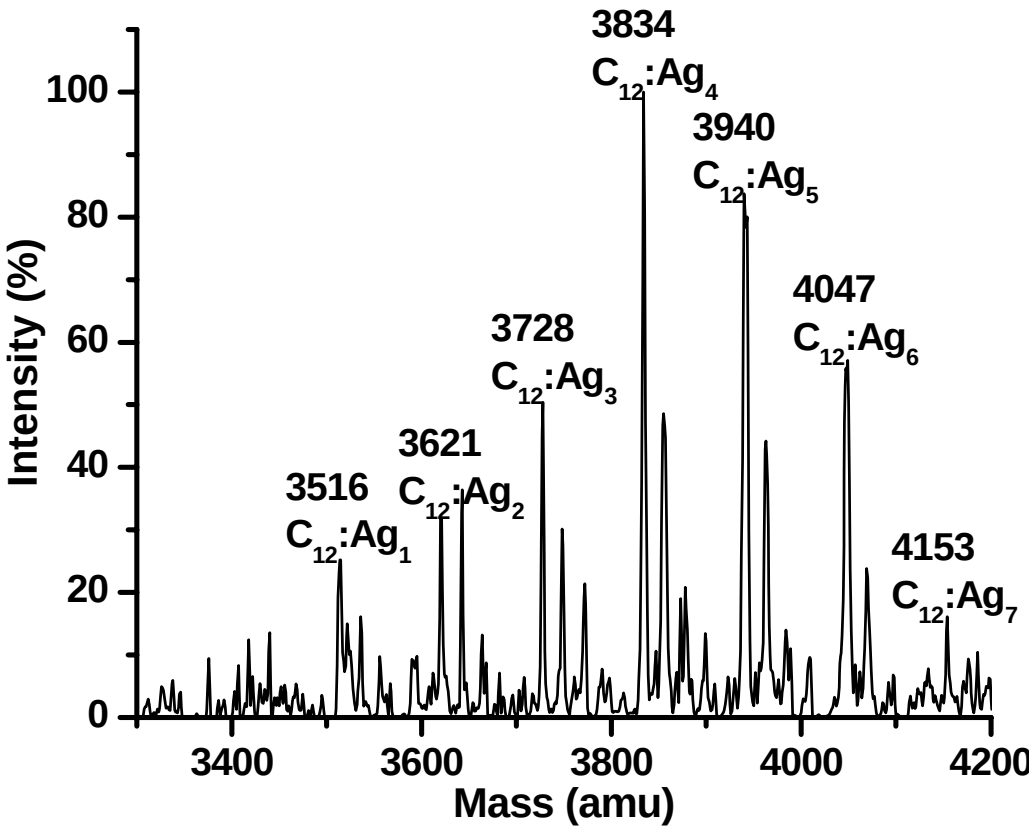

Figure 16. Typical electrospray ionization mass spectrum of C_{12}:Ag_n with [C_{12}] = 60 μM, [Ag^+] = 360 μM, and [BH_4^-] = 360 μM. C_{12} = 3408 amu. Mass spectra were obtained by using a Micromass Quattro LC operated in negative ion mode with 2.5 kV needle and 40 V cone voltage. Experimental conditions: (18 M Ω deionized water, air saturated, measurement within a day after reduction, stored at room temperature under room light, etc).

3.2 Evolution of C_{12}:Ag_n Spectra.

Absorption and emission for C_{12}:Ag_n are recorded with respect to time. Figure 17 shows time-dependent absorption spectra for C_{12}:Ag_n. Immediately after BH_4^- is added, no significant absorption is observed above 300nm. C_{12} itself has an absorption maximum at 260nm. The data represented in figure 3 is shown from 300nm to 700 nm since we are interested in the cluster absorption spectra. After 30 minutes, there is nonzero absorbance from 300 nm to 700 nm with a clear peak at 444 nm. This suggests that silver clusters may form. Each spectrum was taken every 30 minutes for 15 hours to see the changes. From 0.5 hour to 4.5 hours, the absorption maximum at 444 nm shifts to 453 nm. Absorption maxima at 340nm, 580 nm, and 670 nm start to appear. At 15 hours, absorption maxima at 340nm, 450 nm, 580 nm, and 670 nm are observed. Time-dependent emission from C_{12}:Ag_n Figure 18b also shows interesting dynamics. 440 nm excitation of C_{12}:Ag_n (Figure 18b) shows that the green emission (max at 525 nm) increases over 17 hours. While, red (max at 650 nm) in Figure 18c and IR emitters (max at 720 nm) in Figure 18d increase for a few hours and then decrease over time. Here the red and IR emitting species are excited at 580 nm and at 650nm, respectively. Figure 18a shows evolution of emission spectrum for C_{12}:Ag_n excited at 340 nm. As mentioned above, emission spectra from 670 nm to 690 nm were not recorded to avoid detector damage from the second order of the grating. Blue/green and red/IR emitters can be excited by 340 nm simultaneously. Red/IR emission increases for a few hours and decreases over time while blue/green emission continuously increases. An isosbestic

point at 600 nm in Figure 18a indicates that the red and IR species convert into blue and green emitters.

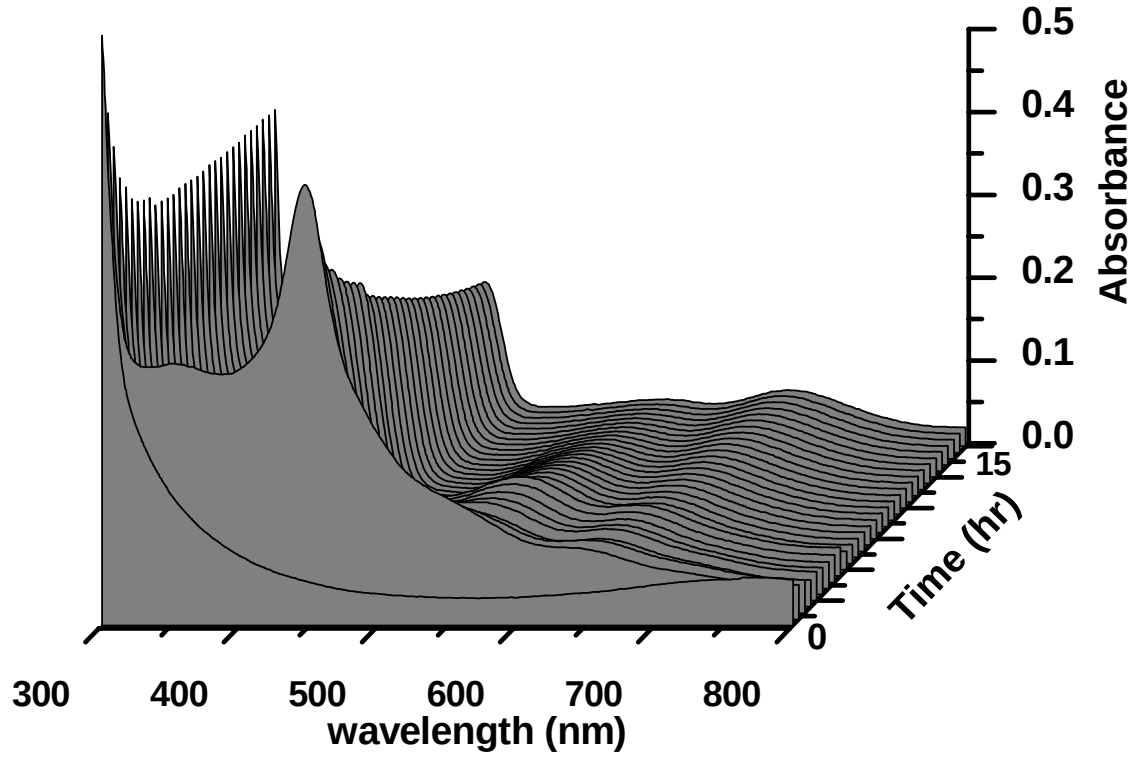

Figure 17. Time-dependent absorption spectra for C_{12}:Ag_n. [C_{12}] = 45 μM, [Ag^+] = 270 μM, and [BH_4^-] = 270 μM (18 MΩ H_2O). The first spectrum is taken immediately after BH_4^- is added to C_{12}:Ag^+ solution. Each spectrum is taken every 30 minutes.

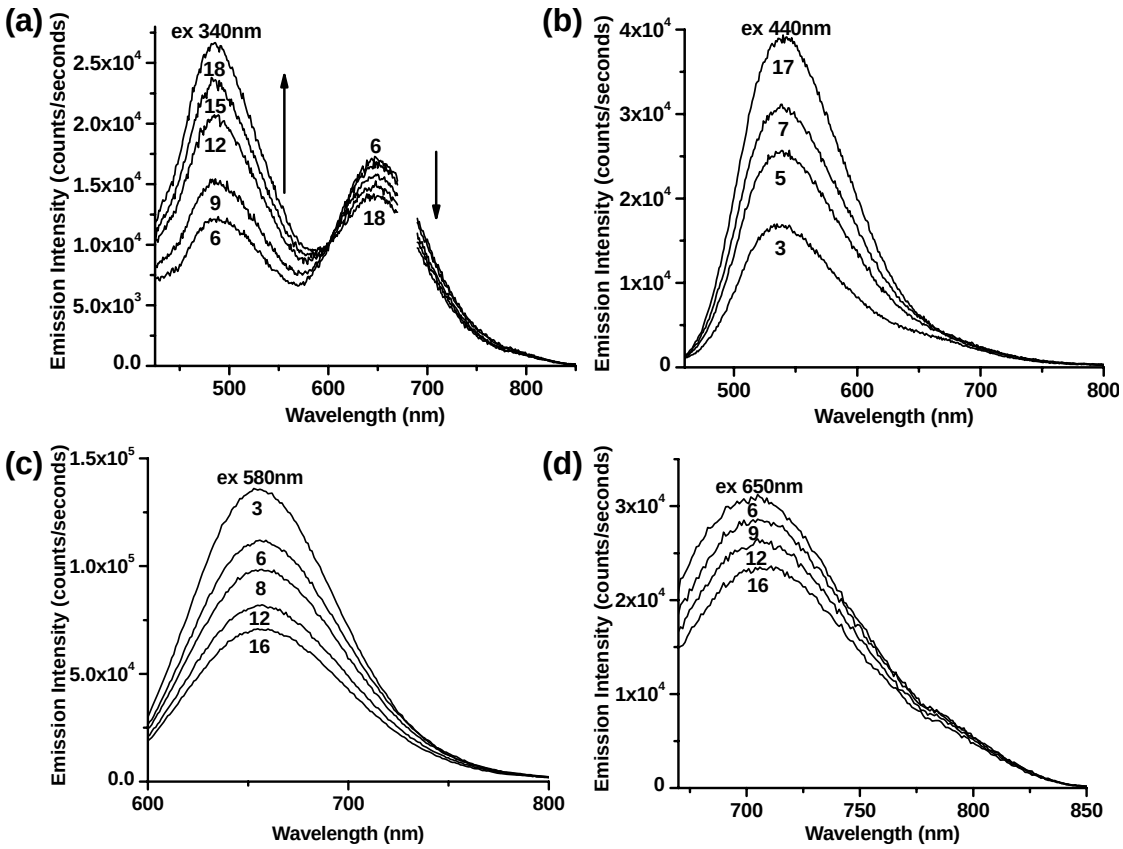

Figure 18. Time-dependent emission spectra for C_{12}:Ag_n excited at (a) 340 nm (b) 440 nm (c) 580 nm (d) 650 nm. [C_{12}] = 60 μM, [Ag^+] = 360 μM, and [BH_4^-] = 360 μM (18 MΩ H_2O). The number shown below each spectrum indicates hours after BH_4^- is added to C_{12}:Ag^+ solution.

3.3 Identification of Silver Nanocluster Size.

Gel Electrophoresis is a useful technique for biological molecules such as proteins and DNA to separate according to charge, mass, and arrangement of molecules.(131) Differences in electrophoretic mobility are used to separate charged macromolecules such as DNA. DNA is negatively charged due to the phosphate backbones. Thus, an electric field will cause DNA to migrate toward the positive electrode generating an electric field. Different gels such as polyacrylamide and agarose have different size pores through which macromolecules migrate with different rates. Using gel electrophoresis, different polycytosine complexes with different silver nanocluster sizes can be separated (60V constant, at 4 °C, running time: 1 and a half day, running buffer: 0.5X TBE, gel: 20% polyacrylamide gel, loading volume: 50 µl). Figure 19 shows an image taken from a fluorescence image scanner (PhosphoImager, Storm) and the corresponding mass spectrum (negative ion mode with 2.5 kV needle and 40 V cone voltage) from the recovered band. This image is taken by using 635 nm excitation and 650 nm long pass filters. The top band is recovered and concentrated by using centrifugal micro tubes. (detail described in section 2.5) The inset in Figure 19 is mass spectrum for the corresponding band. There is a small amount of C_{12}:Ag_2 present in the spectrum while the peak for C_{12}:Ag_3 is dominant. Therefore, this suggests that red species are C_{12}:Ag_3.

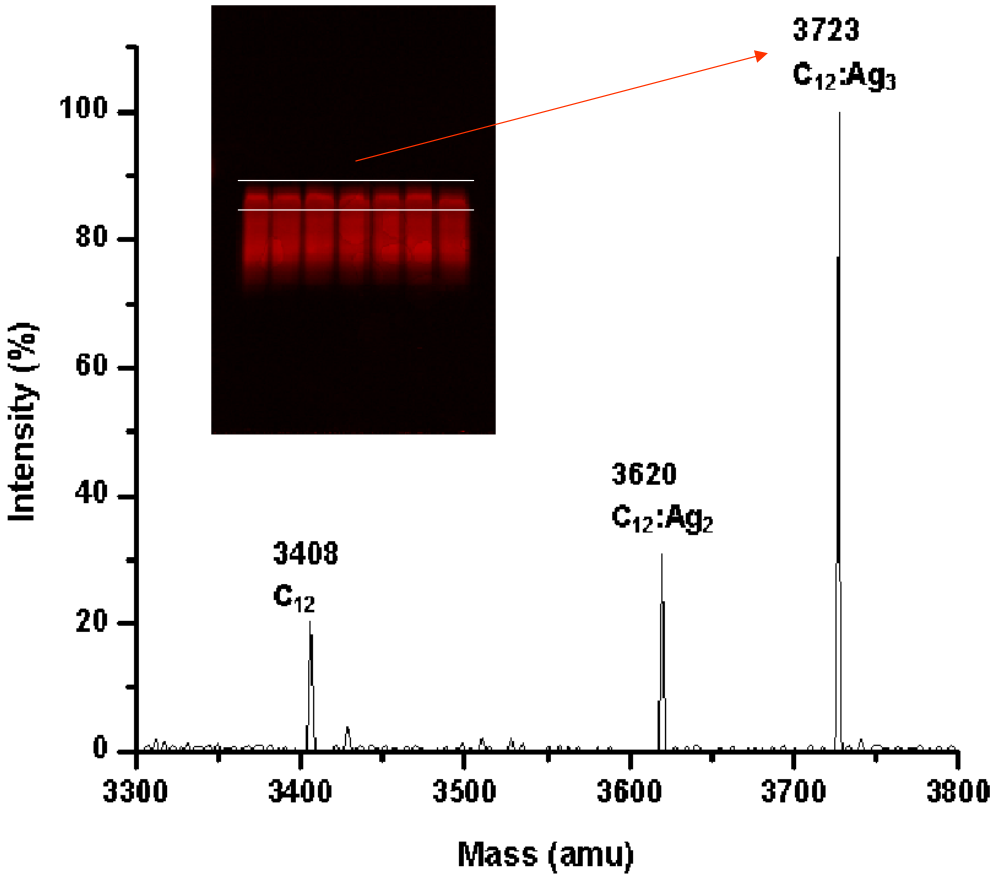

Figure 19. Fluorescence gel image for a band from C_{12}:Ag_n samples (inset) and the corresponding electrospray ionization mass spectrum from the recovery of the bands. 20% polyacrylamide gel in 0.5X TBE buffer solutions is used to run C_{12}:Ag_n samples (18 M Ω H_2O and stored in a dark before use (for a day)) for 1 and a half day at 60V in a cold room (4 °C). C_{12} = 3408 amu. Loading volume of the sample is 50 µl per each lane. Original conditions: [C_{12}] = 500 µM, [Ag^+] = 3 mM, and [BH_4^-] = 3 mM.

It is possible to identify the silver nanocluster sizes by correlating their fluorescence with their mass abundance, but greater discrimination is obtained by also changing DNA length. Figure 20 shows fluorescence-mass correlation of C_8:Ag_n. Since C_8:Ag_n has extremely low blue emission compared to C_{12}:Ag_n and it has comparable IR emission intensities as the red emission, C_8:Ag_n was used for fluorescence-mass correlation to help identify blue and IR emitting species through comparison with data on C_{12}:Ag_n. Figure 20a shows green and red emission excited at 440nm (dotted line), and at 340nm (solid line). To protect the detector, the scan is stopped at 660 nm. As a result of this, the IR emission is not fully shown, but no blue emission at 480 nm is observed in these shorter DNA strands, with green emission (525 nm) and red (650 nm)/IR (705 nm) emission being the dominant peaks. Figure 20b shows strong red (650 nm) emission (solid line) excited at 580nm and IR (720 nm and one shoulder appearing around 780nm) emission (dotted line) excited at 650nm. From the corresponding mass spectrum of C_8:Ag_n in Figure 20c, the cluster distribution ranges from C_8:Ag_1 to C_8:Ag_4 with essentially no abundance of C_8:Ag_5. In order to identify the silver cluster size, several fluorescence and mass spectra at different times have to be taken. All different fluorescent species have different quantum yields and lifetime. Therefore, it cannot be concluded that the most abundant cluster has the most intense fluorescence or percentage increase/decrease from the fluorescence spectra are proportional to the percentage increase/decrease from the mass spectra. Mass and fluorescence spectra of Figure 20d, e, and f were recorded 20 hours after the first mass and fluorescence spectra of C_8:Ag_n were measured. Figure 20d shows green (525 nm) and red (650 nm)/IR (720 nm) emission

excited at 440nm (dotted line). The intensity for green emission increased nearly two fold, while red/IR emission excited at 440nm remains essentially unchanged. Blue/green and red/IR emission excited at 340nm is also unchanged. In Figure 20e, both red (650 nm) emission excited at 580nm and IR emission (720 nm) excited at 650nm slightly decreased compared to the previous spectra (Figure 20b). The shoulder appearing around 780 nm remains the same as before. The corresponding mass spectrum shows the relative abundances have also changed with the most abundant species to higher mass clusters.

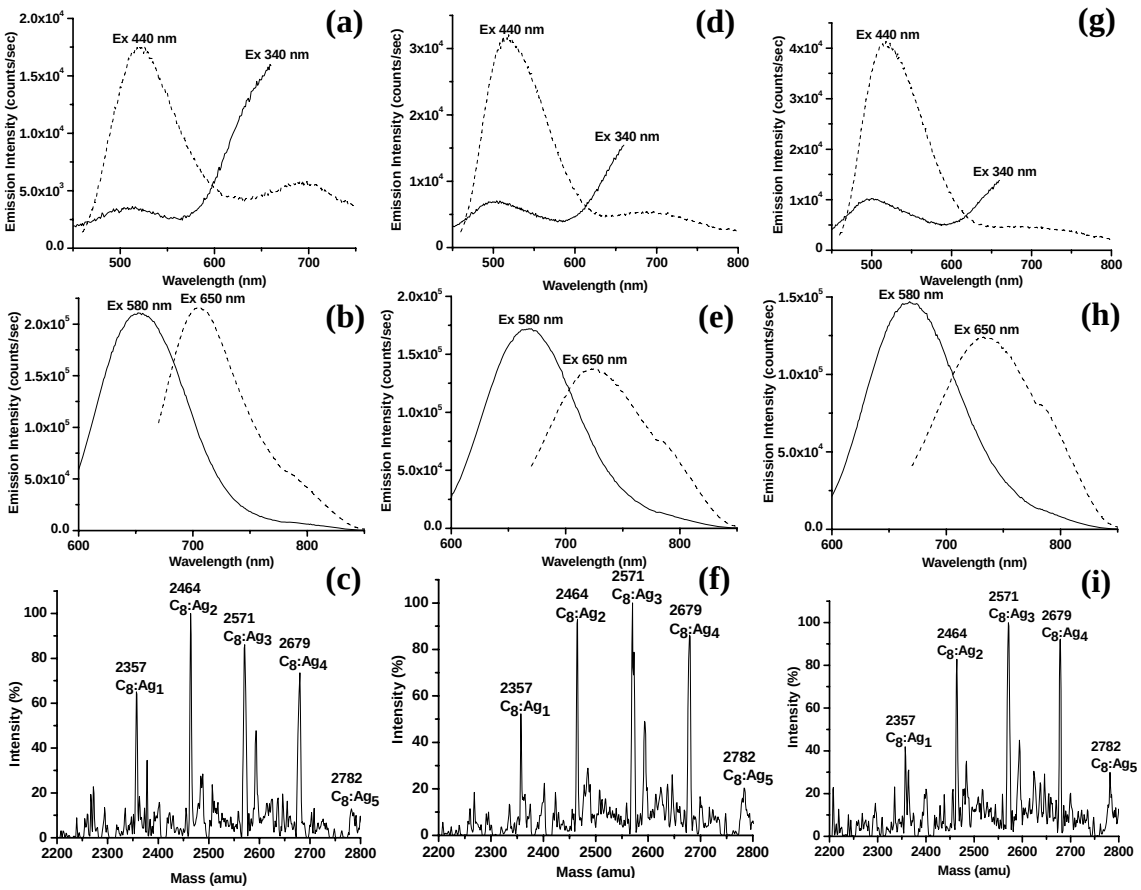

Figure 20. Mass-fluorescence correlation spectra for C_8:Ag_n with [C_8] = 100 μM, [Ag^+] = 400 μM, and [BH_4^-] = 400 μM. (a) Emission excited at 340 nm (solid line) and at 440 nm (dotted line) (b) Emission excited at 580 nm (solid line) and at 650 nm (dotted line) (c) Corresponding mass spectrum from fluorescence spectra in (a) and (b). (d) Emission spectrum excited at 340 nm (solid line) and at 440 nm (dotted line) 20 hours after the previous fluorescence and mass spectra, (a), (b), and (c) were taken. (e) Emission spectra excited at 580 nm (solid line) and at 650 nm (dotted line) 20 hours after the previous spectra were taken. (f) Corresponding mass spectrum from fluorescence spectra in (d) and (e). (g), (h) and (i) are fluorescence and mass spectra 22 hours after the previous spectra, (d), (e) and (f) were taken. (g) Emission excited at 340 nm (solid line) and at 440 nm (dotted line) (h) Emission excited at 580 nm (solid line) and at 650 nm (dotted line). (i) Corresponding mass spectrum from fluorescence spectra in (g) and (h). Experimental conditions: (18 M Ω deionized water, air saturated, measurement within a day after reduction, stored at room temperature under room light, etc). Mass spectra were obtained by using a Micromass Quattro LC operated in negative ion mode with 2.5 kV needle and 40 V cone voltage.

Mass and fluorescence spectra (Figure 20g, h, and I) were recorded 22 hours after the second mass and the fluorescence spectra of C_8:Ag_n were measured. In Figure 20g, the green (525 nm) emission excited at 440nm increased by about 30% from the previous spectrum in Figure 20d. In addition, blue (480 nm)/green (525 nm) emission excited at 340nm increased by 80%. Red (650 nm)/IR (720 nm) emission excited at 340nm and 440nm stay the same as the previous spectrum in Figure 20d. From Figure 20h, both red (650 nm) emission excited at 580nm and IR emission (720 nm) excited at 650nm continue to decrease from the previous spectra in Figure 20b and e. The shoulder appearing around 780nm stays the same. By observing the corresponding mass spectrum in Figure 20i, C_8:Ag_3 is still the most abundant. As the fluorescence intensity for green emitters increases in Figure 20g, the abundance for C_8:Ag_4 increases slightly compared to the previous mass spectrum in Figure 20f. As IR (650 nm) emission decreases (Figure 20h), the abundance for C_8:Ag_2 continues to decrease compared to the previous mass spectrum in Figure 20f.

To summarize this, as the green emission excited at 440nm continued to increase from Figure 20a to g, abundance for C_8:Ag_4 increased relative to the most abundant species. As IR emission (705 nm) excited at 650nm continued to decrease over time from Figure 20b to h, the abundance for C_8:Ag_2 kept decreasing over time relative to the most abundant species. The blue emission excited at 340 nm was hardly formed in Figure 20a, d and g and the least abundant species is C_8:Ag_5. Thus, the following silver cluster assignment can be suggested: Blue (480 nm), green (525 nm), red (650 nm) and IR (720

nm) emitters are Ag_5, Ag_4, Ag_3 and Ag_2, respectively. Much more corroborative evidence will be presented throughout this thesis to further confirm the size-dependent emission.

All of these emitters and formed at different times in C_{12}, but C_8 appears too short to stabilize the Ag_5 species. By taking advantage of formation kinetics producing different emitters in C_{12}, specific nanocluster sizes can be independently identified using correlation of mass spectra with emission spectra as a function of time. To identify the blue emitters, mass spectra were taken as the blue emitters became the dominant species. A typical mass spectrum and the corresponding emission spectra of C_{12}:Ag_n are shown in Figure 21a and b, respectively. As shown in figure Figure 21a, the dominant peaks are Ag_4 and Ag_5. The corresponding emission spectra were taken 30 minutes before the mass spectrum was taken. The dominant emission is blue while the red emission was low due to the conversion of red species into blue species.

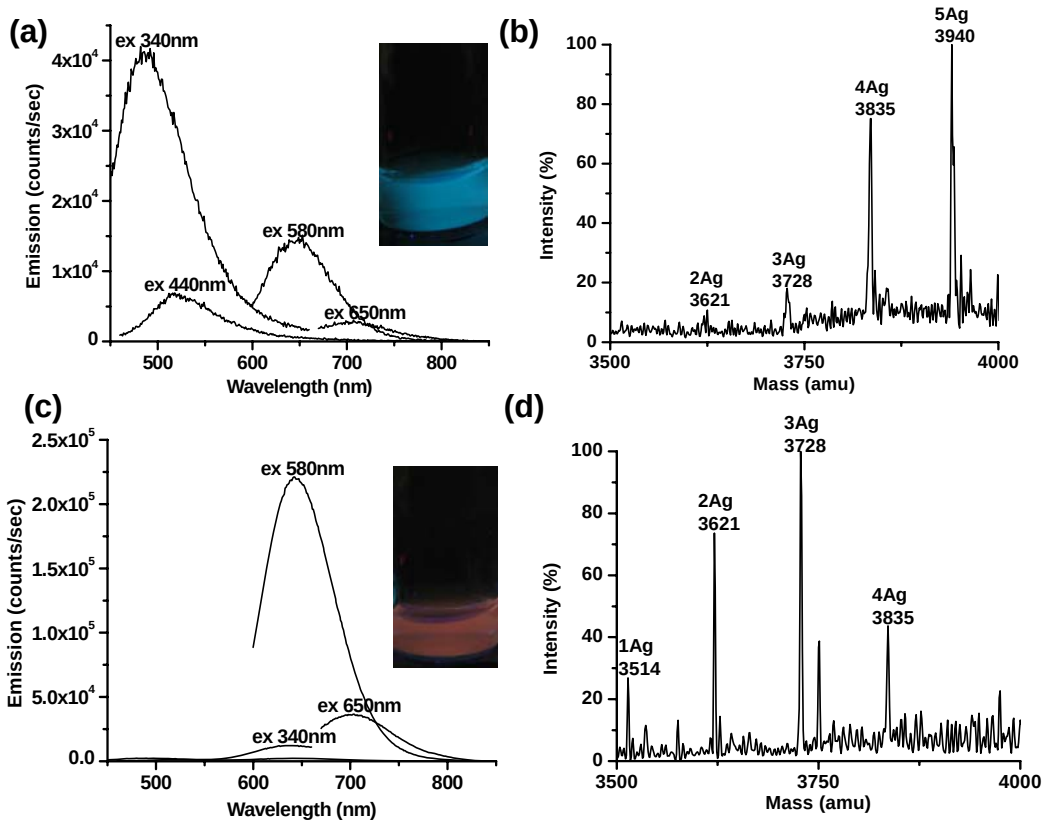

Figure 21. (a) Emission spectra excited at 340 nm, 440 nm, 580 nm and 650 nm 30 minutes before adding another equivalent of BH_4^- to C_{12}:Ag_n, [C_{12}] = 60 μM, [Ag^+] = 360 μM, and [BH_4^-] = 360 μM. Inset is the image of the solution excited with a hand-held UV-lamp. (b) The corresponding electrospray ionization mass spectrum of (a). (c) Emission spectra excited at 340 nm, 440 nm, 580 nm and 650 nm for C_{12}:Ag_n 30 minutes after adding 360 μM BH_4^- to C_{12}:Ag_n, [C_{12}] = 60 μM, [Ag^+] = 360 μM, and [BH_4^-] = 360 μM. Inset is the image of the solution excited with a hand-held UV-lamp. (d) The corresponding electrospray ionization mass spectrum of (c). C_{12} = 3407 amu. Experimental conditions: (18 M Ω deionized water, air saturated, measurement 3 days after reduction, stored at room temperature under room light, etc). Mass spectra were obtained by using a Micromass Quattro LC operated in negative ion mode with 2.5 kV needle and 40 V cone voltage.

One equivalent $NaBH_4$ was added to the blue emitting solution in Figure 21a and b. After 30 minutes, the blue emission completely disappeared while the red emission increased about 10-fold as the previous spectra (Figure 21c). The corresponding mass spectrum in Figure 21d was taken 30 minutes after the emission spectra in Figure 20c were acquired. The dominant peaks in the mass spectra after adding extra 1 equivalent mole of $NaBH_4$ are Ag_2 and Ag_3 while the Ag_5 peak completely disappeared. This strongly suggests that the blue emission corresponds to passively oxidized Ag_5 and red emission corresponds to fully reduced Ag_3. IR emission also increases 5-fold upon addition of equivalent $NaBH_4$, suggesting that the IR emitters corresponds to Ag_2. Finally, Ag_4 might be the green emitter due to decrease in the emission and corresponding abundance change in mass spectrum.

Deoxyribose Nucleic Acid (DNA) consists of bases and a sugar-phosphate backbone while Peptide Nucleic Acid (PNA) consists of bases and backbone in which repeating N-(2-aminoethyl)-glycine groups are linked by peptide bonds. (Figure 22). The bases in DNA are linked to the backbone by β-N -glycosidic bonds, while the bases in PNA are linked to the backbone by methylene carbonyl linkages. The structures of DNA and PNA are quite similar except their backbones. PNA is used to investigate the effect that backbone has.

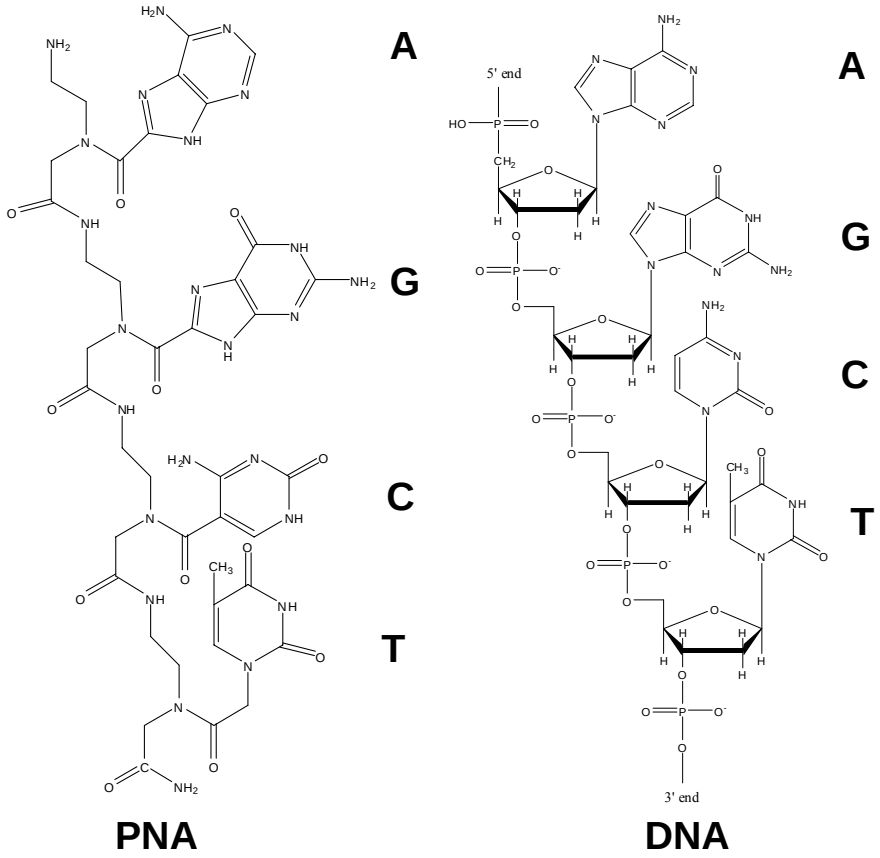

Figure 22. Structures of Peptide Nucleic Acid (PNA) and Deoxyribose Nucleic Acid (DNA).

Figure 23a-b shows emission spectra excited at 340 nm and 440 nm and the corresponding mass spectra for PNA C_{12}:Ag_n, respectively. In Figure 23a, the blue emission excited at 340 nm is the dominant peak while the green emission excited at 440 nm is significantly lower than the blue emission. No other fluorescent species are observed. The corresponding mass spectrum for PNA C_{12}:Ag_n in Figure 23b only shows two peaks, PNA C_{12}:Ag_4 and PNA C_{12}:Ag_5 (the dominant species). This further suggests that blue emitters are Ag_5 and the green emitters are Ag_4.

Taken together, the gel electrophoresis, correlation of DNA-encapsulted Ag_n emission with mass spectra and PNA results all suggest that Ag_2, Ag_3, Ag_4 and Ag_5 are IR (720 nm), red (650 nm), green (525 nm) and blue (480 nm) emitters, respectively. This cluster assignment with emission is in contrast to the jellium model.(1) The jellium model is a model that describes the electronic structure of small metal clusters as strong absorptions of few-atom clusters grow smoothly in to the plasmon that is characteristic of large metal nanoparticles. Many experiments in the early eighties on alkali metal clusters strongly support this model for gas-phase species.(132) This model considers the cluster a uniformly positively charged sphere with conduction electrons that can move freely on this sphere.(1) This model can be used in the case the valence electrons are loosely bound like for alkali and noble metals such as silver and gold.(1) Experimental ionization energies decrease with increasing number of atoms per cluster,(73) which is in good agreement with theoretical calculations using the jellium model.(75) Related to that fact, it was recently shown that the emission energy is correlated with the number of atoms for

gold nanoclusters, even in solution.(44, 45) The emission energy follows the scaling, $E_{Fermi}/N^{1/3}$, in which E_{Fermi} is the Fermi energy of the bulk metal.(52)

Although our silver cluster assignment cannot be explained with the jellium model, this can be explained by determining if silver clusters are oxidized or fully reduced. Unlike bulk metals, small metal clusters have discrete electronic states. Thus, transitions between the electronic states can occur. The larger the particle is, the smaller the energy gap between HOMO and LUMO is. For charged particles such as Ag_5 and Ag_4 although the cluster size is larger, the energy gap between HOMO and LUMO is larger. Since the positively charged clusters (Ag_5 and Ag_4) have fewer electrons, there is less shielding effect from the nucleus. Thus, the electrons will be closer to the nucleus and this will increase the energy gap between HOMO and LUMO.(1)

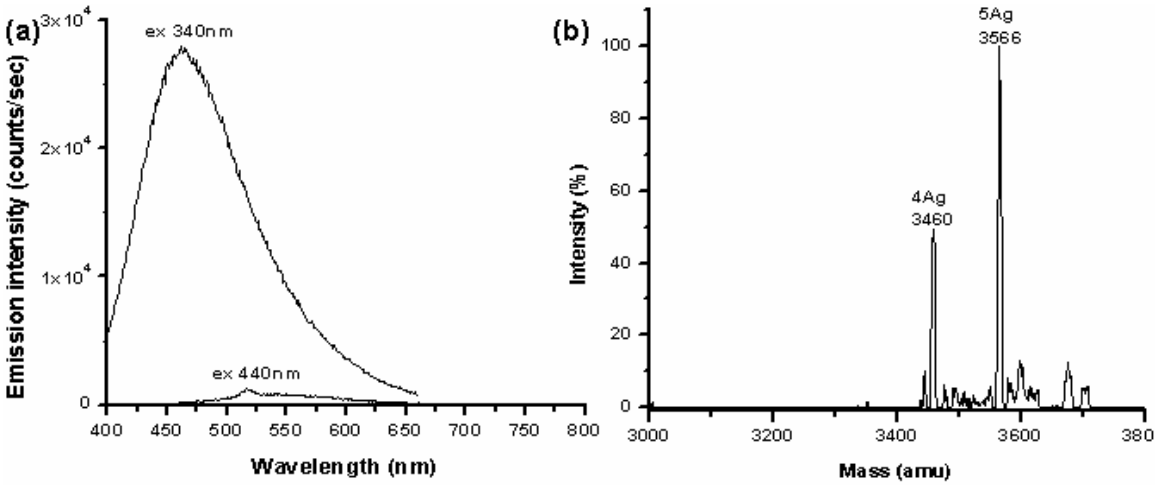

Figure 23. (a) Emission spectra excited at 340 nm and 440 nm for PNA C_{12}:Ag_n. (b) The corresponding electrospray ionization mass spectrum in (a). PNA C_{12} = 3034g. PNA C_{12}:Ag_n. Original conditions: [C_{12}] = 50 μM, [Ag^+] = 300 μM, and [BH_4^-] = 300 μM. Experimental conditions: (18 M Ω deionized water, air saturated, measurement within a day after reduction, stored at room temperature under room light, etc). Mass spectra were obtained by using a Micromass Quattro LC operated in positive ion mode with 2.5 kV needle and 40 V cone voltage.

3.4 Oxidized and Fully Reduced Silver Emitters.

In order to investigate whether or not emitting species are fully reduced, C_{12}:Ag_n solutions were purged with N_2 (dotted lines in Figure 24) before reduction and kept under N_2 in a dark room) while the other C_{12}:Ag_n solution was exposed to air (solid lines in Figure 24) before and after reduction. Figure 24 shows the emission spectra of C_{12}:Ag_n excited at 340 nm, 440 nm, 580 nm and 650 nm at several time points during the first 24 hours after reduction. One hour after reductions (Figure 24a), C_{12}:Ag_n solution exposed to air yields blue emission (max at 480 nm) excited at 340 nm, green emission (max at 525 nm) excited at 440 nm, red emission (max at 650 nm) excited at 580 nm and IR emission (max at 720 nm) excited at 650 nm, while the C_{12}:Ag_n solution kept under N_2 showed five-fold high red emission (max at 650 nm) and IR emission (max at 720 nm) than the C_{12}:Ag_n solution exposed to air. Additionally over the 24-hour observation period, no blue or green emitters formed for C_{12}:Ag_n solution purged with N_2. This indicates that the blue and green emitters are partially oxidized forms and the red and IR emitters are fully reduced.

Blue (480nm), green (525nm), red (650nm) and near IR (720nm) emission from C_{12}:Ag_n were further investigated in the presence of 100mM NaCl. Cl^- will precipitate Ag^+ from solution as AgCl (K_{sp} = 1.82E-10).(133), and etch any oxidized Ag nanoclusters Thus, emission from any oxidized species should decrease. In Figure 25a, the blue emission excited at 340nm is dominant before adding 100mM NaCl.

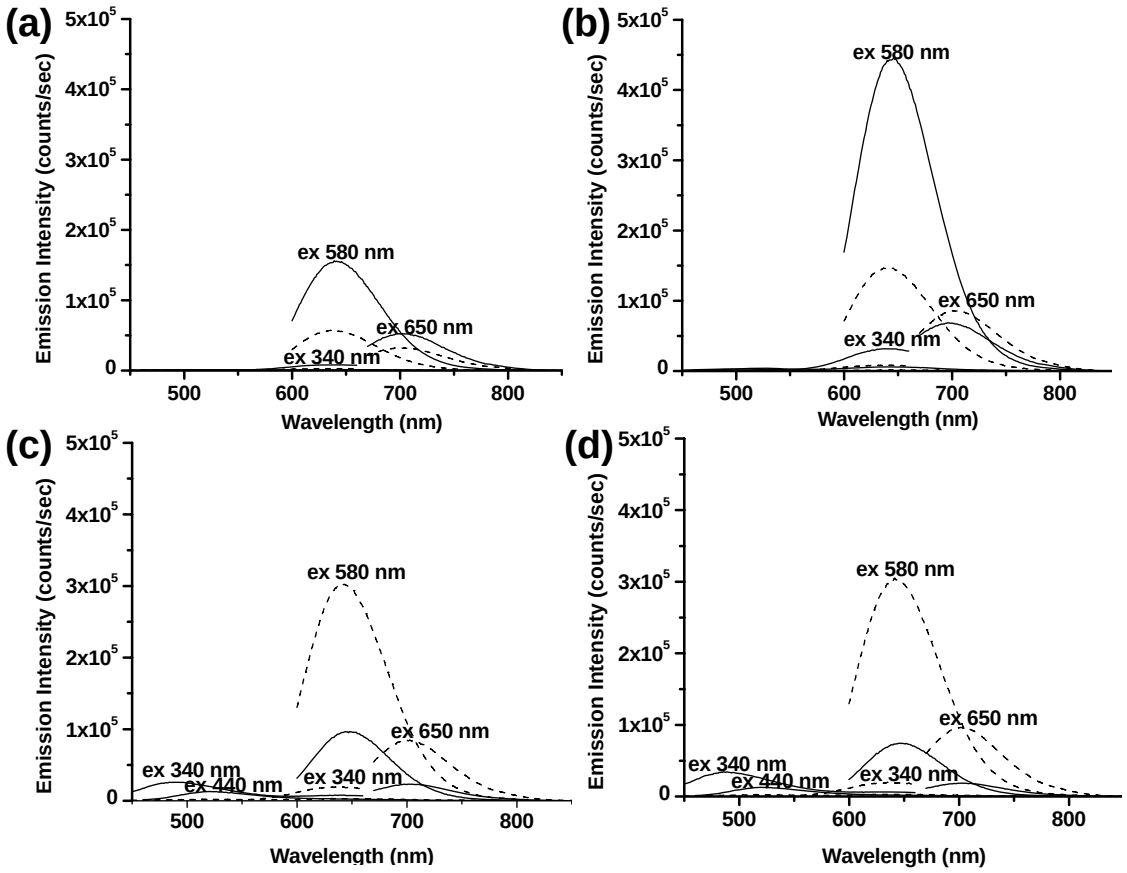

Figure 24. Time-dependent emission spectra of C_{12}:Ag_n excited at 340 nm, 440 nm, 580 nm and 650 nm. The dotted line indicates C_{12}:Ag_n purged with N_2 before and after reduction and the solid line indicates C_{12}:Ag_n exposed to air before and after reduction. (a) 1 hour (b) 4.5 hours (c) 20 hours (d) 24 hours after reduction. Original conditions of both solutions: [C_{12}] = 60 μM, [Ag^+] = 360 μM, and [BH_4^-] = 360 μM. Experimental conditions: (18 M Ω deionized water, stored at room temperature under dark, etc).

Within 25 minutes after adding NaCl shown in Figure 25b, the blue emission decreases significantly (compared to other emission). The green emission excited at 440nm also decreases with time. On the other hand, the red emission excited at 580nm increases two-fold upon upon addition of NaCl and the IR emission excited at 650nm increases four-fold. After the initial increase (Figure 25c), the longer wavelength emitters also eventually decay with time as O_2 is presented in solution. According to our hypothesis, it is possible for Cl^- to remove Ag^+ from the oxidized Ag nanoclusters such as C_{12}:Ag_4 and C_{12}:Ag_5 due to precipitation of AgCl. As a result, the blue and green emission decreases after addition of NaCl.

Another way to test whether or not all observed emitters (blue, green, red and IR) in Figure 26 are fully reduced is one extra equivalent of $NaBH_4$ is added to C_{12}:Ag_n solution. Figure 26a shows the emission spectrum of C_{12}:Ag_n solution one week after initial reduction. The dominant emission is blue while the red emission was low due to the conversion of red species into blue species. After 1 equivalent mole of $NaBH_4$ was added to the same solution used for Figure 26a, the blue emission completely disappears while the red emission increased about 10-fold (Figure 26b). This is strong indication that red and IR emitters are fully reduced.

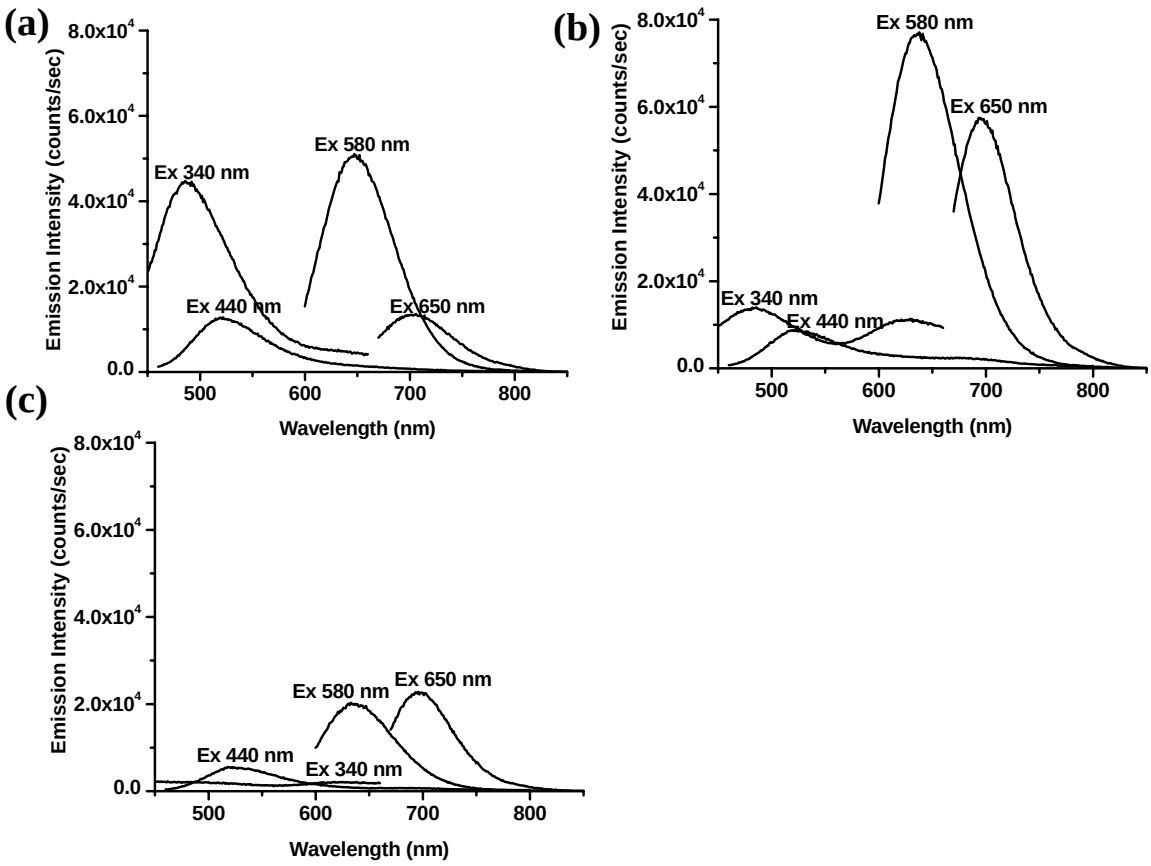

Figure 25. Time-dependent emission spectra of C_{12}:Ag_n excited at 340 nm, 440 nm, 580 nm and 650 nm with addition of 100mM NaCl. (a) before adding100mM NaCl (b) 25 minutes after adding 100mM NaCl (c) 50 minutes after adding 100mM NaCl. Original solution conditions: [C_{12}] = 60 μM, [Ag^+] = 360 μM, and [BH_4^-] = 360 μM. Experimental conditions: (18 M Ω deionized water, air saturated, measurement within two days after reduction, stored at room temperature under room light, etc).

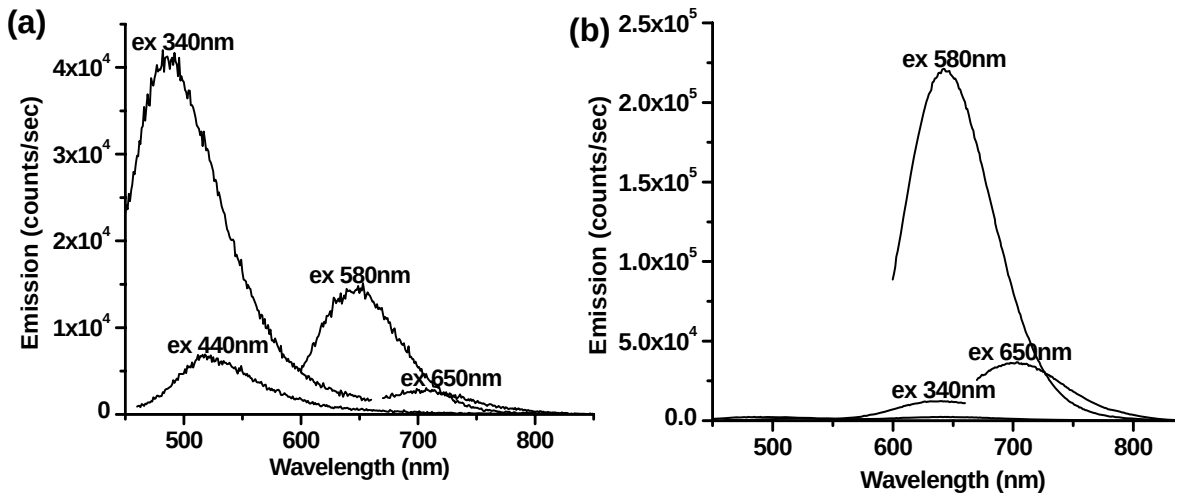

Figure 26. (a) Emission spectra excited at 340 nm, 440 nm, 580 nm and 650 nm 30 minutes before adding a second equivalent (360 μM) of BH_4^- to C_{12}:Ag_n. Original solution conditions: [C_{12}] = 60 μM, [Ag^+] = 360 μM, and [BH_4^-] = 360 μM. (b) Emission spectra excited at 340 nm, 440 nm, 580 nm and 650 nm for C_{12}:Ag_n 30 minutes after adding 360 μM BH_4^- to C_{12}:Ag_n. Experimental conditions: (18 M Ω deionized water, air saturated, measurement within three days after reduction, stored at room temperature under room light, etc).

3.5 Conclusion

Emission spectra excited at 340 nm, 440 nm, 580 nm and 650 nm showed distinct maxima at blue (480nm), green (525nm), red (650nm), and IR (720nm) wavelengths and the silver cluster distribution ranges from Ag_1 to Ag_7. With electrophoresis, correlation of emission with mass spectra and PNA, the Ag cluster sizes were identified with blue emitters as Ag_5, green emitters as Ag_4, red emitters as Ag_3, and IR emitters as Ag_2. With an O_2 free environment, Cl^- addition, and/or extra reducing agent additions, Ag_4 and Ag_5 appear to be partially oxidized while Ag_2 and Ag_3 are likely fully reduced.

4 STABILITY AND DYNAMICS OF C_m:Ag_n

While characterizing the photophysical properties of C_m:Ag_n, interesting silver nanocluster dynamics were observed. The absorption, emission and mass spectra change with respect to time. In order to use this dye for biological applications, dynamics and stability need to be investigated and the dynamics need to be controlled.

4.1 Length-Dependent Ag Cluster Stability in Polycytosine.

The Stability of Ag_n is investigated with varying lengths of polycytosines (C_6, C_8, C_{10}, C_{12} and C_{24}). Due to the kinetic effects of silver clusters, emission spectra of C_6:Ag_n, C_8:Ag_n, C_{10}:Ag_n, C_{12}:Ag_n and C_{24}:Ag_n and mass spectra of C_6:Ag_n, C_8:Ag_n, C_{10}:Ag_n, and C_{12}:Ag_n are taken after they reached equilibrium. The mass spectrum for C_{24}:Ag_n is not shown since clean mass spectra for C_{24}:Ag_n could not be obtained. The mass spectrum of C_6:Ag_n in Figure 27a show cluster sizes ranging from Ag_1 to Ag_3 with Ag_2 as dominant peak. The corresponding emission in Figure 28b spectra show peaks at 650 nm (red) from 340 nm excitation, 650 nm (red)/ 705 nm (IR) from 440 nm excitation, 650 nm (red) from 580 nm excitation and 705 nm (IR) from 640 nm excitation. The emission peak at 650 nm is significantly higher than the emission at 705 nm. The mass spectrum of C_8:Ag_n in Figure 27a show cluster sizes ranging from Ag_1 to Ag_5. The dominant peak is Ag_3, while Ag_5 is hardly formed. The corresponding emission in Figure 28b spectra show peaks at 500 nm (blue and green) from 340 nm excitation, 525 nm (green) from 440 nm excitation, 650 nm (red) from 580 nm excitation and 720 nm (IR) from 650 nm excitation. The emission peaks at 650 nm and 720 nm are significantly higher than the emission at 500

nm. Mass spectra for C_{10}:Ag_n (Figure 28c) indicate clusters ranging from Ag_2 to Ag_6 with Ag_3 as a dominant peak. In Figure 28d, C_{12}:Ag_n shows emission peaks at 480 nm (blue) from 340 nm excitation, 525 nm (green) from 440 nm excitation, 650 nm (red) from 580 nm excitation and 720 nm (IR) from 650 nm excitation. C_{24}:Ag_n in Figure 28e shows emission peaks at 480 nm (blue) from 340 nm excitation and 525 nm (green) from 440 nm excitation. While, emission peaks at 650 nm (red) from 580 nm excitation and 720 nm (IR) from 650 nm excitation were hardly observed from C_{24}:Ag_n.

To summarize, after creation and equilibration C_6:Ag_n shows only red (650nm) and IR (720nm) emissions, while C_8:Ag_n, C_{10}:Ag_n, and C_{12}:Ag_n show distinctive emission peaks, blue (480nm), green (525nm), red (650nm), and IR (705nm). C_{24}:Ag_n yields only blue (480nm) and green (525nm) emission. For C_6:Ag_n, red and IR emission appear while no blue and green emission are observed. For C_8:Ag_n and C_{10}:Ag_n, red and IR emission are dominant while blue emission are very weak. IR emission intensity from C_8:Ag_n is much higher than one from C_{10}:Ag_n. For C_{12}:Ag_n, blue emission dominates while red and IR emission are weak. For C_{24}:Ag_n, blue and green emission are strongest while red and IR emission are barely observed. The corresponding mass spectra of these species indicate that shorter DNA strands can only stabilize small cluster sizes. Additionally, their correlation with emission spectra strongly suggest that the larger clusters give higher energy emission. These data further support assignments that blue, green, red and IR emitters correspond to Ag_5, Ag_4, Ag_3 and Ag_2, respectively.

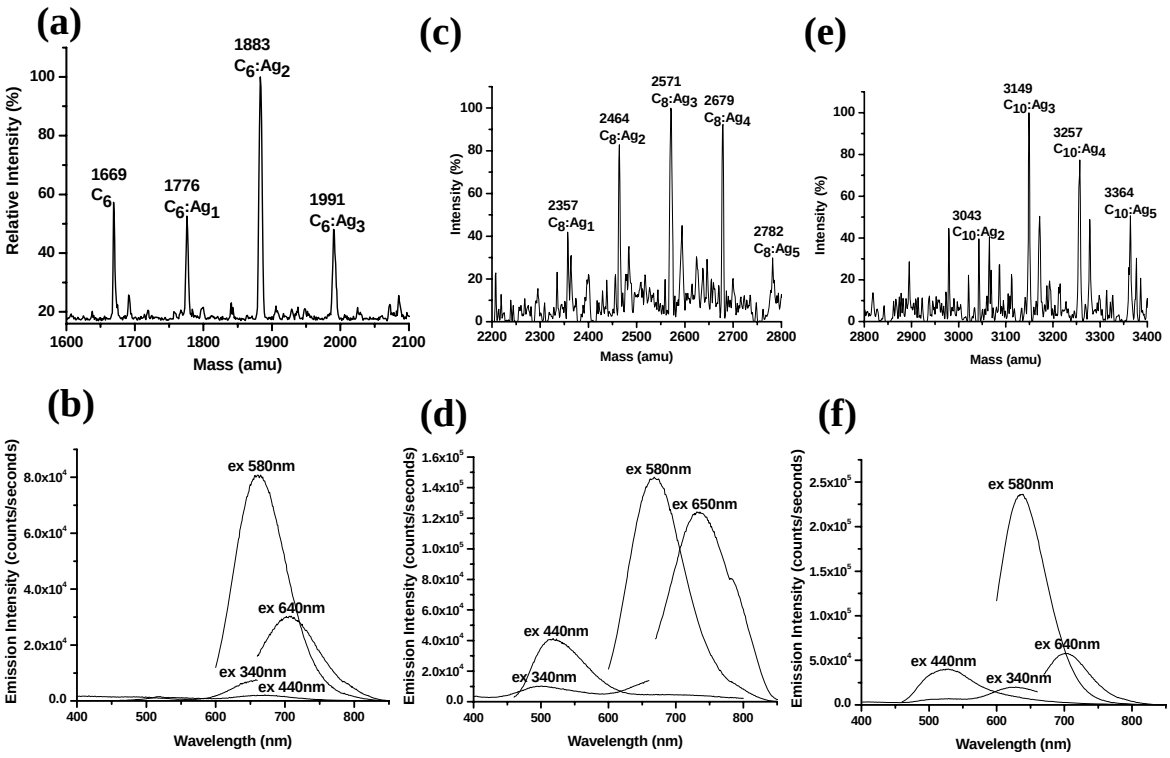

Figure 27. (a) Electrospray ionization mass spectrum of C_6:Ag_n. Original solution conditions: [C_6] = 100 μM, [Ag^+] = 260 μM, and [BH_4^-] = 260 μM. (b) The corresponding emission spectra from C_6:Ag_n excited at 340 nm, 440 nm, 580 nm and 650 nm. (c) Electrospray ionization mass spectrum of C_8:Ag_n. Original solution conditions: [C_8] = 100 μM, [Ag^+] = 350 μM, and [BH_4^-] = 350 μM. (d) Emission spectra from sample in (c) excited at 340 nm, 440 nm, 580 nm and 650 nm. (e) Emission spectra of C_{10}:Ag_n. Original solution conditions: [C_{10}] = 100 μM, [Ag^+] = 720 μM, and [BH_4^-] = 720 μM excited at 340 nm, 440 nm, 580 nm and 650 nm. The samples were dissolved in 18 M Ω H_2O and stored at room temperature under room light. Mass spectra were obtained by using a Micromass Quattro LC operated in negative ion mode with 2.5 kV needle and 40 V cone voltage.

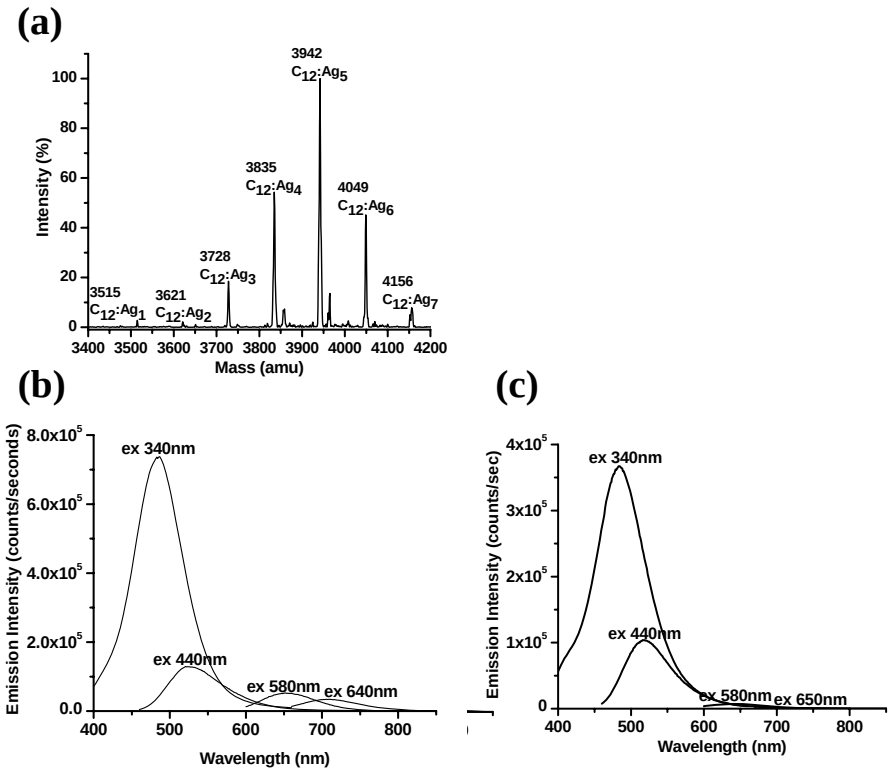

Figure 28. (a) Electrospray ionization mass spectrum of C_{12}:Ag_n. Original solution conditions: [C_{12}] = 60 μM, [Ag^+] = 360 μM, and [BH_4^-] = 360 μM. (b) Emission spectra from sample in (c) excited at 340 nm, 440 nm, 580 nm and 650 nm. (c) Emission spectra of C_{24}:Ag_n. Original solution conditions: [C_{24}] = 60 μM, [Ag^+] = 720 μM, and [BH_4^-] = 720 μM excited at 340 nm, 440 nm, 580 nm and 650 nm. The samples were dissolved in 18 M Ω H_2O and stored at room temperature under room light. Mass spectra were obtained by using a Micromass Quattro LC operated in negative ion mode with 2.5 kV needle and 40 V cone voltage.

4.2 Evolution of Spectra.

To investigate the silver nanocluster formation kinetics, emission spectra for C_m:Ag_n were recorded in time and are shown in Figure 29. In Figure 29a, the green (525 nm) and red (650 nm)/IR (705 nm) emission excited at 340 nm for C_8:Ag_n are shown. The green emission excited at 340 nm increases with time. The red/IR emission excited at 340 nm also increase until 9 hours after C_8:Ag_n reduction, but continuously decrease after that. An isosbestic point is observed at 575 nm, indicating that the red/IR emitters are chemically transformed into the green emitter. The green and red/IR emission are also observed with 440 nm excitation, as shown in Figure 29b. Similar dynamics for the green and red/IR emission excited at 340 nm are observed. The red/IR emission excited at 440 nm also increases over the first 9 hours after initial BH_4^- reduction of C_8:Ag_n, but subsequently decreases. On the other hand, the green emission continuously increases after the reduction of C_8:Ag_n. An isosbestic point is also observed with 440 nm excitation, but at 610 nm, suggesting that an intermediate may be involved in the cluster size dynamics. Not surprisingly then, Figure 29c and d show that the red emission excited at 580 nm and IR emission excited at 650 nm also increase until 9 hours after the reduction of C_8:Ag_n and continuously decrease afterwards. Time-dependent emission from C_{12}:Ag_n is described in section 3.2.

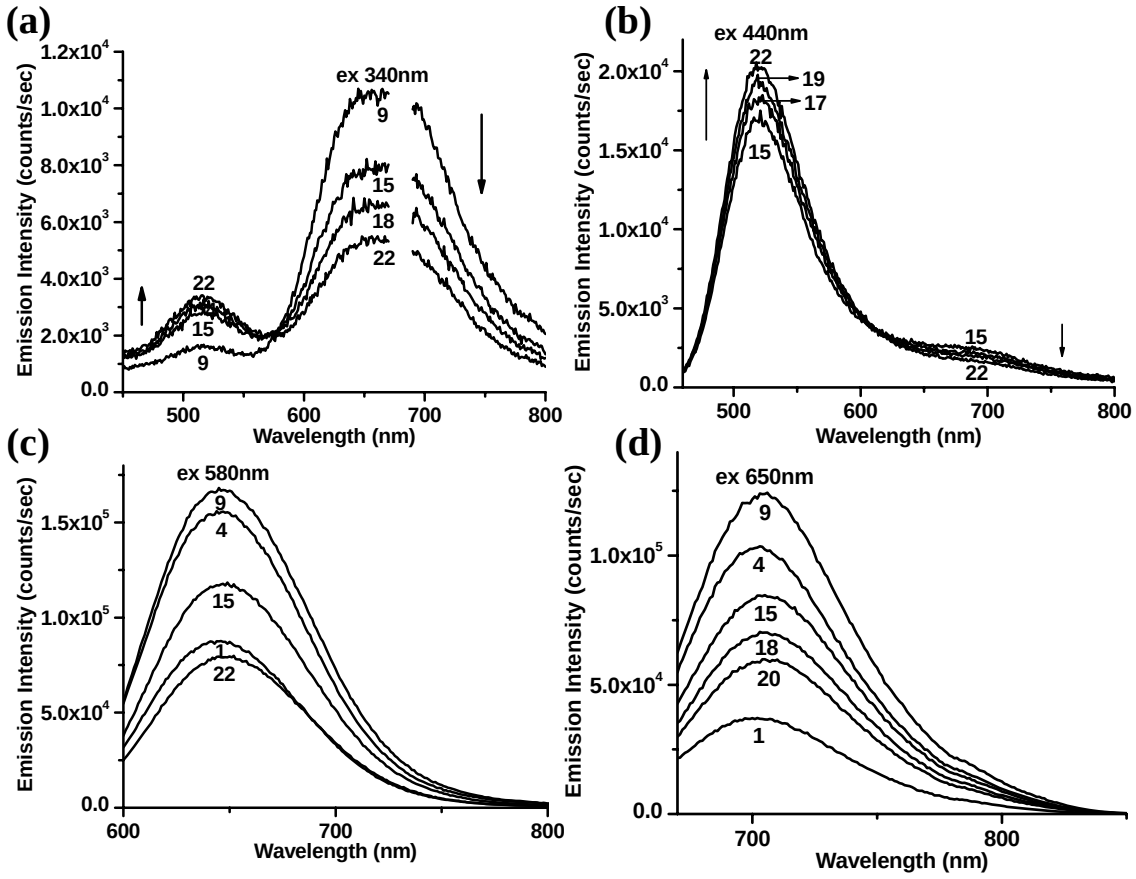

Figure 29. Time-dependent emission spectra for C_8:Ag_n (dissolved in 18 M Ω H_2O) excited at (a) 340 nm (b) 440 nm (c) 580 nm (d) 650 nm. [C_8] = 100 μM, [Ag^+] = 350 μM, and [BH_4^-] = 350 μM. The number shown below each spectrum indicates hours after BH_4^- is added to the C_8:Ag^+ solution. The samples were dissolved in 18 M Ω H_2O and exposed to a room light. The sample had placed in a sample compartment of a fluorometer until all the measurements were over.

C_{24}:Ag_n produced similar emission dynamics were observed. Figure 30b shows the time-dependent emission excited at 440 nm for C_{24}:Ag_n. The green emission (max at 525 nm) increases for 17 hours, while, red (max at 650 nm) in Figure 30c decreases over time. Near IR emission from C_{24}:Ag_n (Figure 30d) exhibits an emission maximum was at 690 nm instead of 720 nm. In spite of the shifted emission peak, IR emitters for C_{24}:Ag_n also decrease over time. Here the red and IR emitting species are exited at 580 nm and at 650nm, respectively. Evolution of the emission spectrum for C_{24}:Ag_n excited at 340 nm is shown in Figure 30a. Blue/green and red/IR emitters were excited by 340 nm simultaneously. Red/IR emission increases for a few hours (not shown in Figure 30a) and decreases over time. On the other hand, blue/green emission continuously increases after reduction. An isosbestic point was observed at 590 nm, again suggesting that the red and IR species are converted into blue and green species.

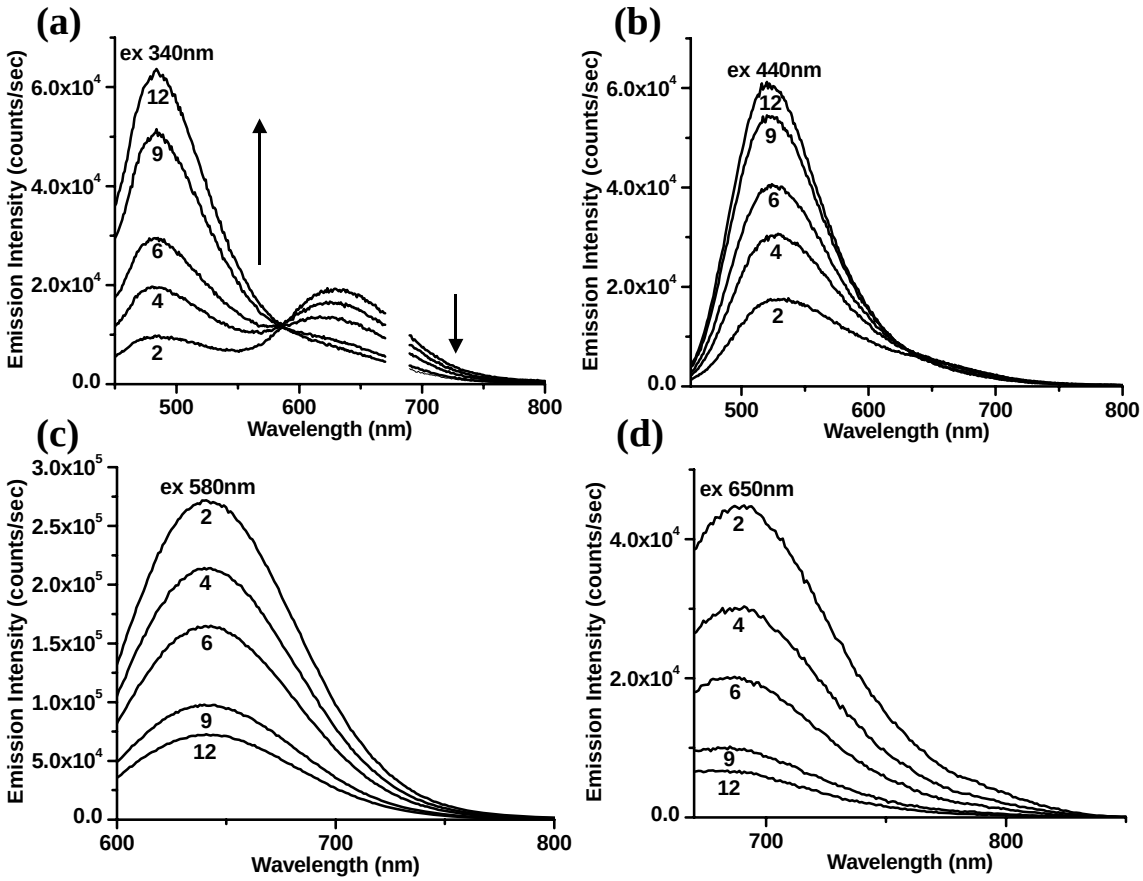

Figure 30. Time-dependent emission spectra for C_{24}:Ag_n (dissolved in 18 M Ω H_2O) excited at (a) 340 nm (b) 440 nm (c) 580 nm (d) 650 nm. [C_{24}] = 60 μM, [Ag^+] = 720 μM, and [BH_4^-] = 720 μM. The number shown below each spectrum indicates hours after BH_4^- is added to C_{24}:Ag^+ solution. The sample had placed in a sample compartment of a fluorometer until all the measurements were over.

Similar trends in silver nanocluster dynamics were observed from C_8:Ag_n, C_{12}:Ag_n and C_{24}:Ag_n. The red emission excited at 580 nm and IR emission excited at 650 nm for C_8:Ag_n, C_{12}:Ag_n and C_{24}:Ag_n increase for a few hours and decreased afterwards. As mentioned in section 4.1 of this thesis, the blue emitters (oxidized Ag_5) were not formed in C_8:Ag_n due to instability of Ag_5 in short lengths of polycytosines. Thus, the green and red/IR emission were excited at 340 nm for C_8:Ag_n, while the blue/green and red/IR emission were excitable with 340 nm for C_{12}:Ag_n and C_{24}:Ag_n. The green and blue/green emission excited at 340 nm for C_8:Ag_n, C_{12}:Ag_n and C_{24}:Ag_n increase with respect to time, while the red/IR emission with 340 nm excitation increases over a few hours and decreases afterwards. Isosbestic points were observed from C_8:Ag_n, C_{12}:Ag_n and C_{24}:Ag_n. The green emission excited at 440 nm for C_8:Ag_n, C_{12}:Ag_n and C_{24}:Ag_n increase over time. The red/IR emission excited at 440 nm for only C_8:Ag_n increased over a few hours and decreased. The isosbestic point (440 nm excitation) was only observed from C_8:Ag_n. Two isosbestic points were observed from C_8:Ag_n, while only one isosbestic point was observed from C_{12}:Ag_n and C_{24}:Ag_n. The isosbestic points indicate that the red and IR emitters turn into blue and green species. Thus, this suggests that under these conditions (18 M Ω deionized water, air saturated, at room temperature, within a day, etc), blue and green emitters are more stable than red and IR species at least in longer DNA strands.

The mechanism suggested in section 1.5 (the standard potentials of the silver electrode as a function of agglomeration number of silvers) in terms of the stability of silver nanoclusters and their dynamics is more or less consistent with our observations from C_m:Ag_n. The red emission (Ag_3) decreased over time after they reached to maximum. This suggests that the following reaction may occur: $Ag_3 \rightarrow Ag_2 + Ag^+ + e^-$.

Through the isosbestic points observed from C_m:Ag_n, the red/IR (Ag_3/Ag_2) species converted into blue/green species (oxidized Ag_5/oxidized Ag_4), thereby indicating the following reaction may be possible: $Ag_2 + 2Ag^+ \rightarrow Ag_4^{2+}$. In the case of Ag_4 for C_m:Ag_n, the oxidation state is yet not known. However, as detailed in section 3.3, our observed Ag_4 species is likely in a positive oxidation state. Since C_m:Ag_4 is also stable, it may be possible that C_m:Ag_4 is Ag_4^{2+}. Since Henglen's work suggests the high stability of Ag_4^{2+}, the question is whether the silver nanocluster dynamics observed from C_m:Ag_n results from silver nanoclusters stabilitie or from interactions with DNA.

4.3 Evolution of Circular Dichroism C_m:Ag_n.

In order to investigate the DNA-mediated contribution to silver nanocluster formation kinetics, Circular Dichroism (CD) spectra for C_8:Ag_n, C_{12}:Ag_n and C_{24}:Ag_n were recorded with time after the reduction of C_m:Ag_n. The CD spectra of C_m are also included to show the difference in C_m configurations between C_m with and without silver nanoclusters. This comparison can tell us whether or not silver nanoclusters are bound to C_m. Since the conformations of C_m remains the same over time, time-dependent CD spectra for C_m without Ag are not shown here. Only wavelengths from 200 nm and 350 nm were monitored due to the weak lamp intensities longer than 400 nm. Figure 31a shows the-independent C_8 CD spectra and the time-dependent CD spectra of C_8:Ag_n after the reduction. For C_8, the positive peak around 285 nm and a negative peak around 265 nm were observed. A positive peak around 285 nm and a negative peak near 260 nm are indications of i-motif structures.(134, 135) The C-rich single strands can form base pair interactions between cytosine and protonated cytosine.(134, 136) These two cytosine base pair interactions are called an i-motif. (134, 136) Since the two peaks around 260 nm and 285 nm were observed for C_8, this suggests that C_8 forms i-motif structures. The potential I-motif signatures disappear upon addition of Ag^+ and reduction produces a positive peak around 290 nm and two negative peaks around 265 and 220 nm for C_8:Ag_n. The peak at 290 nm decreased from 30 mdeg to 7 mdeg after the silver nanoclusters formed with C_8 and a new peak appears at 220 from C_8:Ag_n. Thus, this clearly shows that the silver nanoclusters interacts with C_8.

The time-dependent CD spectra for C_8:Ag_n after reduction (Figure 31a) show the negative peaks at 220 nm and 265 nm growing in. With time, the negative peaks at 220 nm and 265 nm increase. The molar ellipticity at 220 nm changes from –27 mdeg (0 minutes) to –43 mdeg (2.5 hours) and that at 265 nm changes from –8.5 mdeg (0 minutes) to –24 mdeg (2.5 hours). These intensity changes (16 mdeg for both 220 nm and 265 nm peaks) suggest that certain conformations (220 nm and 265 nm) become more dominant as the silver nanoclusters interact with C_8.

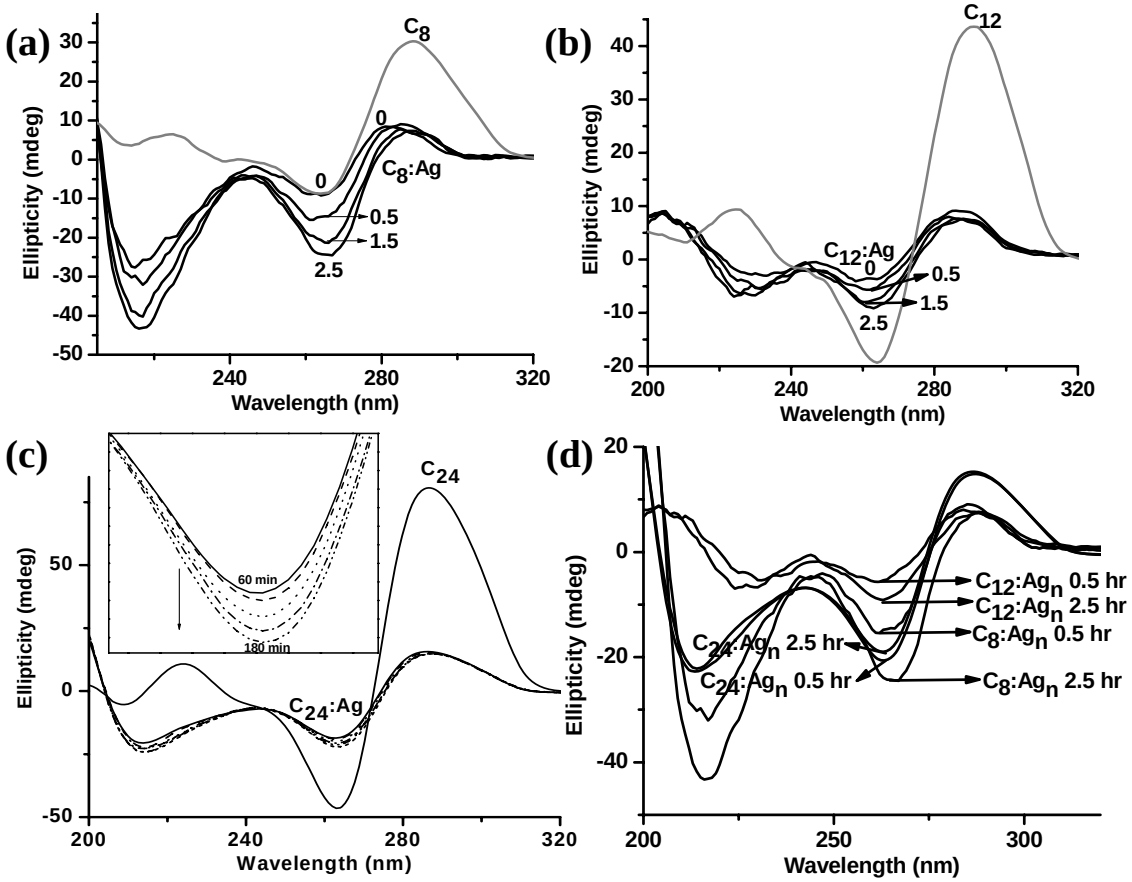

Figure 31. Time-dependent circular dichroism spectra for (a) C_8 (gray line) and C_8:Ag_n (black line). Original conditions: [C_8] = 10 μM, [Ag^+] = 35 μM, and [BH_4^-] = 35 μM. (b) C_{12} (gray line) and C_{12}:Ag_n (black line). Original conditions: [C_{12}] = 10 μM, [Ag^+] = 36 μM, and [BH_4^-] = 36 μM. (c) C_{24} (gray line) and C_{24}:Ag_n (black line). Inset shows time-dependent CD spectra for C_{24}:Ag_n between 250 nm and 270 nm. Original conditions: [C_{24}] = 10 μM, [Ag^+] = 72 μM, and [BH_4^-] = 72 μM. (d) C_8:Ag_n, C_{12}:Ag_n, and C_{24}:Ag_n. The number shown in the figures indicates hours after BH_4^- is added to C_m:Ag^+ solution. Experimental conditions: (18 M Ω deionized water, air saturated, etc).

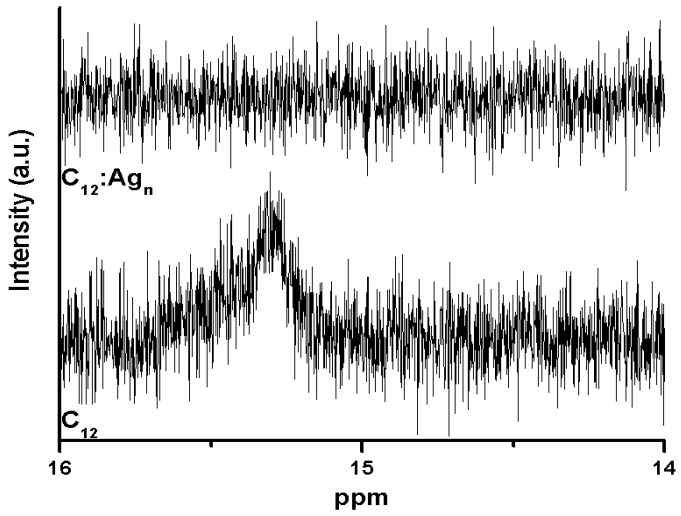

Figure 32. ^{1}H NMR zoom-in spectra for C_{12}:Ag_n(top) and C_{12} (bottom). A peak between 14 and 16 ppm for C_{12} is indicative for i-motif structure. An i-motif peak is not present in C_{12}:Ag_n. For these spectra, [C_{12}] = 0.93 mM, [Ag^+] = 11.16 mM, and [BH_4^-] = 11.16 mM in 90% deionized water and 10% D_2O solution.

For C_{12} shown in Figure 31b, positive peaks were observed around 225 nm and 290 nm and a negative peak was observed at 265 nm. The negative peak around 265 nm and the positive peak around 285 nm are again signatures of i-motif structures. This i-motif structure is also confirmed by NMR (Figure 32). The chemical shift between 15 and 16 p.p.m. in one-dimensional 1H NMR spectra is signature for i-motif structure.(137-139) Figure 32 (bottom line) shows the close-up NMR spectrum for C_{12}. The peak between 15 and 16 p.p.m. is observed. This suggests that C_{12} interact by themselves to form the i-motif structure. Figure 32 (top line) is NMR spectrum for C_{12}:Ag_n. For the top line in Figure 32, the i-motif peak between 15 and 16 p.p.m. disappeared. Upon nanocluster formation, a positive peak at 285 nm and two negative peaks at 225 nm and 265 nm were observed for C_{12}:Ag_n, showing a clear conformation change, and destruction of the i-motif Ag in supported by NMR (Figure 32). The difference in intensities of the peak at 290 nm and at 265 nm between C_{12}:Ag_n and C_{12} are 30 mdeg and 10 mdeg, respectively.

Time-dependent CD for C_{12}:Ag_n (Figure 31b) show the negative peak at 225 nm changing from –4 mdeg (immediately after reduction) to –9 mdeg (2.5 hours after the reduction), while that peak at 265 nm changes from –2.7 mdeg to –6.7 mdeg (2.5 hours after the reduction). Since single stranded DNA is more flexible than double strands, the structures of the single strands can be readily changed. Therefore, the small differences (within 5 mdeg) are insufficient to say that the conformations are changed drastically after the initial reduction occurs.

Similar to C_{12}, peaks at 225 and 285 nm (positive peaks) and at 265 nm (negative peak) were observed from C_{24} (Figure 31c). Therefore, C_{24} also likely forms i-motif

structures. However, the i-motif structures similarly disappear after formation of silver nanoclusters. The positive peak at 285 nm decreased from 80 mdeg to 15 mdeg, whereas the negative peak at 265 nm changed from –45 mdeg to –22 mdeg. The peak observed at 225 nm for C_{24} was shifted to 215 nm and a polarity change from positive to negative was also observed. These observed changes indicate that C_{24} conformations also significantly change as a result of silver nanocluster formation.

The time dependence of C_{24}:Ag_n is similar to that of C_{12}:Ag_n (Figure 31c). After initial reduction of C_{24}:Ag_n, the peak intensities at 215 nm and 265 nm changed slightly. However, as mentioned above, the intensity changes are slight, thereby indicating only minor conformation changes.

Since silver nanocluster dynamics of were observed via C_m:Ag_n emission, CD spectra for C_m:Ag_n were taken in order to test if the silver nanoclusters dynamics resulted from conformationals change in C_m. As observed above, after initial reduction of C_m:Ag_n, the C_{12} and C_{24} ss-DNA conformations did not significantly change with time, while C_8 showed more significant conformational evolution. Clearly the DNA plays an important role in nanocluster creation and stabilization, but nanocluster stability is likely an even more important factor in determining the final nanocluster distribution under a given set of conditions. The strong DNA-Ag interaction stabilizes and seems to protect the nanoclusters through interaction with the cytosine bases, but the silver nanocluster dynamics are fundamentally related to stabilities of the silver nanoclusters as suggested from Henglen's work.(85)

4.4 Temperature-dependent Optical Properties of C_m:Ag_n.

In order to investigate silver nanocluster stability, a temperature-dependent study on C_m:Ag_n was performed. As mentioned above, the emission intensities of distinctive emission peaks, blue (480nm), green (525nm), red (650nm), and IR (700nm) for C_m:Ag_n change with time. Thus, the temperature-dependent optical properties for C_m:Ag_n were investigated after different emitters reached equilibrium (5<pH<6, 18 M Ω deionized water, air saturated, at room temperature, within a day, etc). The temperature-dependent absorption and emission for C_8:Ag_n are shown in Figure 33a. Figure 33b is the absorption difference between 50 °C and 20 °C to clearly show the changes in the absorption with changing temperature. As temperature increase from 20 °C to 50 °C, absorption at wavelengths below 550 nm and above 630 nm decrease, while the absorption between 550 nm and 630 nm increases with increasing temperature. Isosbestic points at 550 nm and 632 nm were observed from temperature-dependent absorption of C_8:Ag_n in Figure 33a when changing temperature from 20 ºC to 50 ºC. The 550-nm isosbestic point suggests that the higher energy absorbers (Ag_4 and/or Ag_5) are converted to the lower energy absorber (Ag_3). While the isosbestic point at 632 nm suggests that the lower energy absorber Ag_2 is converted into Ag_3. Figure 33c-f shows the corresponding temperature-dependent emission spectra of C_8:Ag_n, excited at 340 nm, 440 nm, 580 nm, and 650 nm, respectively. At 340 nm excitation, the blue (oxidized Ag_5)/green (oxidized Ag_4) and red (Ag_3) /IR (Ag_2) emitters can be observed. The emission intensity for blue/green decreases with increasing temperature from 20 ºC to 50 ºC. While, the emission intensity for red/IR increases with increasing temperature from 20 ºC to 50 ºC. An isosbestic point is observed at 608 nm, suggesting that the blue/green species are

converted into red/IR species. This is consistent with the observation from temperature-dependent absorption (Figure 33b). Figure 33d shows the temperature-dependent emission excited at 440 nm, which exhibits the same trend as C_{12}:Ag_n excited at 340 nm. The green emission intensity decreased with increasing temperature. The red/IR emission increased with increasing temperature from 20 ºC to 50 ºC. The near isosbestic point at 626 nm suggests that the green species is converted to red/IR species, again consistent with absorption measurements. Figure 33e and f are temperature-dependent emission of C_8:Ag_n excited at 580 nm and at 650 nm, respectively. The emission intensity excited at 580 nm increases with temperature, while emission intensity excited at 650 nm decreases with increasing temperature. The observations from the temperature-dependent emission of C_8:Ag_n are consistent with the corresponding temperature-dependent absorption shown in Figure 33a and b. It appears to be that blue (oxidized Ag_5)/green (oxidized Ag_4) and IR (Ag_2) emitters were converted into red (Ag_3) emitters under the experimental conditions: (18 M Ω deionized water, air saturated, measurement within a day after reduction, etc).

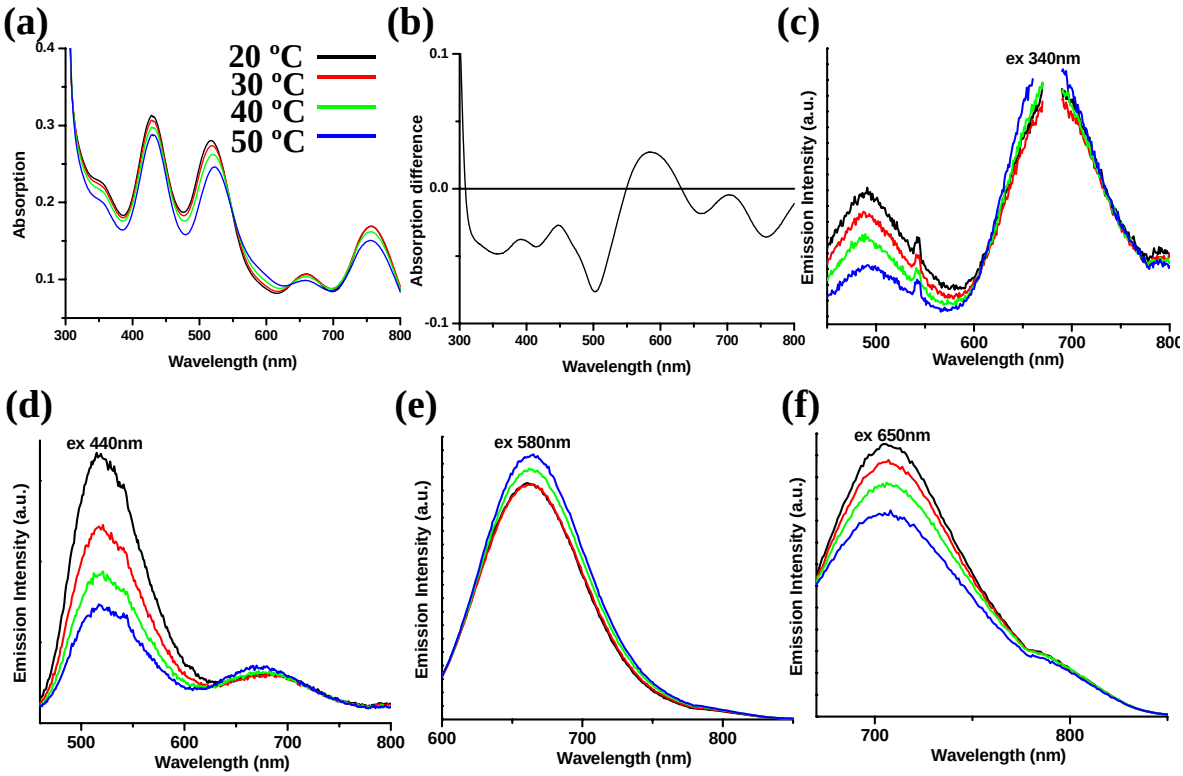

Figure 33. (a) Temperature-dependent absorption of C_8:Ag_n. (b) Absorption difference of C_8:Ag_n between 50 °C and 20 °C in (a). (c)-(f) Temperature-dependent emission spectra excited at (c) 340 nm (d) 440 nm (e) 580 nm (f) 650 nm for C_8:Ag_n. Original conditions: [C_8] = 100 μM, [Ag^+] = 350 μM, and [BH_4^-] = 350 μM. Experimental conditions: (18 M Ω deionized water, air saturated, measurement within a day after reduction, stored at room temperature under room light, etc). The spectra were taken 10 minutes after the temperature was set.

Temperature-dependent absorption for C_{12}:Ag_n and C_{24}:Ag_n are shown in Figure 34a and Figure 35a, respectively. In the case of temperature-dependent absorption for C_8:Ag_n, two isosbestic points were observed at 550 nm and 632 nm. Only one isosbestic point at 529 nm for C_{12}:Ag_n and at 544 nm for C_{24}:Ag_n are observed. The absorptions at shorter wavelengths of the isosbestic points for both C_{12}:Ag_n and C_{24}:Ag_n decrease with increasing temperature, while the absorption at longer wavelengths of the isosbestic points for both C_{12}:Ag_n and C_{24}:Ag_n increased with increasing temperature. Thus, this suggests that the blue (oxidized Ag_5) and green (oxidized Ag_4) emitters are converted into the red (Ag_3) and IR (Ag_2) species. The corresponding temperature-dependent emission C_{12}:Ag_n and C_{24}:Ag_n are shown in Figure 34c-f and Figure 35c-f, respectively. For C_{12}:Ag_n excited at 340 nm and 440 nm shown in Figure 34c and d, blue and green emission intensities decreased with increasing temperature. Similar emission trends as for C_{12}:Ag_n were observed for C_{24}:Ag_n excited at 340 nm and 440 nm (shown in Figure 35c and d). Emission intensities for blue and green emitters of C_{24}:Ag_n also decreased by increasing temperature. On the othe other hand, the red and IR intensities excited at 580 nm and 650 nm for C_{12}:Ag_n (shown in Figure 34e and f) and for C_{24}:Ag_n (shown in Figure 35e and f) increased with increasing temperature. One can see from Figure 35f that the IR emission excited at 650 nm for C_{24}:Ag_n were shifted to 690 nm instead of 720 nm observed from C_{12}:Ag_n. This may be due to the different silver cluster stability with different lengths of polycytosine. The temperature-dependent emission from C_{12}:Ag_n and C_{24}:Ag_n are consistent with the temperature-dependent absorption observed in Figure 34c-f and Figure 35c-f above.

To summarise, the temperature-dependent optical properties observed from C_{12}:Ag_n and C_{24}:Ag_n are similar. In the case of the temperature-dependent absorption for C_{12}:Ag_n and C_{24}:Ag_n, one isosbestic point was observed at 529 nm from C_{12}:Ag_n and at 544 nm from C_{24}:Ag_n, with shorter wavelengths having decreased absorption and longer wavelengths increased absorption with increasing temperature from 20 °C to 50 °C. The temperature-dependent emission for C_{12}:Ag_n and C_{24}:Ag_n are consistent with the temperature-dependent absorption observed above. The blue and green emission excited at 340 nm and 440 nm for C_{12}:Ag_n and C_{24}:Ag_n decreased with increasing temperature from 20 °C to 50 °C. It appears to be that by increasing temperature (energy), the larger clusters such as the blue (oxidized Ag_5) and green (oxidized Ag_4) emitters may dissociate to the smaller clusters such as the red (Ag_3) and IR (Ag_2) emitters, while in C_8, Ag_3 may be more stable than even Ag_2.

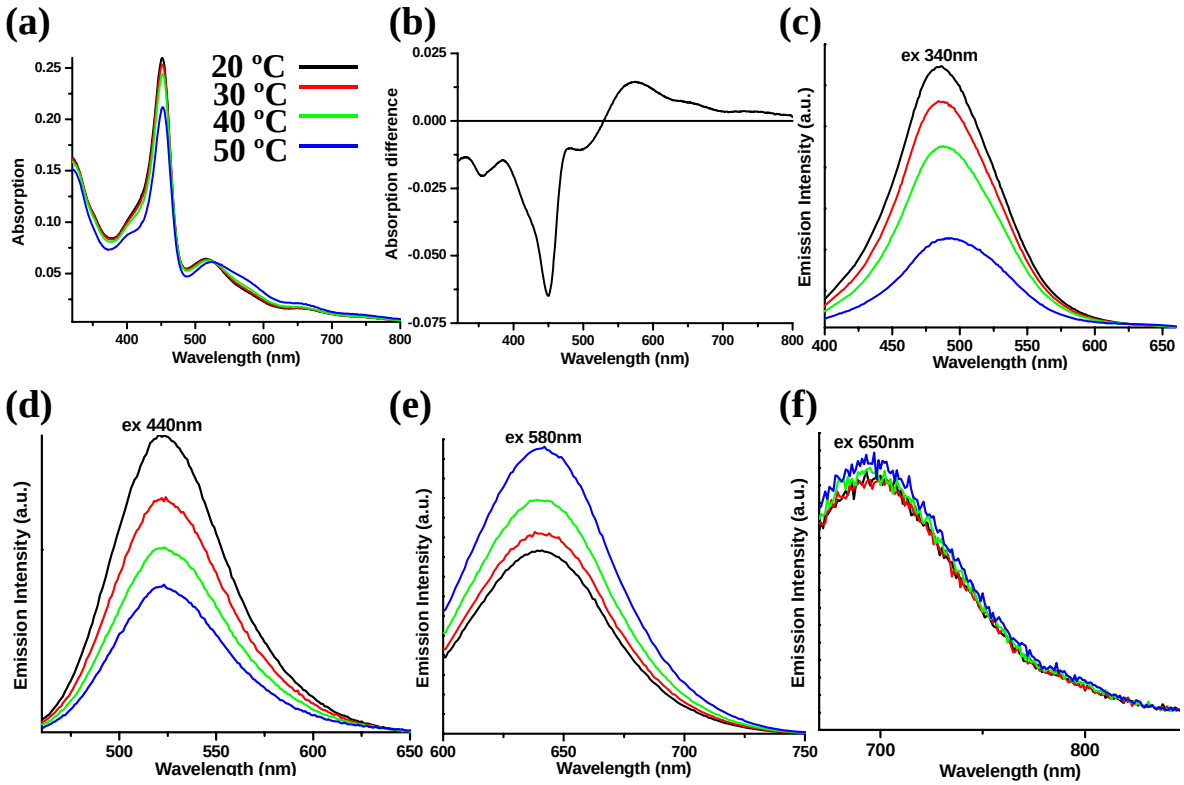

Figure 34. (a) Temperature-dependent absorption of C_{12}:Ag_n. (b) Absorption difference of C_{12}:Ag_n between 50°C and 20°C in (a). (c)-(f) Temperature-dependent emission spectra excited at (c) 340 nm (d) 440 nm (e) 580 nm (f) 650 nm for C_{12}:Ag_n. Original conditions: [C_{12}] = 60 μM, [Ag^+] = 360 μM, and [BH_4^-] = 360 μM. Temperature is increases by 10°C for (a)-(f) except (b). Experimental conditions: (18 M Ω deionized water, air saturated, measurement within a day after reduction, stored at room temperature under room light, etc). The spectra were taken 10 minutes after the temperature was set.

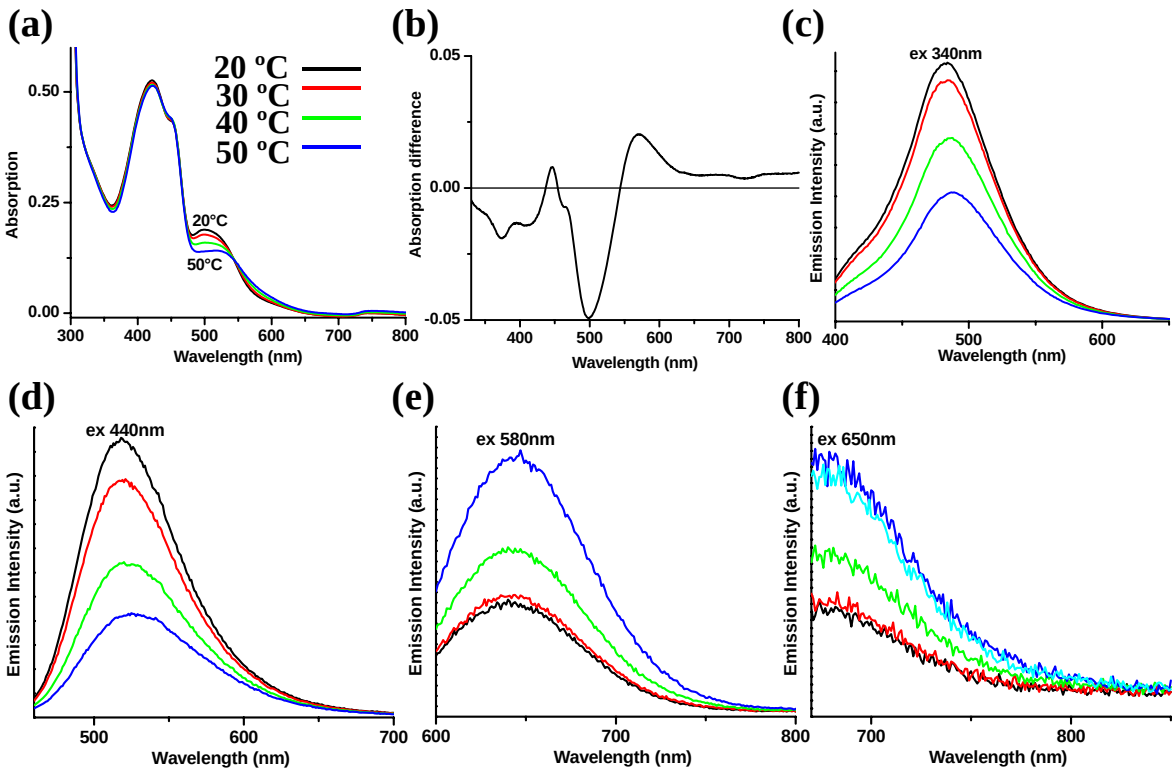

Figure 35. (a) Temperature-dependent absorption of C_{24}:Ag_n. (b) Absorption difference of C_{24}:Ag_n between 50 °C and 20 °C in (a). (c)-(f) Temperature-dependent emission spectra excited at (c) 340 nm (d) 440 nm (e) 580 nm (f) 650 nm for C_{24}:Ag_n. [C_{24}] = 60 μM, [Ag^+] = 720 μM, and [BH_4^-] = 720 μM. Experimental conditions: (18 M Ω deionized water, air saturated, measurement within a day after reduction, stored at room temperature under room light, etc). The spectra were taken 10 minutes after the temperature was set.

In the case of C_8:Ag_n, two isosbestic points were observed at 550 nm and 632 nm, with absorption between the two increasing with temperature. Similar to observations in longer strands, the blue (oxidized Ag_5)/green (oxidized Ag_4) and appear to turn into red (Ag_3) emitters, but the Ag_2 species also appears destabilized with respect to Ag_3 at higher temperatures. The silver nanocluster stability with increased temperature (energy) is the opposite trend from that suggested from Henglein's work,(85) and likely results from the strong interaction with cytosine. Therefore, Ag-cytosine interactions and possibly DNA conformational changes appear to significantly modify Henglein's observed stabilities. DNA conformational contributions are investigated in C_m and C_m:Ag_n by variable temperatures circular dichroism studies.

4.5 Temperature-Dependent Circular Dichroism C_m:Ag_n.

In order to investigate effects of DNA conformation on silver nanocluster stabilities, Circular Dichroism (CD) spectra for C_8:Ag_n, C_{12}:Ag_n, C_{24}:Ag_n C_8:Ag^+, C_{12}:Ag^+, and C_{24}:Ag^+ were recorded with increasing temperature. The CD spectra of C_m are also included to show the difference in C_m configurations between C_m with and without silver nanoclusters. This comparison also indicates whether or not silver nanoclusters are bound to C_m. As mentioned above, C-rich single strands can form base pair interactions between cytosine and protonated cytosine (i-motif).(134, 136) The indications for base pair between cytosine and protonated cytosine in CD are a positive peak around 285 nm and a negative peak near 260 nm and is confirmed by a hydrogen bonded proton resonance in the NMR spectra (Figure 32) Figure 36a, b and c show the temperature-dependent circular dichroism of C_8, C_8:Ag^+ and C_8:Ag_n, C_{12}, C_{12}:Ag^+ and

C_{12}:Ag_n, and C_{24}, C_{24}:Ag^+, and C_{24}:Ag_n. C_8 in Figure 36a (black lines) shows similar trends as C_{12} in Figure 36b (black lines) and C_{24} in Figure 36c (black lines). In Figure 36a-c between 20°C and 40°C, positive peaks around 285 nm and also negative peaks around 260 nm were observed from each of C_8, C_{12}, and C_{24}. This may be suggestive that C_8, C_{12} and C_{24} interact with themselves to form base pair between cytosine and protonated cytosine.(134, 136) In Figure 36a and b, C_8 and C_{12} begin to change their conformation around 50 °C, while for C_{24}, the positive peak at 290 nm shifts slightly to 287 nm only at 60 °C, again indicative of forming base pair between cytosine and protonated cytosine. Gray lines in Figure 36a-c show the temperature-dependent circular dichroism of C_8:Ag_n, C_{12}:Ag_n and C_{24}:Ag_n, respectively. Clearly, peaks in the CD spectra for C_8:Ag_n, C_{12}:Ag_n, and C_{24}:Ag_n significantly differ from those of C_8, C_{12}, and C_{24}, respectively. Negative peaks around 265 nm and 225 nm are observed for C_8:Ag_n (Figure 36a) and negative peaks around 265 nm and 220 nm are observed for C_{12}:Ag_n and C_{24}:Ag_n (Figure 36b and c), strongly suggesting that the cytosine-silver nanocluster interaction significantly changes the conformation of C_m (C_8, C_{12} and C_{24}). With increasing temperature from 20 °C to 60 °C, the conformation for C_m:Ag_n (C_8:Ag_n, C_{12}:Ag_n and C_{24}:Ag_n) remains essentially unchanged, even at 60 °C. Temperature-dependent circular dichroism of C_8:Ag^+, C_{12}:Ag^+ and C_{24}:Ag^+ (black lines) in Figure 36a-c show similar trends as C_m:Ag_n with greater mole ellipcity for C_m:Ag^+, thereby indicating that C_m:Ag^+ have more ordered structures than C_m:Ag_n. This suggests that the silver nanocluster dynamics observed from temperature-dependent emission of C_m:Ag_n (C_8:Ag_n, C_{12}:Ag_n and C_{24}:Ag_n) by increasing temperature can not be as a result of conformation changes in DNA. With comparison of temperature-dependent CD for C_m

(C_8, C_{12} and C_{24}) to C_m:Ag_n (C_8:Ag_n, C_{12}:Ag_n and C_{24}:Ag_n) and C_m:Ag^+ (C_8:Ag^+, C_{12}:Ag^+ and C_{24}:Ag^+), the interaction between C_m and silver nanoclusters and also silver ions is stronger than interaction between C_m (C_8, C_{12} and C_{24}) themselves.

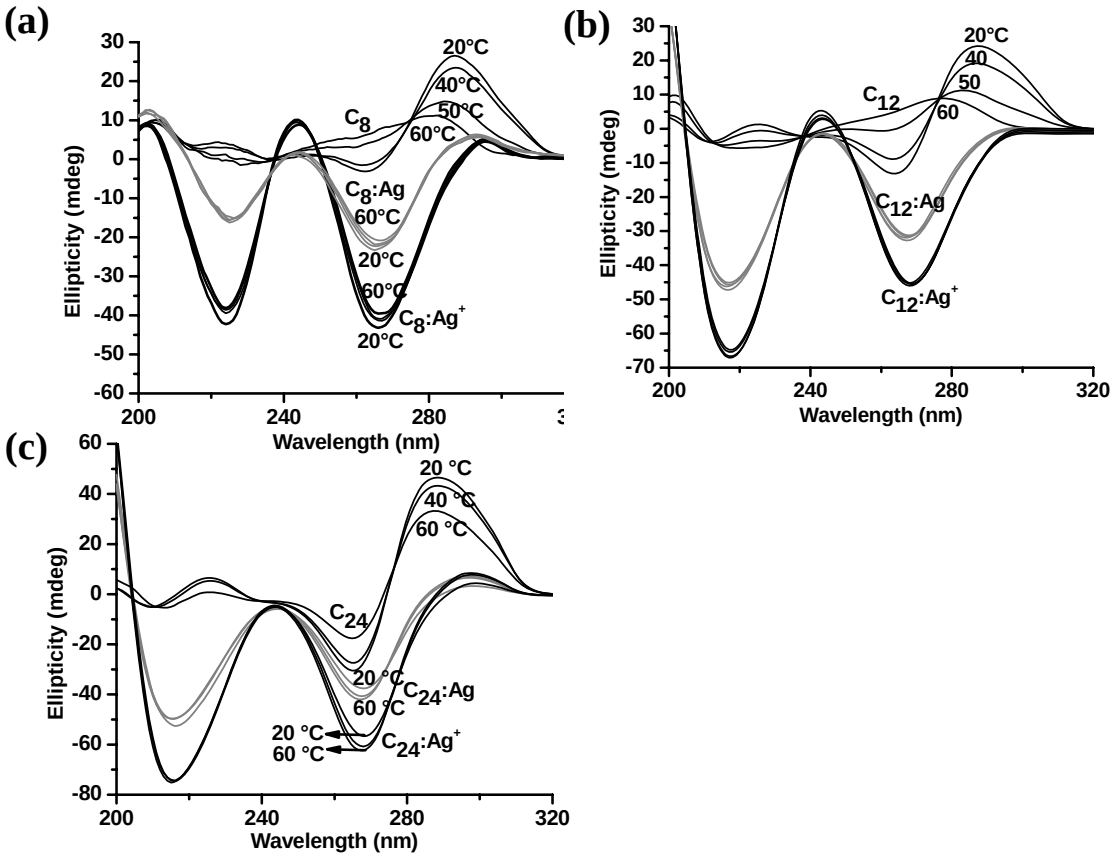

Figure 36. (a) Temperature-dependent circular dichroism spectra for (a) C_8 (black lines), C_8:Ag_n (gray lines) and C_8:Ag^+ (black lines) [C_8] = 10 μM, [Ag^+] = 35 μM, and [BH_4^-] = 35 μM. (b) C_{12} (gray lines), C_{12}:Ag_n (black lines) and C_{12}:Ag^+ (black lines). [C_{12}] = 10 μM, [Ag^+] = 36 μM, and [BH_4^-] = 36 μM. (c) C_{24} (gray lines), C_{24}:Ag_n (black lines) and C_{24}:Ag^+ (black lines). [C_{24}] = 10 μM, [Ag^+] = 72 μM, and [BH_4^-] = 72 μM. Temperature is increased by increment of 10°C. Experimental conditions: (18 M Ω deionized water, air saturated, measurement within a day after reduction, stored at room temperature under room light, etc). The spectra were taken 5 minutes after the temperature was set.

4.6 Stability and Dynamics of Silver Nanoclusters for C_8:Ag_n, C_{12}:Ag_n and C_{24}:Ag_n in 100mM NaCl.

Ag based fluorophores must overcome significant challenges when utilized as biological labels. Perhaps the most daunting is precipitations of silver salts AgCl (K_{sp} = 1.82E-10).(133) Biological media typically have > 100 mM Cl^-, which is likely to etch oxidized Ag clusters from solutions. While simultaneously assaying for cluster stability and biological relevance, monitoring fluorescence intensively upon addition of Cl^- should further indicate oxidation states of each species. Blue (480nm), green (525nm), red (650nm) and IR (720nm) emission from C_m:Ag_n have been investigated by adding sufficient NaCl to create C_m:Ag_n solutions that are 100 mM NaCl. The blue/green emission excited at 340nm (black line) observed from C_8:Ag_n (Figure 37a) changes significantly even after just five minutes after being brought to 100mM (NaCl) The blue/green emission excited at 340nm decreases and shifts to green emission (525 nm). As time passes, the green emission excited at 340 nm also decreases. Shown in Figure 37a, the green emission (530 nm) excited at 440 nm (red line) also decreases with 5 minutes (red dash line) of NaCl addition (final concentration 100 mM NaCl), and continues to decrease with time. Red emission excited at 580 nm (green line), however, increases three-fold and the emission wavelength is blue-shifted from 665 nm to 633 nm (green dashed line). After 45 minutes (green dotted line), the red emission (633 nm) decreased four-fold and continued to decrease with time. Initially near IR emission excited at 650nm also increased two-fold with 20-nm blue shift (blue dashed line), and 45 minutes, the IR (695 nm) decreased nearly two-fold and continued to decrease with time.

For C_{12}:Ag_n (Figure 37b) blue emission excited at 340nm dominates before NaCl addition to reach 100 mM NaCl (black line). Within 5 minutes after adding NaCl (black dashed line), the blue emission decreased significantly (compared to other emission). The green emission excited at 440nm also decreased with respect to time. On the other hand, the red and IR emission excited at 580nm and 650nm increased 10-fold. Following the initial increase, red emission subsequently decreases with respect to time. The near IR emission, however, remains constant for at least 90 minutes.

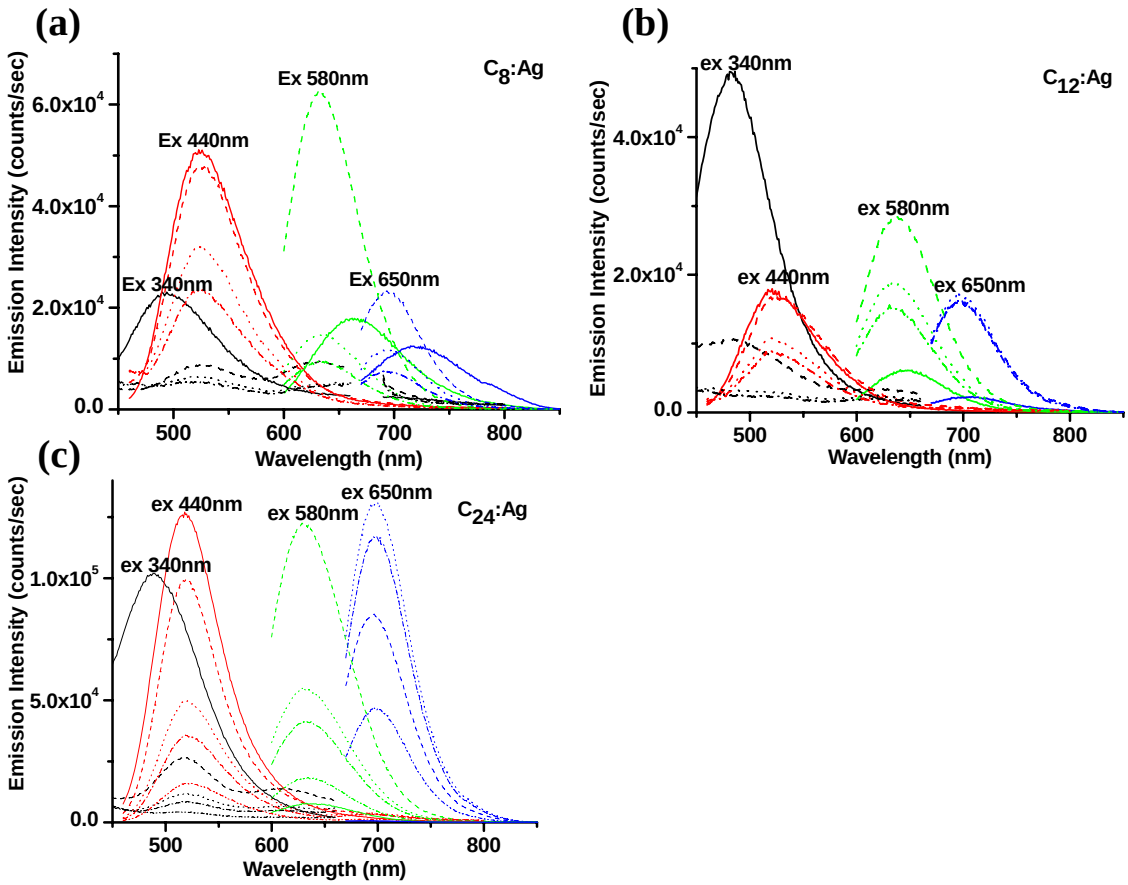

Figure 37. Time-dependent emission spectra of (a) C_8:Ag_n, (b)C_{12}:Ag_n and (c) C_{24}:Ag_n excited at 340 nm, 440 nm, 580 nm and 650 nm with addition of 100mM NaCl. Before bringing solutions to a concentration of 100mM NaCl (solid line), 5 minutes after adding NaCl (dashed line), 45 minutes after adding NaCl (dotted line) and 90 minutes after adding 100mM NaCl (dash dotted line). In a case of C_{24}:Ag_n, before adding100mM NaCl (solid line), 1 hour after adding NaCl (dashed line), 4 hours after adding NaCl (dotted line), 7 hours after adding NaCl (dash dot line) and 1 day after adding 100mM NaCl (dash dot dotted line). Original solution conditions: [C_8] = 100 μM, [Ag^+] = 350 μM, and [BH_4^-] = 350 μM. [C_{12}] = 60 μM, [Ag^+] = 360 μM, and [BH_4^-] = 360 μM. [C_{24}] = 60 μM, [Ag^+] = 720 μM, and [BH_4^-] = 720 μM. Experimental conditions: (18 M Ω deionized water, air saturated, measurement within a day after reduction, stored at room temperature under room light, etc).

C_{24}:Ag_n (Figure 37c) exhibits similar emission trends as for C_{12}:Ag_n, but the rate of emission changes is slowed. One hour after the addition of NaCl (black line), the blue emission excited at 340nm decreased 10-fold and are shifted to the green emission (525nm). Red emission excited at 340nm also started to appear. The green and red emissions subsequently decrease and completely disappear within one day. The green emission excited at 440nm is the most dominant of all the emission observed from C_{24}:Ag_n before adding 100mM NaCl (red line). Within an hour after the addition of NaCl to C_{24}:Ag_n (red dashed line), the green emission decreases and continues to decrease for one day. The red emission excited at 580nm before adding NaCl (green line) has an extremely low intensity compared to blue and green emission. The IR emission excited at 650nm is barely present. However, within one hour after the addition of NaCl (green dashed line), the red emission increases ~ 10-fold and the IR emission increased from no emission to ~10^5 counts/sec. After the initial gain, the red emission decreases over time and in one day, the red emission intensities returned to the original intensities (before adding NaCl). The IR emission excited at 650nm continued to increase for 7 hours (blue dash dot line). Within one day (blue dash dot dot line), the IR emission intensity was lower than the intensity at 1 hour (blue dashed line) after adding NaCl. However, the IR emission intensity at 1 day is still greater than the original emission intensity (before adding NaCl).

As C_8:Ag_n and C_{12}:Ag_n are compared with C_{24}:Ag_n, significant differences in rate of emission change are observed. The blue/green emission excited at 340nm for C_8:Ag_n and the blue emission excited at 340nm for C_{12}:Ag_n disappeared within 90 minutes after

adding NaCl, while the blue emission excited at 340nm for C_{24}:Ag_n took one day to disappear. The green emission excited at 440 nm for C_8:Ag_n and C_{12}:Ag_n decreased by about 50% within 90 minutes after adding 100mM NaCl. In the case of C_{24}:Ag_n, the green emission excited at 440nm took ~4 hours to decrease by the same amount. The red emission excited at 580nm for C_8:Ag_n and C_{12}:Ag_n increased within 5 minutes and then decreased by 50% (C_{12}:Ag_n) and by 75% (C_8:Ag_n) from the previous emission intensities (5 minutes after adding NaCl) within 90 minutes, while the red emission excited at 580nm for C_{24}:Ag_n took 1 hour and 3 hours to increase and decrease, respectively by the same amount. The IR emission excited at 650nm for C_8:Ag_n and C_{12}:Ag_n increased within 5 minutes after adding NaCl and remained constant for 90 minutes, but subsequently disappeared. The IR emission excited at 650nm for C_{24}:Ag_n increased for 7 hours after adding NaCl and decreased by 50% from the 1 hour post addition intensity within a day. This suggests that the stability of the emission with addition of NaCl to biologically related concentrations for C_{24}:Ag_n is significantly greater than of the short polycytosine, and the rate of change in emission for C_{24}:Ag_n is diminished compared to that for C_8:Ag_n and C_{12}:Ag_n. As mentioned in section 4.1, this probably results from the length difference of the polycytosines. The longer the length of polycytosine is, the better the silver nanoclusters are protected from Cl^-. A significant point observed from C_8:Ag_n, C_{12}:Ag_n and C_{24}:Ag_n is that as the blue and green emission excited at 340nm and 440nm for C_8:Ag_n, C_{12}:Ag_n and C_{24}:Ag_n decrease, the red and IR emission excited at 580nm and 650nm increase. As previously mentioned, the blue, green, red, and near IR emitters appear to correspond to Ag_5, Ag_4, Ag_3, and Ag_2, respectively. This NaCl-dependent emission observed from C_8:Ag_n, C_{12}:Ag_n and C_{24}:Ag_n support assignments of the silver

nanocluster size and oxidation state. The blue (oxidized Ag_5) and green (oxidized Ag_4) emitters turn into red (Ag_3) and IR (Ag_2) emitters. The dynamics of silver nanoclusters observed in 100mM NaCl are not consistent with the dynamics observed from time dependence in air-saturated, non-buffered, extremely low ionic strength solutions. In terms of time dependency, the red (Ag_3)/IR (Ag_2) emitters converted into blue (oxidized Ag_5)/green (oxidized Ag_4) emitters. The obvious difference in these two experiments is the addition of NaCl. As mentioned above, Cl^- prefers to bind to Ag^+. From NaCl observations, the following can be suggested. As NaCl was added, Cl^- may remove Ag^+ from the oxidized blue (oxidized Ag_5) and green (oxidized Ag_4) emitters and those blue and green emitters might turn into smaller clusters such as Ag_3 and Ag_2. As a result, the emission from blue (oxidized Ag_5) and green (oxidized Ag_4) emitters decreases, while the emission from red (Ag_3) and IR (Ag_2) increases with respect to time. Since the red and IR emitters are fully reduced species, Cl^- should not remove reduced silver. However, one can see that after the red and IR emission increased, they started to decrease. Another possibility is that with addition of Na^+, the conformations of C_m may change and silver clusters are no longer protected from C_m. Thus, aggregation may occur. To investigate whether or not the conformations of C_m change, CD are performed on C_8:Ag_n, C_{12}:Ag_n and C_{24}:Ag_n before and after bringing solutions to 100mM [NaCl].

4.7 Conformations of C_8, C_{12} and C_{24} in 100mM NaCl.

As mentioned previously, Circular Dichroism (CD) is sensitive to conformation changes in DNA. By using CD, we investigated NaCl affects DNA conformation and possibly leads to changes in emission intensities for the red (Ag_3) and IR (Ag_2) emitters.

The CD spectra of C_8, C_{12} and C_{24}, displayed in Figure 38 are recorded to compare the conformational changes in C_m with the changes in C_m:Ag_n. As mentioned above, the C-rich single strands can form base pairs between cytosine and protonated cytosine.(134, 136) The CD spectra of C_8 before (black lines) and after (grey lines) adding NaCl to C_8 are shown in Figure 38a. The CD spectra for C_8 in 100mM NaCl solutions were recorded 1 hour after adding NaCl to C_8. The positive peak around 275nm and the negative peak around 230nm appeared for both C_8 with and without addition of NaCl. Thus, no change was observed by adding the NaCl solutions. In a case of C_{12} and C_{24} shown in Figure 38b and c, the positive peak around 285nm and a negative peak around 260nm before adding NaCl were observed. This may indicate that i-motif structures are formed on C_{12} and C_{24} but not on C_8. With addition of NaCl to C_{12} and C_{24} solutions, the positive peak around 275nm and the negative peak around 230nm appeared and the positive peak around 285nm and a negative peak around 260nm disappeared. With addition of NaCl, the i-motif structures for C_{12} and C_{24} disappeared. In fact, in 100 mM NaCl, the CD of all C_m species look very similar.

CD spectra of C_8:Ag_n are shown in Figure 39a. The conformations of C_8:Ag with and without addition of 100mM NaCl are different from the conformations of C_8 with and without NaCl. This suggests that the silver nanoclusters interact with C_8. The negative peaks at 220nm and 265nm were observed for both C_8:Ag_n with and without NaCl. In terms of peak intensity, the intensity for C_8:Ag with NaCl is 10 mdeg less than the intensity for C_8:Ag_n without NaCl. The positive peak at 293nm was observed for C_8:Ag_n without NaCl, while the positive peak for C_8:Ag_n with NaCl was shifted to 285nm. This suggests that the conformation of C_8:Ag_n changes at least slightly with addition of

100mM NaCl. In the case of C_{12}:Ag_n and C_{24}:Ag_n (Figure 39b and c), spectra similar to these from C_8:Ag_n are observed. The negative peaks were observed at 225nm and 265nm for both C_{12}:Ag and C_{24}:Ag with and without NaCl. The intensity difference between C_{12}:Ag with and without NaCl and also between C_{24}:Ag with and without NaCl are within 5 mdeg, making determinations of conformational changes difficult.

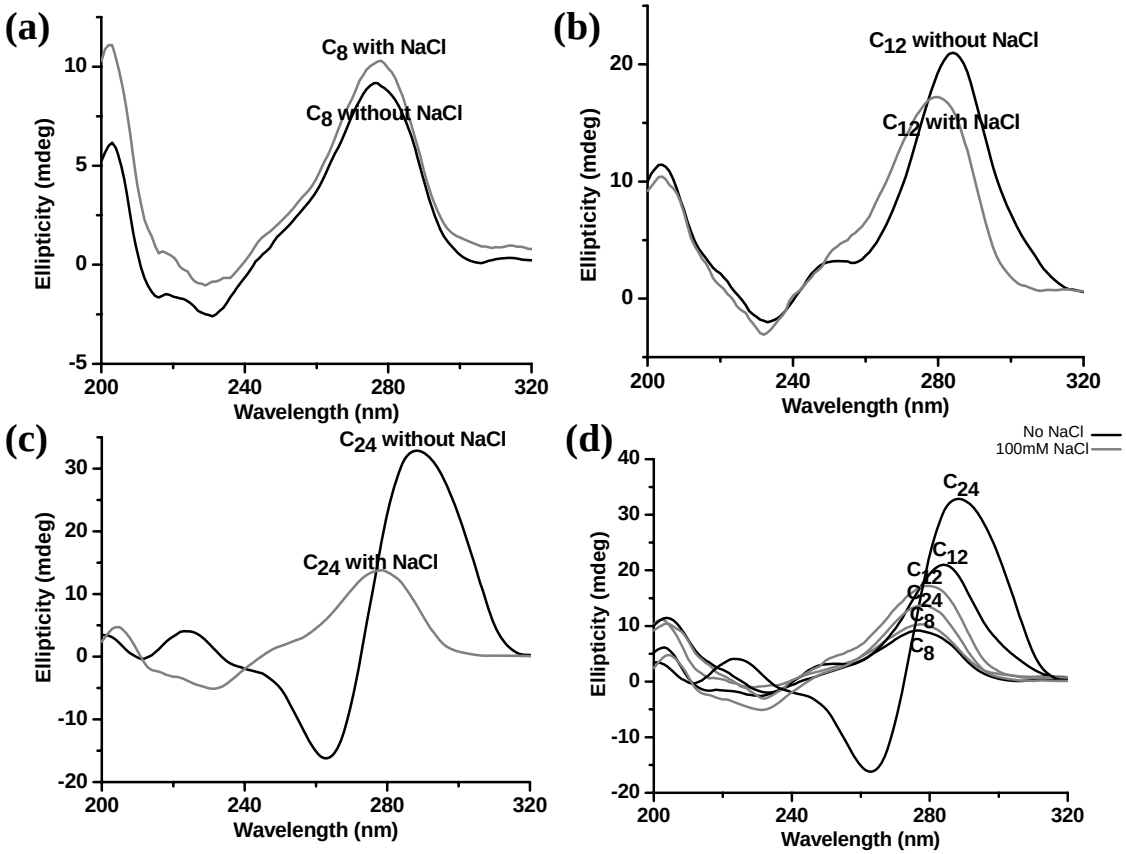

Figure 38. Time-dependent circular dichroism spectra for (a) C_8 in pure H_2O (black line) and C_8 in 100mM NaCl (gray line). [C_8] = 10 μM. (b) C_{12} in pure water (black line) and C_{12} in 100mM NaCl (gray line). [C_{12}] = 10 μM. (c) C_{24} in pure H_2O (black line) and C_{24} in 100mM NaCl (gray line). [C_{24}] = 10 μM. (d) C_m in pure H_2O (black line) and C_m in 100mM NaCl (gray line). C_m spectra (with 100mM NaCl) were recorded 1 hr after adding NaCl to reach 100mM. Experimental conditions: (18 M Ω deionized water, air saturated, measurement within a day after reduction, stored at room temperature under room light, etc).

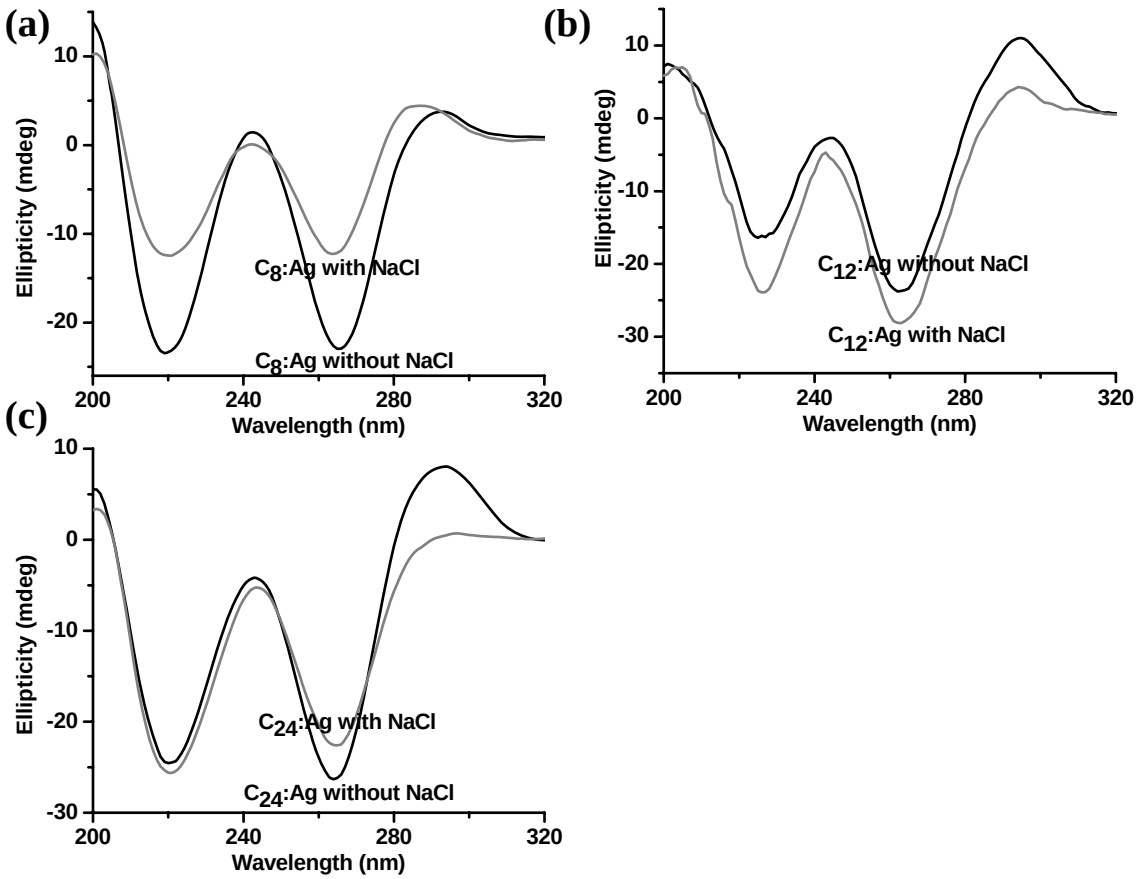

Figure 39. Time-dependent circular dichroism spectra for (a) C_8:Ag_n in H_2O (black line) and C_8:Ag_n in 100mM NaCl (gray line). Original conditions: [C_8] = 10 μM, [Ag^+] = 35 μM, and [BH_4^-] = 35 μM. (b) C_{12}:Ag_n in water (black line) and C_{12}:Ag_n in 100mM NaCl (gray line). Original conditions: [C_{12}] = 10 μM, [Ag^+] = 36 μM, and [BH_4^-] = 36 μM. (c) C_{24}:Ag_n in water (black line) and C_{24}:Ag_n with 100mM NaCl (gray line). Original conditions: [C_{24}] = 10 μM, [Ag^+] = 72 μM, and [BH_4^-] = 72 μM. C_m:Ag_n spectra (in 100mM NaCl) were recorded 1 hr after adding NaCl to reach 100 mM. Experimental conditions: (18 M Ω deionized water, air saturated, measurement within a day after reduction, stored at room temperature under room light, etc).

Both intensity differences between C_{12}:Ag with and without NaCl are about 7 mdeg, while the positive peak for C_{24}:Ag without NaCl is observed at 295nm and for C_{24}:Ag with NaCl disappeared. Therefore, this may indicate that the conformation of C_{12} and C_{24} are changed with addition of 100mM NaCl.

With addition of 100mM to C_m:Ag (m = 8, 12 and 24), the blue (480 nm) emission excited at 340 nm, and green (525 nm) emission excited at 440 nm decrease, while the red (650 nm) emission excited at 580nm and the IR (720 nm) emission excited at 650nm increased. To investigate whether or not the decrease in emission intensities for the red (Ag_3) and IR (Ag_2) emitters with addition of 100mM NaCl result from the conformational change in DNA structures, CD was used. For C_8:Ag, C_{12}:Ag and C_{24}:Ag, the conformation change in C_8, C_{12} and C_{24} were observed. Thus, the decrease in emission intensities for the red (Ag_3) and IR (Ag_2) emitters with addition of 100mM NaCl may be due to the conformational change in DNA structures.

4.8 pH-dependent Emission of C_m:Ag_n.

As seen above, the dynamics of silver nanoclusters were observed with introducing stimuli such as changing temperature and salt concentrations. In spite of absence of the stimulus, the dynamics of silver nanoclusters were still observed with respect to time. Since buffer solutions are resistive to changes in pH, buffer solutions can make the environment nearly constant. Therefore, buffer solutions were introduced in order to control the dynamics of silver nanoclusters. With different pH, the stability of silver nanoclusters is also investigated. Besides considering the stability of silver nanoclusters, DNA also needs to be stable in buffer medium. Since the pK_a value of

cytosine is ~4, C_m:Ag_n solutions were made in citrate buffer solutions with pH 4. Figure 40a-d shows emission spectra of C_8:Ag_n in citrate buffer solutions with pH 4 (20 mM sodium citrate ($Na_3C_6H_5O_7$), Fluka) and 5 (20 mM sodium citrate ($Na_3C_6H_5O_7$), Fluka) and in phosphate buffer solutions with pH 6 ([KH_2PO_4]=90mM and [NaOH]=10mM)(140) and 7 ([KH_2PO_4]=63.2mM and [NaOH]=36.7mM).(140) All the emission spectra were recorded 12 hours after the reduction of C_8:Ag_n solutions and are shown in the Figure 40 with solid lines. Dashed lines in Figure 40 indicate 4 hours after the first emission spectra (solid lines) were taken. The blue/green emission excited at 340 nm, green emission excited at 440 nm, red emission excited at 580 nm and IR emission excited at 640 nm appeared in the emission spectra of C_8:Ag_n between pH 4 and pH 7. At pH 4 and 5, the green emission excited at 440 nm is dominant, while red emission excited at 580 nm is dominant at pH 6 and 7. The dynamics of blue/green, green, red and IR emitters are similar to that of C_8:Ag_n in deionized water shown in Figure 29. At pH 8 (phosphate buffer, [KH_2PO_4]=5.2mM and [NaOH]=4.8mM, Figure 41a), significant changes in emission become clear. Instead of red emission (650 nm) excited at 580 nm being the highest peak, a new peak at 600 nm, emission excited at 520 nm dominates the spectrum and 580 nm emission excited at 480 nm is the second highest peak. At pH 10 ([$Na_2B_4O_710H_2O$]=8.3mM and [NaOH]=27mM)(140) and 12 ([Na_2HPO_4]=32.5mM and [NaOH]=35mM)(140) shown in Figure 41b and c, all emission is significantly lower (more than 10-fold less than the emission at other pH from 4 to 8). This suggests that at basic conditions such as pH 10 and 12, silver nanocluster formation might be disfavored.

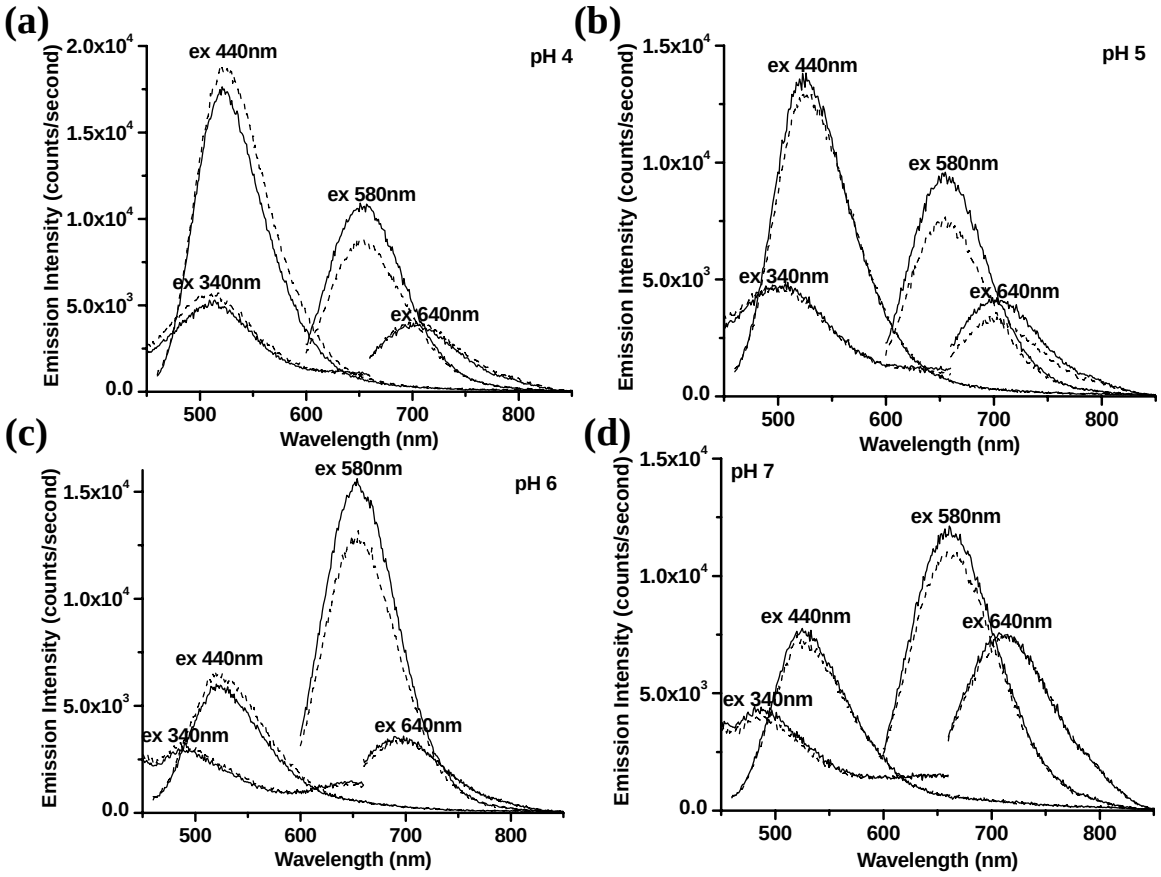

Figure 40. Emission spectra of C_8:Ag_n at (a) pH 4 (b) pH 5 (c) pH 6 and (d) pH 7. Solid lines indicate the emission spectra taken 12 hours after reduction of C_8:Ag_n. Dashed lines indicate the emission spectra 4 hours after the first emission spectra (solid line) C_8:Ag_n were recorded. [C_8] = 100 μM, [Ag^+] = 350 μM, and [BH_4^-] = 350 μM. The samples were stored at room temperature in a dark.

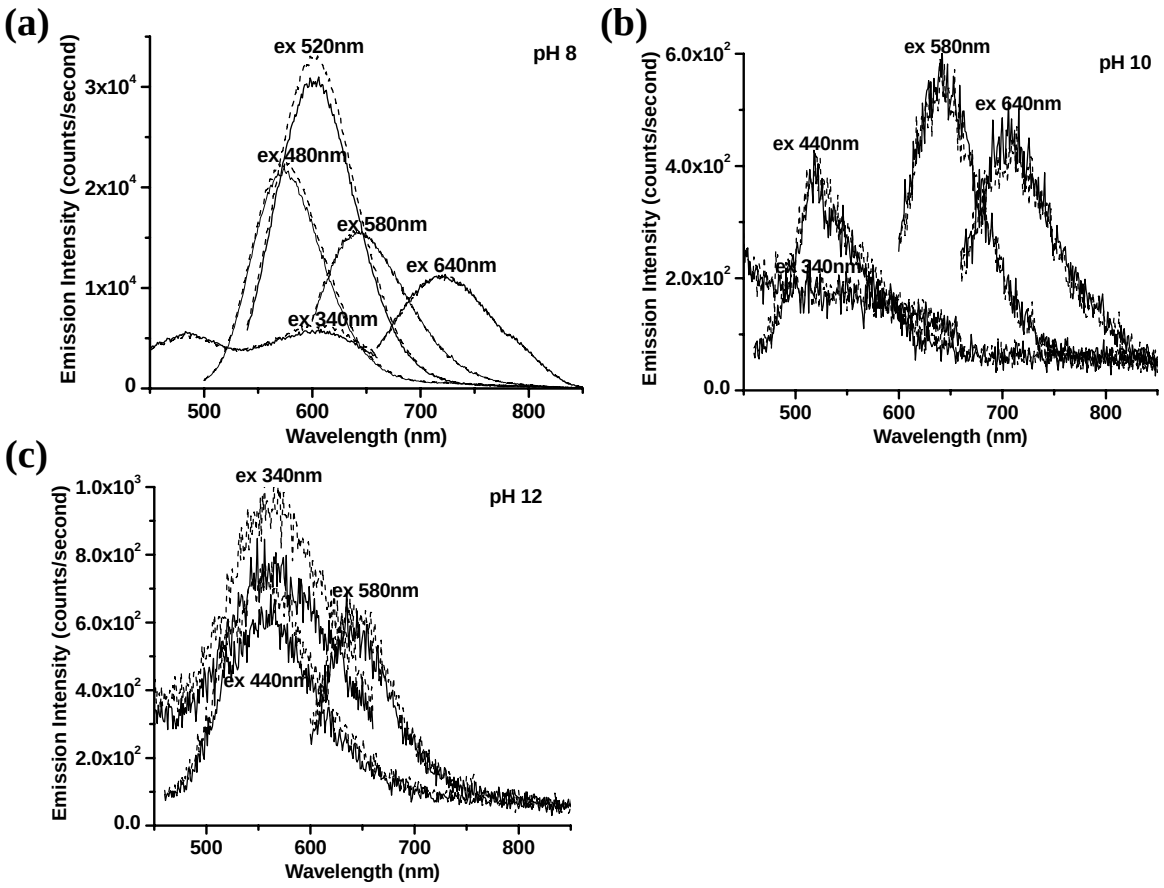

Figure 41. Emission spectra of C_8:Ag_n at (a) pH 8 (b) pH 10 and (c) pH 12. Solid lines indicate the emission spectra taken 12 hours after reduction of C_8:Ag_n. Dashed lines indicate the emission spectra 4 hours after the first emission spectra (solid line) C_8:Ag_n were recorded. $[C_8]$ = 100 μM, $[Ag^+]$ = 350 μM, and $[BH_4^-]$ = 350 μM. The samples were stored at room temperature in a dark.

In the case of emission spectra for C_{12}:Ag_n at pH 4 and 5 (citrate buffer) shown in Figure 42a and b, the blue emission excited at 340 nm, the green emission excited at 440 nm, red emission excited at 580 nm and IR emission excited at 640 nm were observed. The dynamics of different emitters are similar as the ones observed from C_{12}:Ag_n in the Figure 25. As red and IR emission decrease, the blue and green emission increases. The emission intensities of red and IR emitters at pH 5 are five times higher than those at pH 4. Since the pK_a for N3 of cytosine is ~4,(141) this suggests that the red and IR emitters may bind to N3, as previously suggested by NMR. At pH 6 and 7 (phosphate buffer), the red emission excited at 580 nm and IR emission excited at 640 nm were observed from C_{12}:Ag_n, while the blue emitters were hardly formed and green emission excited at 440 nm was quite low compared to the red and IR emission, (Figure 42c and d). The dynamics of red and IR emitters are similar to those in deionized water. Emission and dynamics of silver nanoclusters at pH 8-10 (Figure 43 a-c) were observed (Figure 43a). The dynamics of green, red and IR emitters are much slower than the dynamics below pH 8, however. Above pH 8, the solid lines indicate emission spectra taken 12 hours after the reduction of C_{12}:Ag_n, which is the same as for C_8:Ag_n. On the other hand, the dashed lines indicate emission spectra taken a day after the first emission spectra (solid lines) were recorded.

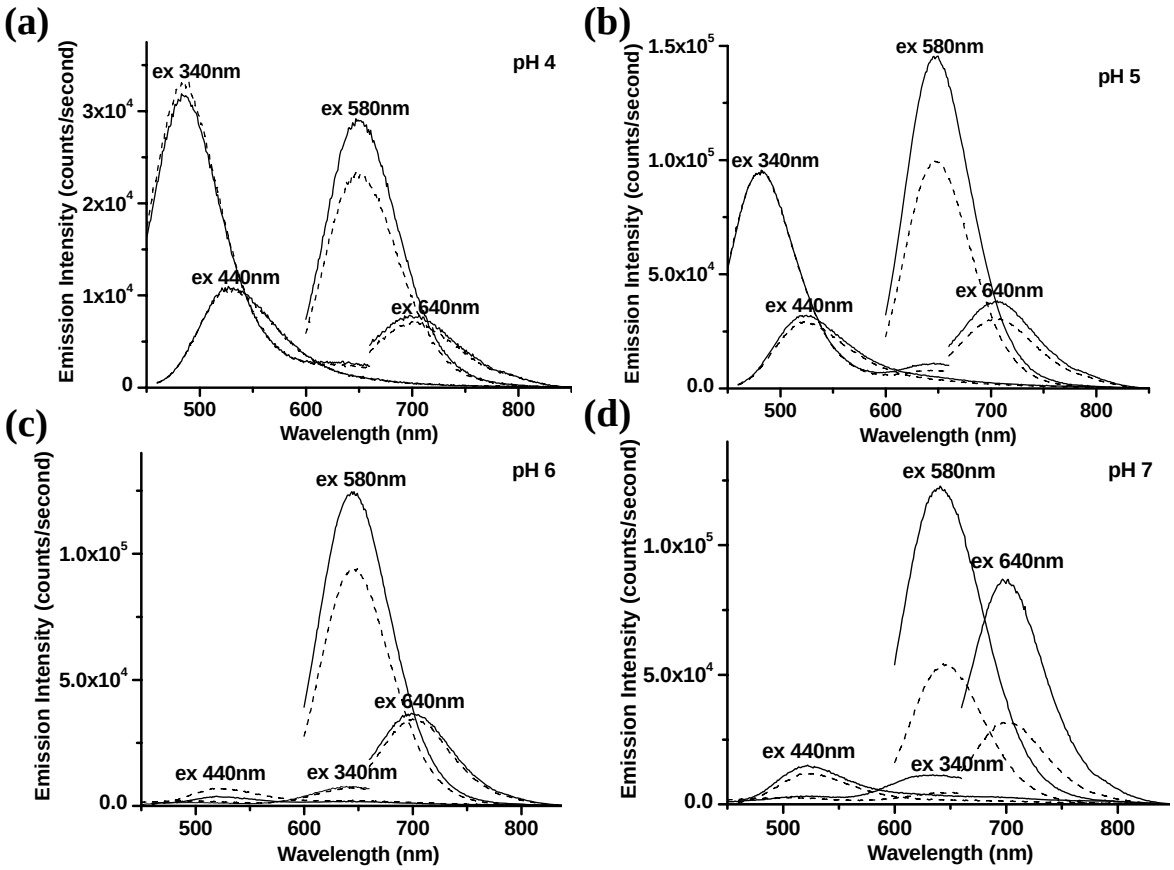

Figure 42. Emission spectra of C_{12}:Ag_n at (a) pH 4 (b) pH 5 (c) pH 6 and (d) pH 7. Solid lines indicate the emission spectra taken 12 hours after reduction of C_{12}:Ag_n. Dashed lines indicate the emission spectra 4 hours after the first emission spectra (solid line) C_{12}:Ag_n were recorded. Original conditions: $[C_{12}]$ = 60 μM, $[Ag^+]$ = 360 μM, and $[BH_4^-]$ = 360 μM. The samples were stored at room temperature in a dark.

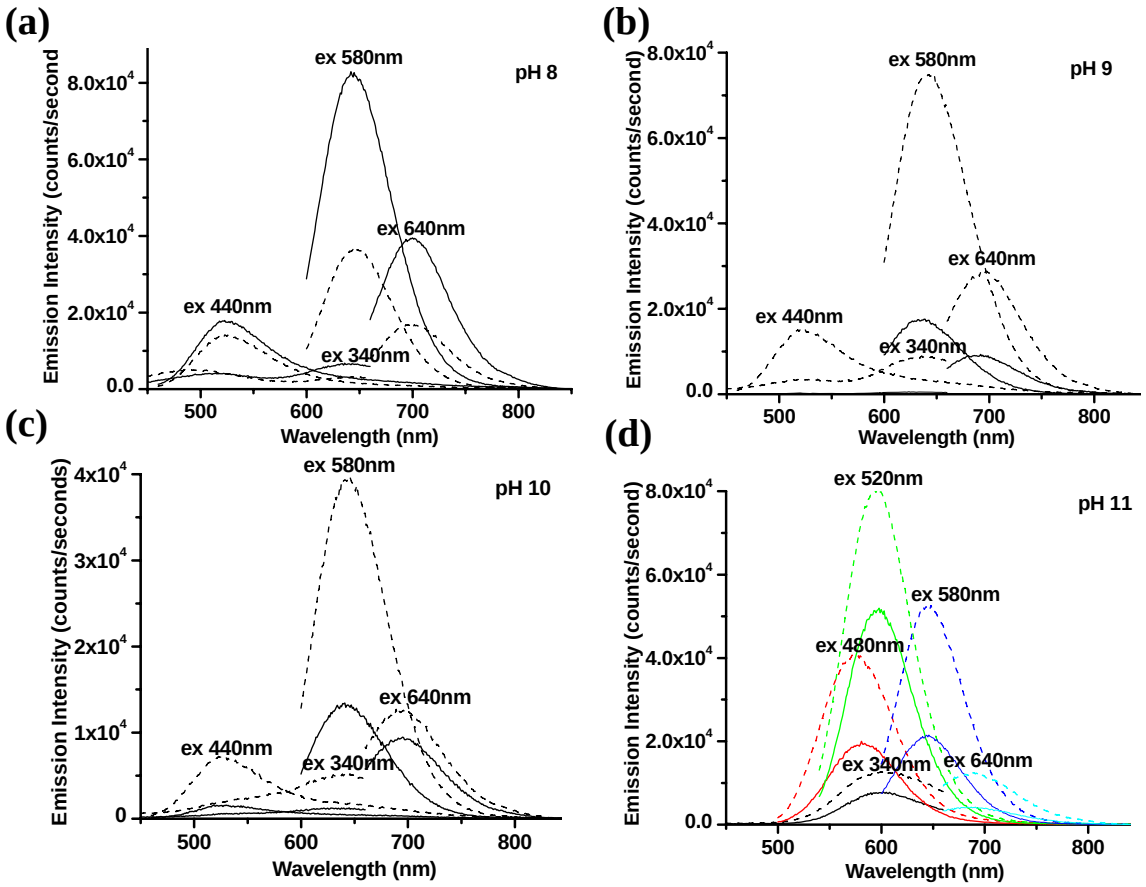

Figure 43. Emission spectra of C_{12}:Ag_n at (a) pH 8 (b) pH 9 (c) pH 10 and (d) pH 11. Solid lines indicate the emission spectra taken 12 hours after reduction of C_{12}:Ag_n. Dashed lines indicate the emission spectra 4 hours for pH 8 and a day for pH 9, 10, 11 after the first emission spectra (solid line) C_{12}:Ag_n were recorded. Since the different emission of C_{12}:Ag_n at pH 11 are crowded and hard to distinguish between different emission, the emission spectra are shown in color. Original conditions: [C_{12}] = 60 μM, [Ag^+] = 360 μM, and [BH_4^-] = 360 μM. The samples were stored at room temperature in a dark.

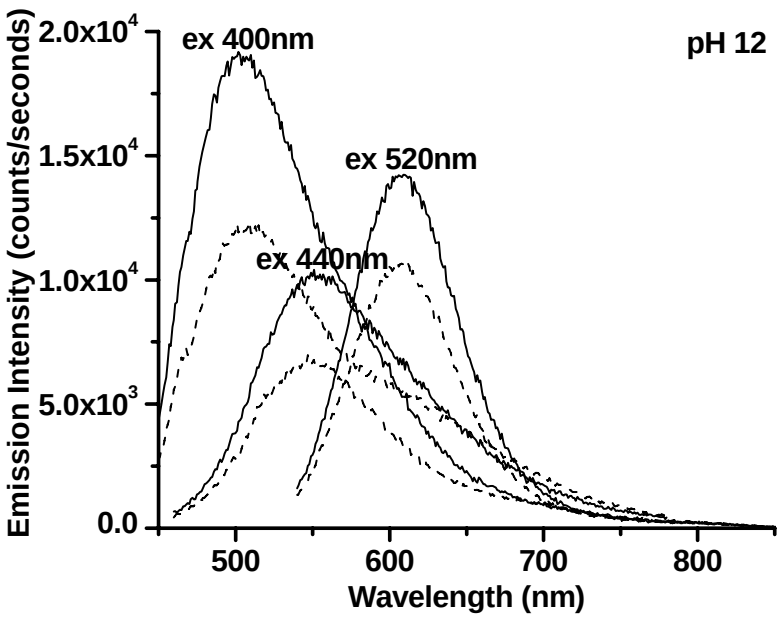

Figure 44. Emission spectra of C_{12}:Ag_n at pH 12. Solid lines indicate the emission spectra taken 12 hours after reduction of C_{12}:Ag_n. Dashed lines indicate the emission spectra 4 hours after the first emission spectra (solid line) C_{12}:Ag_n were recorded. Original conditions: [C_{12}] = 60 μM, [Ag^+] = 360 μM, and [BH_4^-] = 360 μM. The samples were stored at room temperature in a dark.

Above pH 8 even after a day, the green emission excited at 440 nm, the red emission excited at 580 nm and the IR emission excited at 640 nm are still increasing. In contrast, below pH 8, the red and IR emission for the second emission scans (dashed line) decrease with time (solid lines). At pH 11 ($[Na_2HPO_4]$=46.2mM and [NaOH]=7.6mM)(140) shown in Figure 43d, the different emitters at 600 nm excited at 520 nm and 580 nm excited at 480 nm appear with the red and IR emission. The dynamics of different emitters are also slow as seen in pH 9 ($[Na_2B_4O_7 \cdot 10H_2O]$=2.3mM and [NaOH]=8.4mM)(140) and 10. Although different emission appeared from C_{12}:Ag_n at pH 12 (borate buffer) in Figure 44, the emission maximum reached is similar to that at pH 4. Therefore, the silver nanoclusters may not be stable at pH 12. Overall, this suggests that the dynamics of silver nanoclusters slow down as the solutions become basic except pH 12 (too basic). Since OH^- is abundant at high pH, the solutions are more reducing conditions than one at low pH (H^+ is abundant). At high pH, the fully reduced species such as Ag_2 (IR) and Ag_3 (red) are less likely oxidized to form the oxidized silver clusters such as Ag_5 (blue) and Ag_4 (green). Therefore, at high pH, the slow silver nanocluster dynamics are observed, thereby reducing the conversion from the fully reduced species (Ag_2 and Ag_3) to the oxidized silver clusters such (Ag_5 and Ag_4).

Similar trends as the dynamics and emission of C_{12}:Ag_n with different pH were observed from C_{24}:Ag_n. At pH 4 and 5 (citrate buffer) shown in Figure 45a and b, the blue emission excited at 340 nm, the green emission excited at 440 nm, red emission excited at 580 nm and IR emission excited at 640 nm are all observed. The dynamics of different emitters are similar as the ones observed from C_{24}:Ag_n in the Figure 30. As red and IR emission decrease, the blue and green emission increases. As observed from the

emission of C_{24}:Ag_n at pH 5 in the Figure 45, the emission intensities of red and IR emitters at pH 5 are about five times as higher than at pH 4. As mentioned above that pK_a for N3 of cytosine is around 4, indicating that the red and IR emitters also bind to N3. At pH 6 and 7 (phosphate buffer) shown in Figure 45c and d, the red emission excited at 580 nm and IR emission excited at 640 nm are observed from C_{24}:Ag_n, with only weak blue and green emission excited at 340 nm and 440 nm, respectively. The dynamics of red and IR emitters at pH 6 are similar as the dynamics of C_{24}:Ag_n in deionized water. While the dynamics of red and IR emitters for pH 7 are significantly slowed. Similar slow dynamics of the red and IR emitters were also observed from C_{12}:Ag_n, however only at pH 9. Since the red and IR emission intensities increase, the red and IR emitters are not converted into blue and green species under higher reducing conditions. As a result, the blue and green emission excited at 340 nm and 440 nm decreased with respect to time. At pH 8 (phosphate buffer) shown in Figure 46a, the new emission maxima at 540 nm from 480 nm excitation appears beside the green, red and IR emission. As observed from pH 7, the dynamics of red and IR emitters at pH 8 slowed down and as mentioned above, the blue/green and green emission excited at 340 nm and 440 nm decreased with respect to time. At pH 9 and 10 (borate buffer) in Figure 46b and c, similar emission as at pH 8 was observed, but the dynamics of green, red and IR emitters are slower than those at pH 8 since the 550 nm emission excited at 480 nm still increases. Above pH 9, the solid lines indicate emission spectra taken 12 hours after the reduction of C_{12}:Ag_n, which is the same as C_8:Ag_n and C_{12}:Ag_n. On the other hand, the dashed lines indicate emission spectra taken a day after the first emission spectra (solid lines) were recorded. Although a day had passed, the green emission excited at 440 nm, the red emission excited at 580 nm and

the IR emission excited at 640 continue to increase. At pH 11 (borate buffer) shown in Figure 46d, the different emitters such as 600 nm excited at 520 nm and 580 nm excited at 480 nm also appear with the red and IR emitters. The dynamics of different emitters are also slowed relative to those at lower pH. Although blue, green, and 600 nm emission were observed from C_{24}:Ag_n at pH 12 (borate buffer) in Figure 47, the blue emission are not only excited by 340 nm but also by 400 nm. This excitation peak (blue emission) for C_{24}:Ag_n was also observed from C_{12}:Ag_n at pH 12. Although the silver nanoclusters for C_{12}:Ag_n were not stable at pH 12, the silver nanoclusters for C_{24}:Ag_n at pH 12 seem to be more stable.

Two aspects in terms of stability of silver nanoclusters and their dynamics were observed. One is stability of silver nanoclusters with length-dependent polycytosine described in section 4.1. In that section, blue emitters (oxidized Ag_5) were not formed due to stabilities of the clusters with different polycytosine length. The longer the polycytosine is, the easier it is to stabilize larger cluster size. In a case of pH dependent emission, all the emission intensities of C_8:Ag_n in phosphate buffer such as pH 6, 7 and 8 were lower than the emission intensities of C_{12}:Ag_n in phosphate buffer (pH 6, 7 and 8) even though Ag^+ concentrations added to C_8:Ag_n (350 uM) and C_{12}:Ag_n (360 uM) were nearly identical. Since the K_{sp} of Ag_3PO_4 is 10^{-17}, Ag^+ is in competition to bind PO_4^{3-} vs polycytosine. As observed from above that emission appeared from C_m:Ag_n in phosphate buffer, it seems that polycytosine may compete favorably with PO_4^{3-}. Since the emission intensity for C_8:Ag_n was the lowest of all with considering concentrations of Ag^+ with different length of polycytosine, this suggests that the longer the polycytosine, the better Ag^+ and Ag are protected. Therefore, the silver nanoclusters formed from C_{12}:Ag_n and

C_{24}:Ag_n may be well protected compared to the silver nanoclusters formed from C_8:Ag_n, thereby producing higher emission intensity from C_{12}:Ag_n and C_{24}:Ag_n than from C_8:Ag_n. Another intriguing feature observed from pH-dependent emission of C_{12}:Ag_n and C_{24}:Ag_n is dynamic effect on silver nanoclusters with increasing pH. This is a more reducing environment, thus silver nanocluster dynamic especially red emitters is slow.

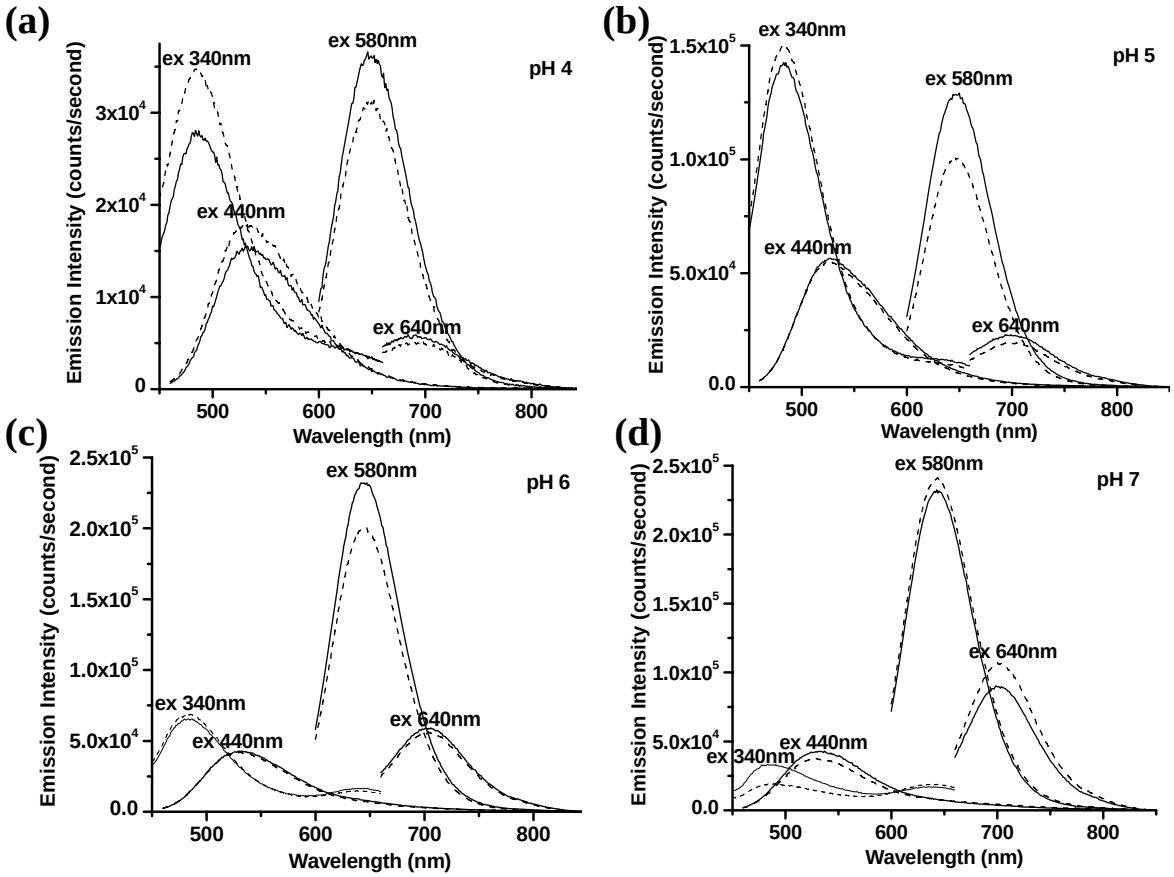

Figure 45. Emission spectra of C_{24}:Ag_n at (a) pH 4 (b) pH 5 (c) pH 6 and (d) pH 7. Solid lines indicate the emission spectra taken 12 hours after reduction of C_{24}:Ag_n. Dashed lines indicate the emission spectra 4 hours after the first emission spectra (solid line) C_{24}:Ag_n were recorded. Original conditions: [C_{24}] = 60 μM, [Ag^+] = 720 μM, and [BH_4^-] = 720 μM. The samples were stored at room temperature in a dark.

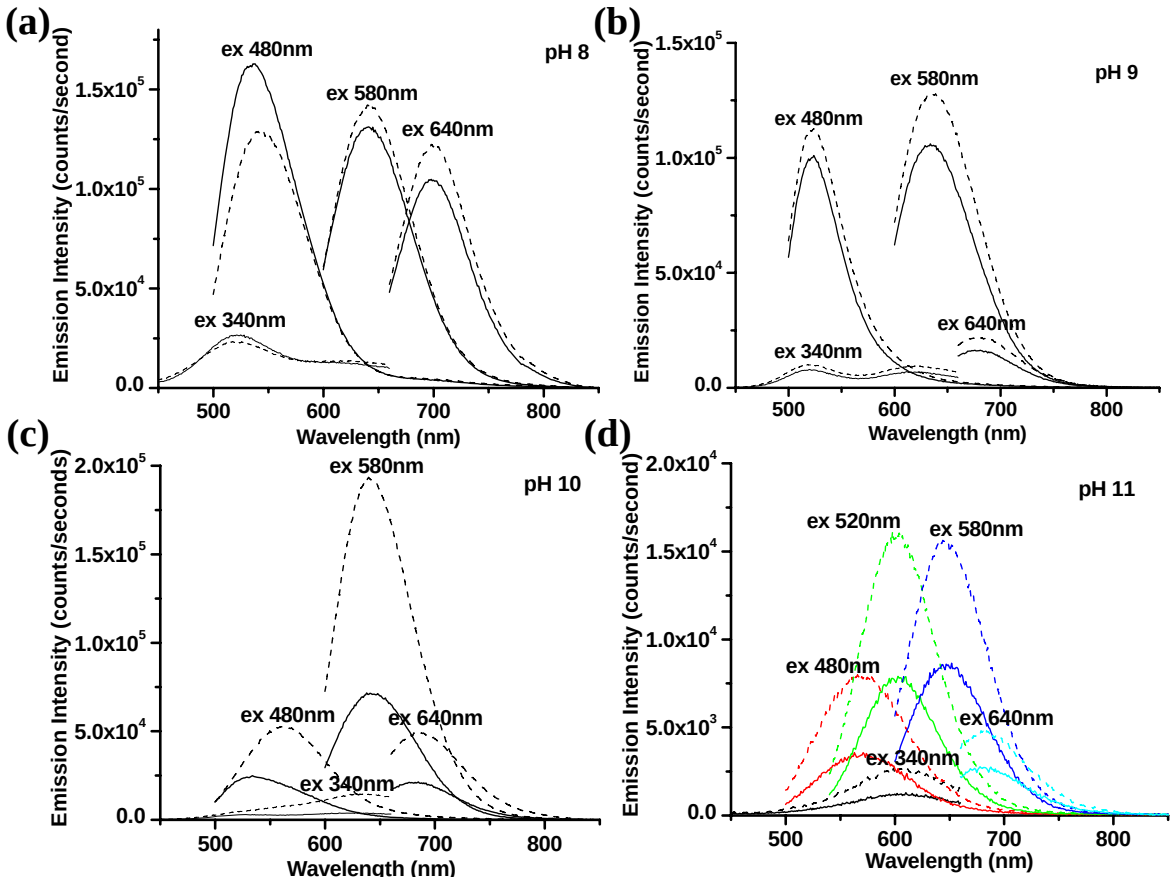

Figure 46. Emission spectra of C_{24}:Ag_n at (a) pH 8 (b) pH 9 (c) pH 10 and (d) pH 11. Solid lines indicate the emission spectra taken 12 hours after reduction of C_{24}:Ag_n. Dashed lines indicate the emission spectra 4 hours for pH 8 and 9 and one day for pH 10 and 11 after the first emission spectra (solid line) C_{24}:Ag_n were recorded. Since the different emission of C_{24}:Ag_n at pH 11 are crowded and hard to distinguish between different emission, the emission spectra are shown in color. Original conditions: [C_{24}] = 60 μM, [Ag^+] = 720 μM, and [BH_4^-] = 720 μM. The samples were stored at room temperature in a dark.

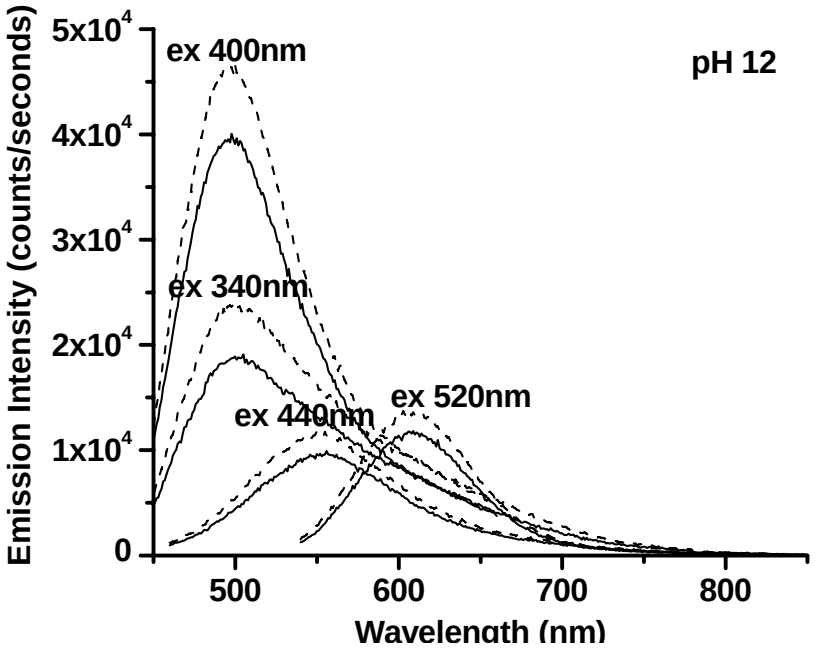

Figure 47. Emission spectra of C_{24}:Ag_n at pH 12. Solid lines indicate the emission spectra taken 12 hours after reduction of C_{24}:Ag_n. Dashed lines indicate the emission spectra 4 hours after the first emission spectra (solid line) C_{24}:Ag_n were recorded. Original conditions: [C_{24}] = 60 μM, [Ag^+] = 720 μM, and [BH_4^-] = 720 μM. The samples were stored at room temperature in a dark.

Due to lack of careful studies on dynamics of silver nanoclusters, their dynamics are investigated at different pH (pH 5, 8 and 10). Since C_8:Ag_n is not well protected from O_2 and from ions in solution, only C_{12}:Ag_n and C_{24}:Ag_n are used to study the kinetic effects on silver nanoclusters. Figure 48 shows the time-dependent emission of C_{12}:Ag_n at pH 5 (citrate buffer). In Figure 48a, red and IR emission excited at 580 nm and 640 nm appear 50 minutes after the reduction of C_{12}:Ag_n. In Figure 48b, the red and IR emission reach maxima 6 hours after the reduction. The blue and red emissions excited at 340 nm and the green emission excited at 440 nm also appeared. The blue, green, red and IR emissions remain unchanged for two hours and are shown in Figure 48c. Subsequently, the red and IR emissions started to decrease and the blue and green emissions continue to increase. 2.5 days after the reduction shown in Figure 48d, the red and IR emissions decrease by 70%.

At pH 8 (phosphate buffer), the red and IR emissions excited at 580 nm and 640 nm were observed 50 minutes after the reduction of C_{12}:Ag_n (Figure 49a). The red and IR emissions reached maximum intensities 7 hours after the reduction (Figure 49b). The red and green emissions excited at 340 nm and 440 nm also appeared at that time. The green, red and IR emission intensities stayed constant for 3 hours (Figure 49c). 2.5 days after the reduction (Figure 49d), the red and IR emissions decreased by about 30% and 25%, while the green emission increased.

Figure 50 shows the time-dependent emission of C_{12}:Ag_n at pH 10 (borate buffer). Similar emission as those at pH 5 and pH 8 appeared 50 minutes after the reduction of C_{12}:Ag_n. At pH 10, it took 5 days for the red and IR emission intensities to be maximized

(Figure 50b). Besides the green emission excited at 440 nm, 570 nm emission excited at 480 nm also appeared (Figure 50b). As shown in Figure 50c, the green, red, and IR emissions remained unchanged for 2 days, while the 570 nm emission excited at 480 nm increased. When the dynamics of red emitters of C_{12}:Ag_n at pH 10 are compared with the dynamics of red emitters at pH 5 and 8, the dynamics of the red emitters at pH 10 are the slowest of all (pH 5 and pH 8). As mentioned above, high pH is more reducing condition, thereby causing the silver cluster kinetics to slow down.

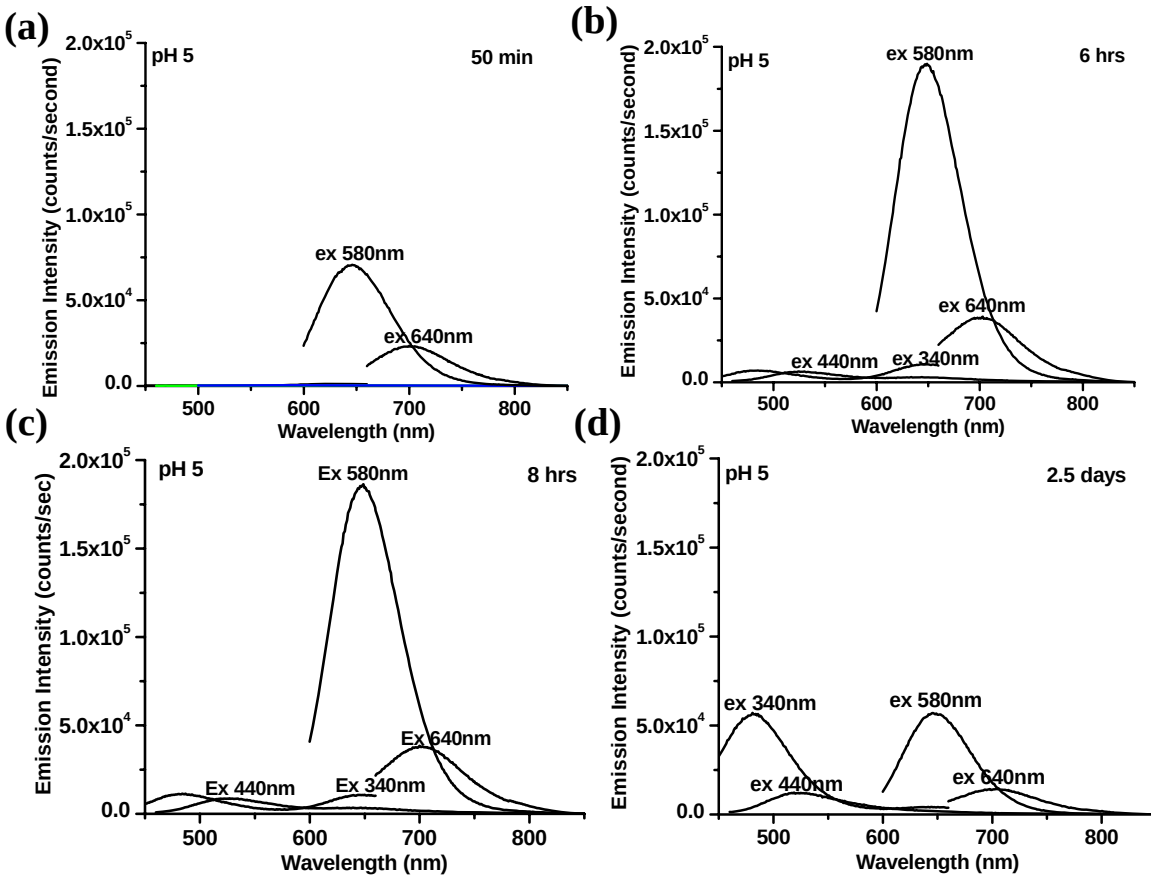

Figure 48. Time-dependent emission of C_{12}:Ag_n at pH 5 (a) 50 minutes (b) 6 hours (c) 8 hours (d) 2.5 days. Sodium Citrate buffer was used for pH 5. Original conditions: [C_{12}] = 60 μM, [Ag^+] = 360 μM, and [BH_4^-] = 360 μM. The samples were stored at room temperature in a dark.

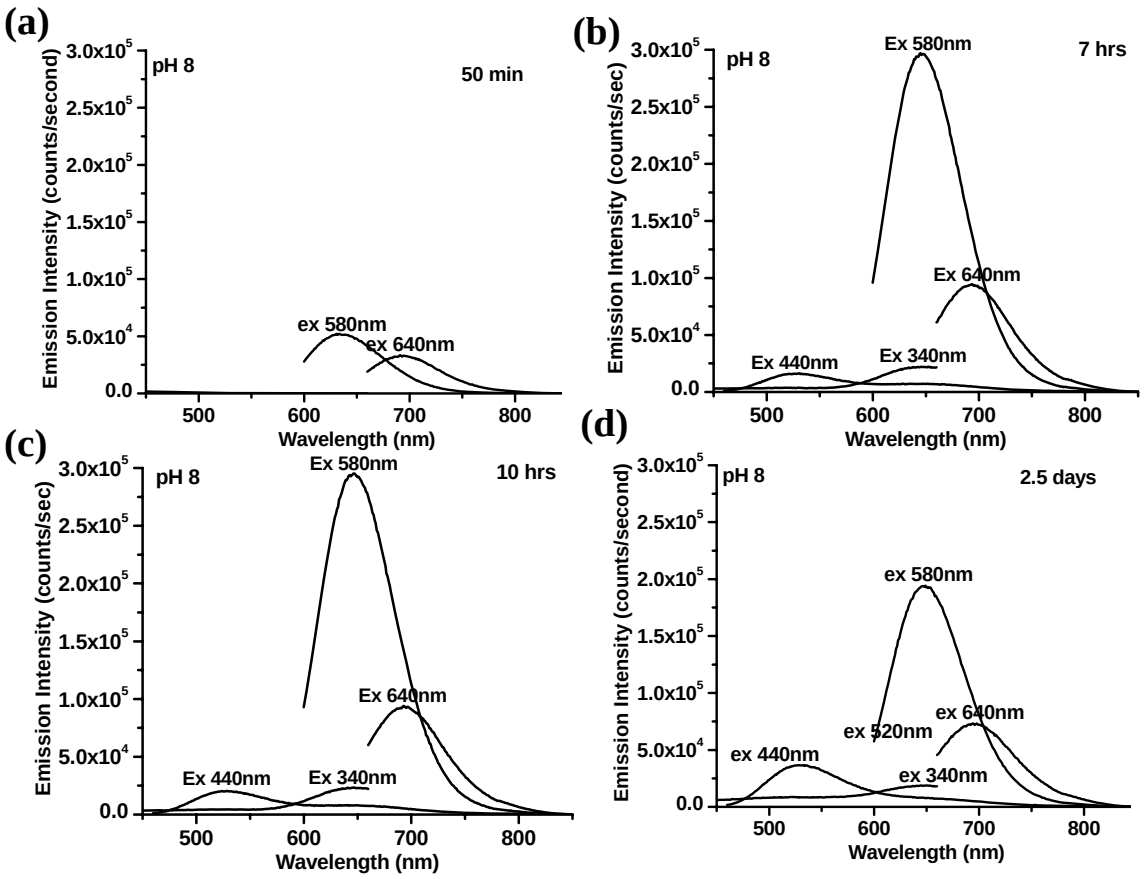

Figure 49. Time-dependent emission of C_{12}:Ag_n at pH 8 (a) 50 minutes (b) 7 hours (c) 10 hours (d) 2.5 days. Potassium phosphate buffer was used for pH 8. Original conditions: $[C_{12}]$ = 60 μM, $[Ag^+]$ = 360 μM, and $[BH_4^-]$ = 360 μM. The samples were stored at room temperature in a dark.

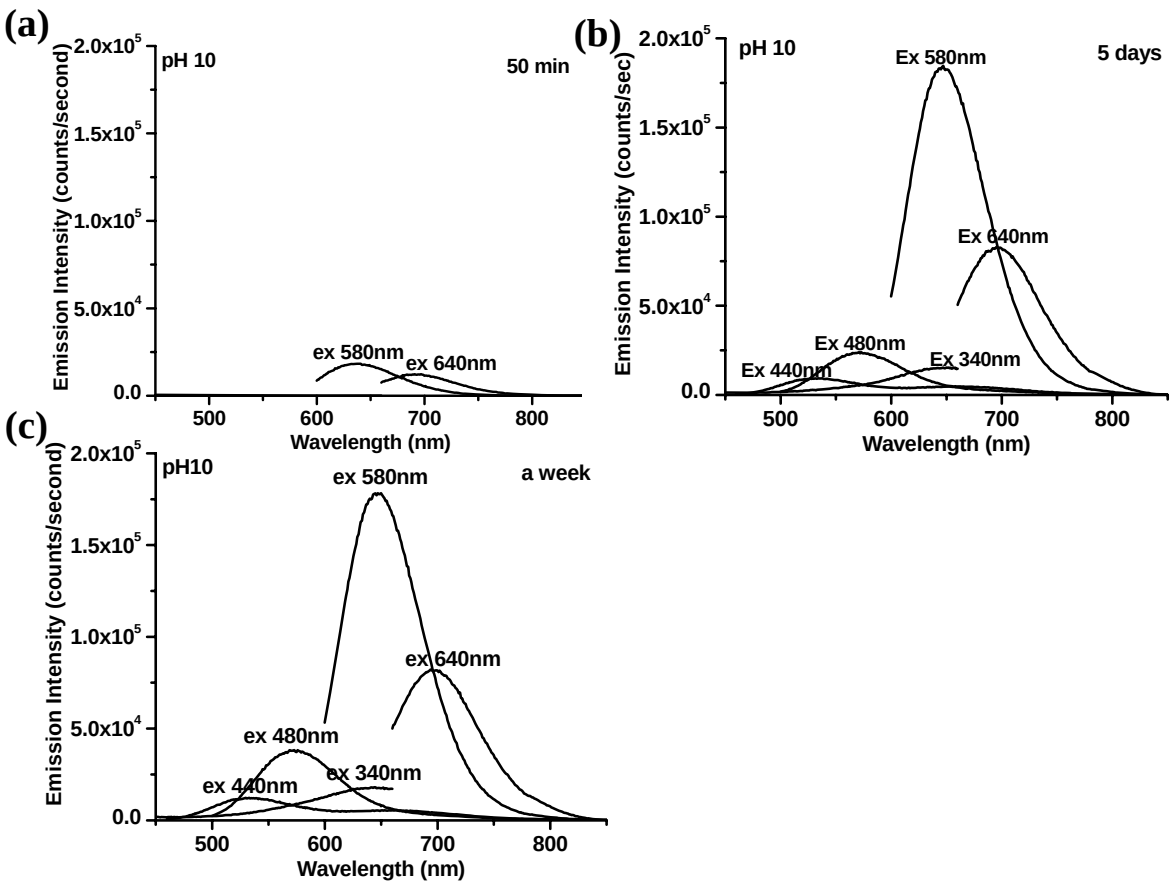

Figure 50. Time-dependent emission of C_{12}:Ag_n at pH 10 (a) 50 minutes (b) 5 days (c) one week. Sodium borate buffer was used for pH 10. Original conditions: [C_{12}] = 60 μM, [Ag^+] = 360 μM, and [BH_4^-] = 360 μM. The samples were stored at room temperature in a dark.

The time-dependent emission of C_{24}:Ag_n at pH 5 (citrate buffer) was also studied. Similar dynamics as for C_{12}:Ag_n are observed from C_{24}:Ag_n. In Figure 51a, red and IR emission excited at 580 nm and 640 nm appeared 50 minutes after the reduction of C_{24}:Ag_n. The red and IR emission intensities of C_{24}:Ag_n at 50 minutes after the reduction are much higher, however, than the corresponding intensities for C_{12}:Ag_n. In Figure 51b, the red and IR emission reached maximum intensities 150 minutes after reduction. The red and IR emissions shown in Figure 51c remained the same for 100 minutes and the green emission excited at 440 nm appeared. 3 days after reduction (Figure 51c), the red and IR emissions decreased by 80 % and 70 % and the green emission continued to increase. The dynamics of the red emitters at pH 5 for C_{24}:Ag_n are faster than the dynamics of the red emitters at pH 5 for C_{12}:Ag_n.

At pH 8 (phosphate buffer), the red and IR emissions excited at 560 nm and 640 nm were observed 50 minutes after the reduction of C_{24}:Ag_n (Figure 52a). The red and IR emissions reached maximum intensities 9 hours after reduction (Figure 52b). The green emission excited at 480 nm appeared at that time. The red and IR emission intensities remained unchanged for 3 hours shown in Figure 52c and the green emission excited at 480 nm increased. 2.5 days after the reduction (Figure 52d), the red emission decreased by about 25% and the IR emission intensity still remained the same, while the green emission increased. At pH 8, the excitation for the green changed to 480 nm and a new red emission peak at 620 nm was observed from 560 nm excitation. This is probably due to the different silver cluster stability with different lengths of polycytosine under slightly reducing basic conditions.

Figure 53 shows time-dependent emission of C_{24}:Ag_n at pH 10 (borate buffer). Similar emission to that at pH 5 appeared 50 minutes after the reduction of C_{24}:Ag_n. At 1.5 days after the reduction (Figure 53b), the red and IR emission intensities reached maximum. The red emission excited at 340 nm, the 570 nm emission excited at 480 nm and the 600 nm emission excited at 520 nm all appeared by this time (Figure 53b). In Figure 53c, the red emission excited at 580 nm remained unchanged for 4 days, while the 570 nm emission excited at 480 nm, the 600 nm emission excited at 520 nm and IR emission excited at 640 nm increased. At 10 days after the reduction, the red and IR emissions decreased, while the 570 nm emission excited at 480 nm and the 600 nm emission excited at 520 nm continued to increase.

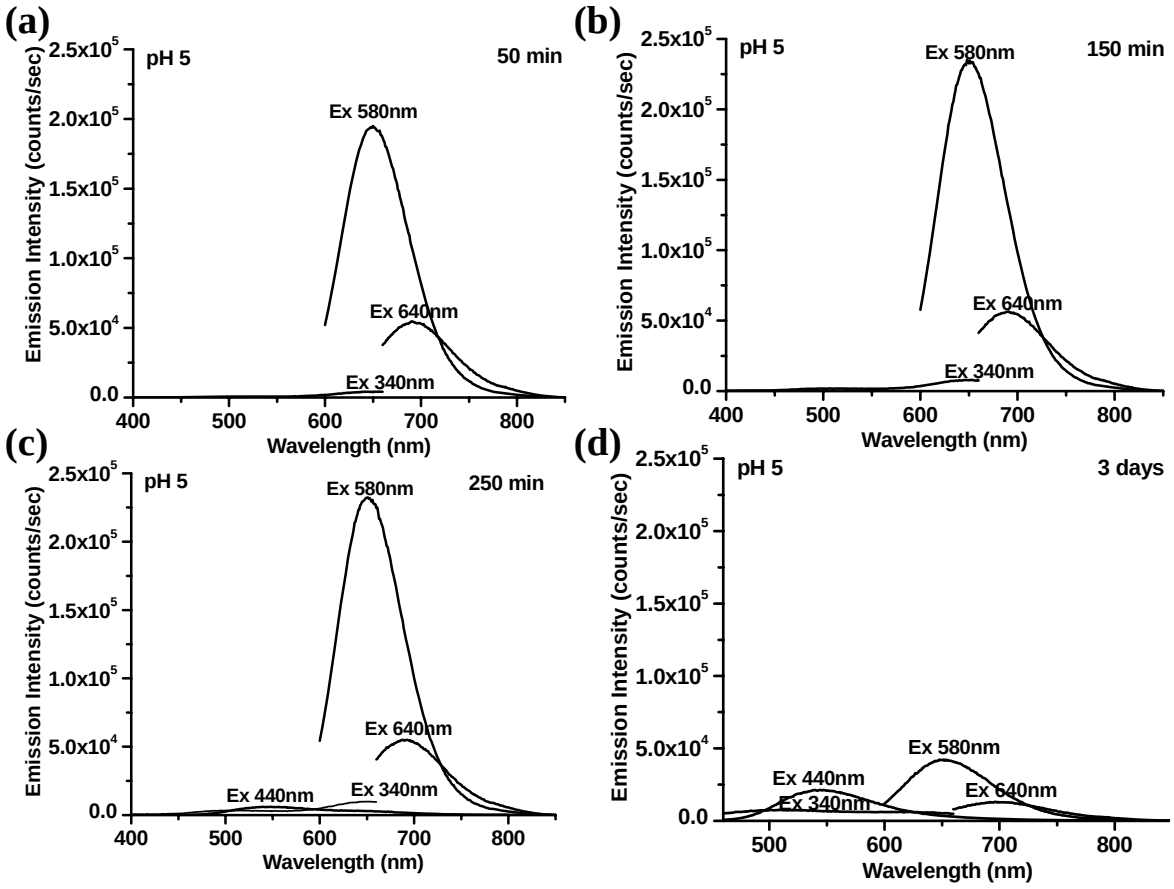

Figure 51. Time-dependent emission of C_{24}:Ag_n at pH 5 (a) 50 minutes (b) 150 minutes (c) 250 minutes (d) 3 days. Sodium Citrate buffer was used for pH 5. Original conditions: $[C_{24}]$ = 60 μM, $[Ag^+]$ = 720 μM, and $[BH_4^-]$ = 720 μM. The samples were stored at room temperature in a dark.

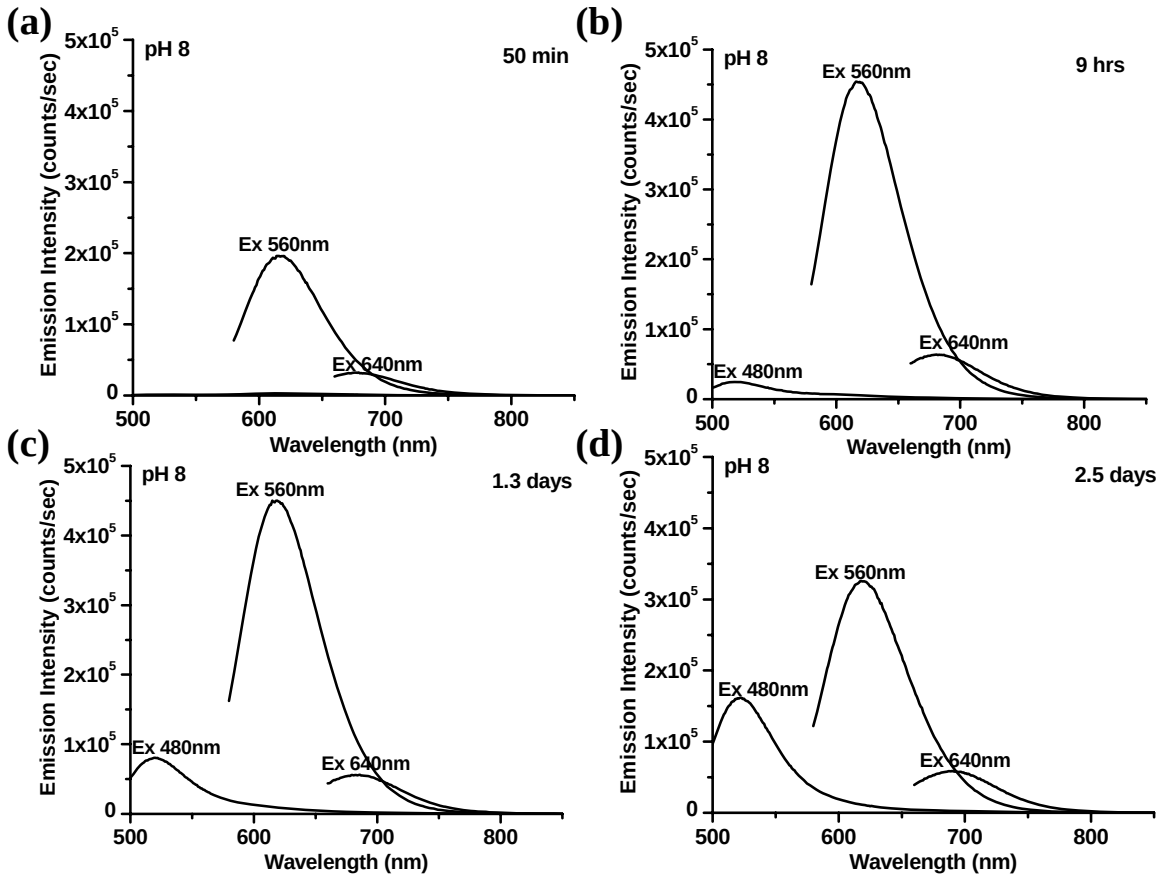

Figure 52. Time-dependent emission of C_{24}:Ag_n at pH 8 (a) 50 minutes (b) 9 hours (c) 1.3 days (d) 2.5 days. Potassium phosphate buffer was used for pH 8. Original conditions: $[C_{24}]$ = 60 μM, $[Ag^+]$ = 720 μM, and $[BH_4^-]$ = 720 μM. The samples were stored at room temperature in a dark.

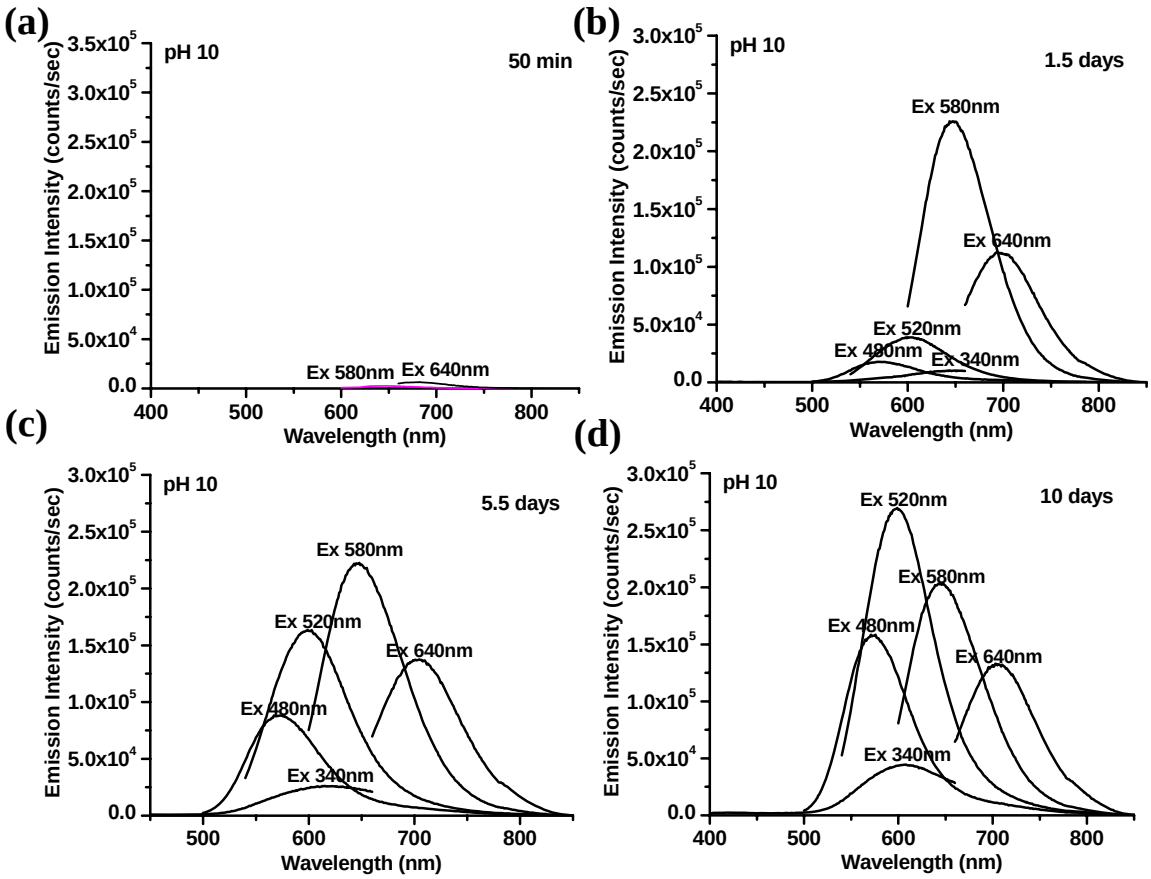

Figure 53. Time-dependent emission of C_{24}:Ag_n at pH 10 (a) 50 minutes (b) 1.5 days (c) 5.5 days (d) 10 days. Sodium borate buffer was used for pH 10. Original conditions: [C_{24}] = 60 μM, [Ag^+] = 720 μM, and [BH_4^-] = 720 μM. The samples were stored at room temperature in a dark.

From the time dependent emission of C_{12}:Ag_n and C_{24}:Ag_n at various pH (5, 8 and 10), the following results are found. New species are formed at higher pH, and these species (570 nm emission excited at 480 nm and the 600 nm emission excited at 520) are more stable in C_{24}. Therefore, they were not shown in the time dependent emission of C_{12}:Ag_n at pH 5, 8 and 10. This different emission abundance is probably due to the different silver cluster stability with different lengths of polycytosine under reducing conditions. Another difference is the dynamics of the red emitters. The dynamics of the red emitters slowed down under more basic conditions (more reducing condition). The slow dynamics of the red emitters were observed from both C_{12}:Ag_n and C_{24}:Ag_n. The more the pH is basic, the slower the dynamics of the red emitters are.

4.9 Conclusions

With comparison of mass spectra and the corresponding emission spectra for C_8:Ag_n with ones for C_{12}:Ag_n, it is suggestive that the longer the polycytosine is, the more stable the larger clusters such as Ag_5 are. In time-dependent emission spectra, an isosbestic point is observed from C_8:Ag_n, C_{12}:Ag_n and C_{24}:Ag_n by converting red and IR species into blue and green species. CD spectra for C_m:Ag_n were measured to investigate if the silver nanoclusters dynamics were due to conformation change in C_m. The conformations in C_m were not changed with respect to time except C_8. This is not conclusive to say that the dynamics observed from silver nanoclusters can be due to stabilities of the silver nanoclusters. Isosbestic points were observed from temperature-dependent absorption and emissions of C_m:Ag_n. By increasing temperature (energy), the larger clusters such as the blue (oxidized Ag_5) and green (oxidized Ag_4) emitters may dissociate to the smaller

clusters such as the red (Ag_3) and IR (Ag_2) emitters. Cytosine interacts with itself to form an i-motif structure.(134, 136, 142) With increase of temperatures from 20 °C to 60 °C, the conformation for C_m changes, while the conformation for C_m:Ag_n remained the same even at 60 °C. Therefore, the interaction between C_m and silver nanoclusters is stronger than interaction between C_m themselves and the silver nanocluster dynamics observed from temperature-dependent absorption and emission of C_m:Ag_n can not be as a result of conformation changes in DNA. By adding NaCl to reach 100 mM NaCl, the blue (oxidized Ag_5) and green (oxidized Ag_4) emitters turn into red (Ag_3) and IR (Ag_2) emitters due to the conformation change in C_m. From pH-dependent emission study of C_{12}:Ag and C_{24}:Ag, the dynamics of the red emitters slowed down when pH was more basic (more reducing conditions)

The different dynamics of silver nanoclusters were observed from different parameters such as time, temperature, salt and pH. Buffer solutions at higher pH (between 7 and 9) are most effective way to control the dynamics of silver clusters. Tuning kinetics of emissive species with different pH buffer solution, single molecules as well as ensembles for each emitter can be studied separately.

5 SINGLE MOLECULE STUDY ON C_m:Ag_n AND ITS APPLICATION

While myriad dyes exist with varying photophysical properties, (95, 96) organic dye-based single molecule and even bulk in vivo imaging dynamics studies suffer from low probe brightness, poor photostability, (99) and oxygen sensitivity. (101) Advances in nanotechnology such as the use of quantum dots (143, 144) have ameliorated some of these issues but at the cost of toxicity, (104) broad excitation,(145, 146) power-law blinking, (105, 107, 147) and large probe size.(109, 110) While quantum dots are readily excited with low intensity sources, their fluorescence exhibits intermittency on all timescales, (105, 107, 147) thereby causing problems when utilized for tracking or imaging studies. Arising from Auger processes,(148) these photophysical dynamics are apparent at all excitation intensities and appear without characteristic times. While functionalization, large size (10~20 nm diameter), and cellular uptake are potential problems, the strong non-molecular power-law fluorescence intermittency is a major drawback of these materials as single molecule reporters.(105, 107, 147) Consequently, for both in vitro and in vivo single molecule studies, fluorophores with high emission rates and excellent photostability must be identified that are completely devoid of blinking on all relevant timescales.

By combining the virtues of chemistry and nanotechnology, we have developed few-atom, molecular scale noble metal nanoclusters as a new class of emitters that simultaneously exhibit bright, highly polarizable discrete transitions, good photostability, and small size, all within biocompatible scaffolds.(13, 23, 149) Recent observations that DNA

encapsulates Ag nanoclusters to yield a range of absorption and emission features throughout the visible region, (150) have enabled the detailed investigation of Ag nanocluster size and nanocluster interactions with cytosine bases in particular.(149) Here we report a new, bright near IR emitting Ag nanocluster created in C_{12} single-stranded DNA (ss-DNA) that shows very high emission rates, excellent photostability, strong antibunching, and essentially no intensity fluctuations on experimentally relevant timescales.

5.1 Ensemble photophysical properties of C_m:Ag_n.

Due to distinctive fluorescent emission in the blue, green, red and IR, the photophysical parameters, quantum yield ϕ_F, lifetime τ_F and absorption coefficient ε for C_{12}:Ag_n have been investigated. The quantum yield of fluorescence of a molecule of interest can be calculated with a reference dye by using Equation 5.1.1,

$$Q_F = Q_R \frac{I_F A_R n_F^2}{I_R A_F n_R^2} \qquad \text{Equation 5.1.1}$$

were Q_F is the quantum yield of fluorescence of the molecule of interest and Q_R is the quantum yield of the reference dye. The parameters I, A and n are the total fluorescence intensity of the emission spectrum, the absorption and the refractive index of the solution in which the molecules are dissolved, respectively. The subscript F and R indicate whether the parameters I, A and n are from the molecule of interest or the reference dye. At first, ϕ_F excited at 340 nm (ϕ_{F340}), 580 nm (ϕ_{F580}) and 650 nm (ϕ_{F650}) for C_{12}:Ag_n are calculated using Coumarin 120,(151) Cresyl Violet(152) and Cyanine Dye(119) as references dyes, respectively. Since the absorption at 440 nm is much higher than the ones at 580 nm and 650 nm and the corresponding emission excited at 440 nm is much

lower than the ones excited at 580 nm and 650 nm, the ϕ_F excited at 440 nm is not calculated. The ϕ_{F340}, ϕ_{F580} and ϕ_{F650} for C_{12}:Ag_n are 1%, 23%, and 17 %, respectively. Since the green and red emitters can both be excited by 375 nm simultaneously, a 375 nm pulsed laser was used to determine the lifetimes of both emitters. The different emitters were spectrally selected by using a monochromator and monitoring the fluorescence at 550 nm (for the green emitter) and 650 nm (for the red emitter). The fluorescence was collected with a PMT that was attached at the exit of the monochromator. The signals from the PMT were sent to a TCSPC board (LifeSpec) together with a synchronization pulse from the pulsed laser. In the way a histogram of time differences between the pulsed excitation (synchronization pulse) and the arrival of the fluorescence at the PMT can be constructed which represents the fluorescence decay. The lifetime for green emitters is 400 ps while the lifetime for red emitters shown in Figure 54 consists of 2 components: One component is 60 % of 483 ps and the other is 40 % of 2.87 ns. Also, the lifetime of C_{12}:Ag_n excited at 640 nm shown in Figure 55 and emission collected at 700 nm is 2.8 ns. As a result, the nanosecond component of two components obtained from 375nm excitation is from the IR component. The lifetime for blue emitters excited at 336 nm was also obtained and it is 3 ns.

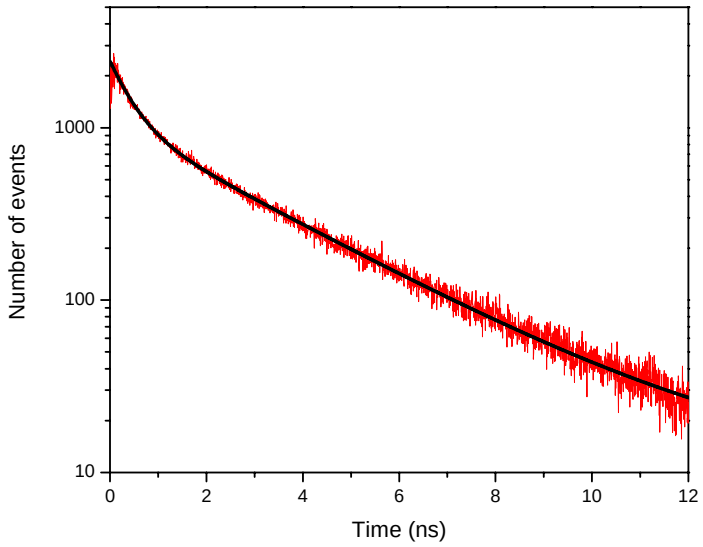

Figure 54. Lifetime measurement of red and IR emitting silver nanoclusters, C_{12}:Ag_n excited at 375 nm. Red line is from C_{12}:Ag_n and black line is a fit. Lifetime of C_{12}:Ag_n consists of two components: 483 ps (60 %) and 2.87 ns (40 %).

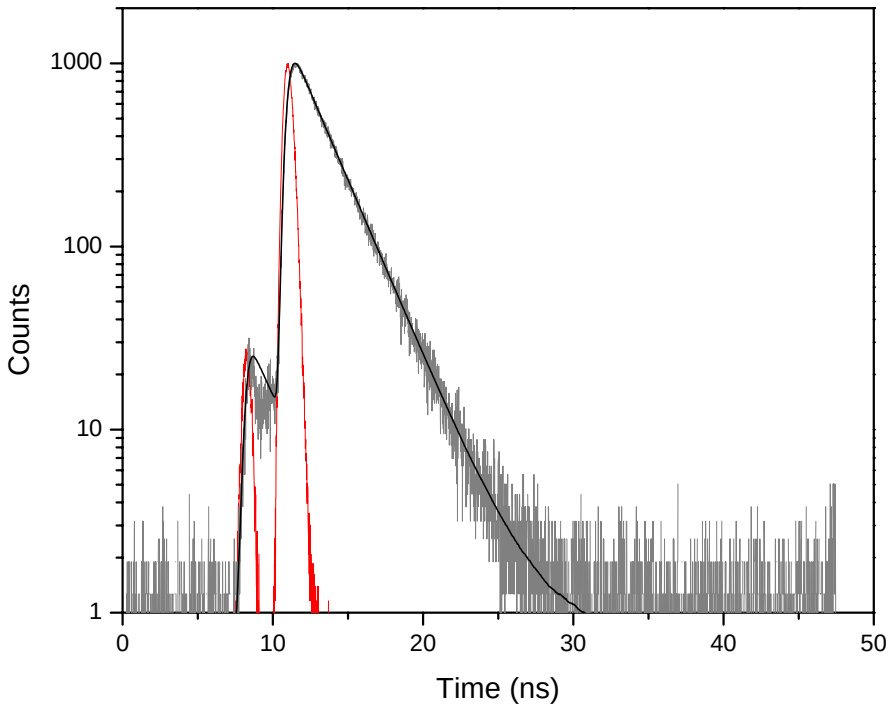

Figure 55. Lifetime measurement of IR emitting silver nanoclusters, C_{12}:Ag_n excited at 647 nm. Red line is an instrument response, gray line is from C_{12}:Ag_n, and black line is a fit. Lifetime of C_{12}:Ag_n is 2.8 ns.

In order to obtain the absorption coefficient of C_m:Ag_n, Fluorescence Correlation Spectroscopy (FCS)(129, 153, 154) was performed on C_m:Ag_n. Figure 58.a shows the fluorescence intensity time traces of a C_{24}:Ag_n sample dissolved in PBS. An autocorrelation can be performed on the fluorescence intensity time traces of C_{24}:Ag_n to obtain the information about the average number of molecules in the detection volume, triplet lifetime and diffusion time. The autocorrelation function $G_{11}(\tau)$ is defined as Equation 5.1.2,

$$G_{11}(\tau) = \frac{< \delta F_1(t) \delta F_1(t+\tau) >}{< F_1 >< F_1 >} \qquad \text{Equation 5.1.2}$$

where F_1 is the fluorescence trajectory constructed from detector 1 and $<F_1>$ represents the average fluorescence. In the top part of the Equation 5.1.2, $\delta F_1(t)$ represents the fluorescence intensity at time (t) and $\delta F_1(t+\tau)$ is the fluorescence intensity later at time $(t+\tau)$.(155)

For the diffusion process of single molecules in solution through a tightly focused laser spot, one can obtain values like diffusion time and number of molecules in the confocal volume (concentration) from the autocorrelation of fluorescence intensity data by fitting the autocorrelation curve to Equation 5.1.3,

$$G(\tau) = \left(1 + \frac{1}{N}\right)\left(\frac{1}{\left(1+\frac{\tau}{\tau_C}\right)\sqrt{\left(1+\frac{\tau}{\omega^2 \tau_C}\right)}}\right) \qquad \text{Equation 5.1.3}$$

where N is the average number of molecules in the detection volume, τ_C is the average transit time of the molecule diffusing through the focus (diffusion time) and ω is a term related to the z-axis diffusion component in the 3D confocal volume. (154) Besides the simple process of diffusion, other processes that contribute to fluorescence fluctuations can occur. Figure 56 shows the typical timescales of various processes that lead to fluorescence fluctuations that can be obtained from single molecules in solution.

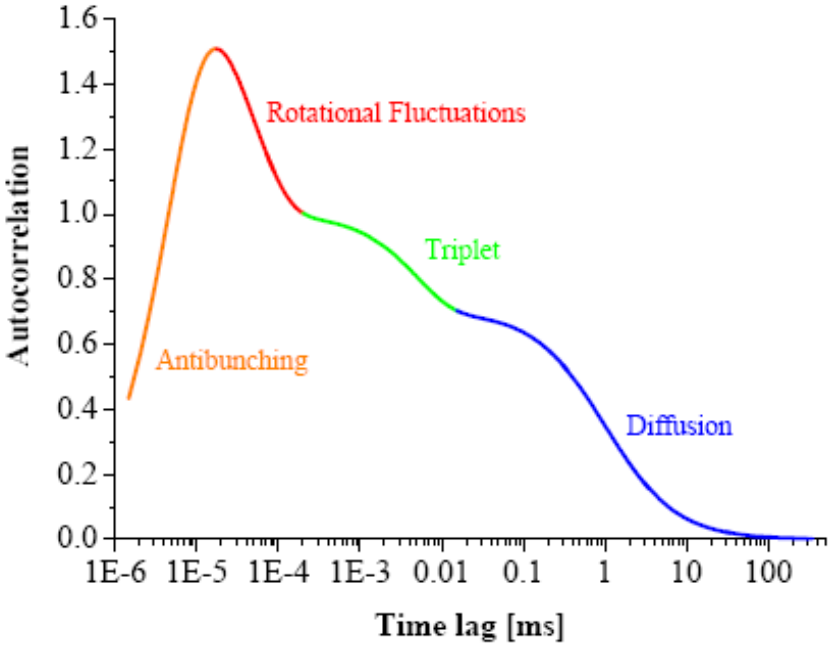

Figure 56. Autocorrelation curve where 1 is subtracted from the Y-axis. Timescale of various fluorescence fluctuation processes that can be obtained from single molecules in solution and can be seen in the autocorrelation curve.(154)

When only one detector is used, the autocorrelation curve is similar to the dotted line shown in Figure 57 due to the afterpulsing from the detector (APD).(129)

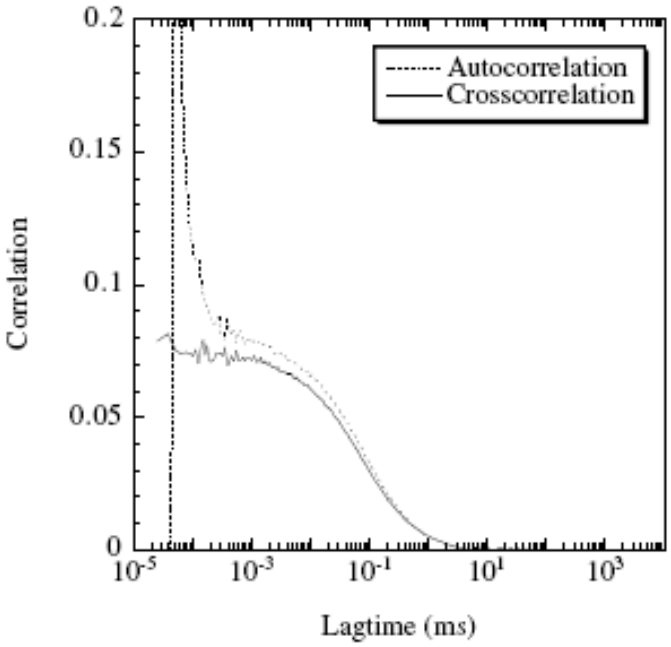

Figure 57. Comparison of cross correlation with autocorrelation (1 is subtracted from the Y-axis). The peak on the autocorrelation curve is due to the afterpulsing of APD. Reproduced from reference (129).

To remove the peak resulted from the afterpulsing of the APD, two detectors are used and cross correlation is performed on the fluorescence intensity trajectory and is shown in Figure 57. The cross correlation function is similar to that in Equation 5.1.2 and defined as Equation 5.1.4,

$$G_{12}(\tau) = \frac{< \delta F_1(t) \delta F_2(t+\tau) >}{< F_1 >< F_2 >} \qquad \text{Equation 5.1.4}$$

where F_1 and F_2 are fluorescence trajectories constructed from detector 1 and 2. (153) Figure 58(a) shows the cross correlation curve (black) and fits of the curve (red) of an FCS experiment of C_{24}:Ag_n (Figure 58.a). In order to calculate a concentration of the C_{24}:Ag_n solution, several dilutions of a C_{24}:Ag_n solution and a Cy5 reference solution of known concentration were measured. The Cy5 dilutions are used to calculate the excitation volume. This is done by plotting the known concentration of the Cy5 solutions versus the number of molecules that was obtained from the cross correlation fits of these solutions. Now we know the focal volume and since we also know the absorption of the undiluted C_{24}:Ag_n sample, a concentration and molar extinction coefficient can be calculated. A value for ε_{647} of 3.2E5 L/mole cm and for ε_{594} a value of 1.95E5 L/mole cm for C_{12}:Ag_n was found in this way. This ε_{647} value is comparable to that of Cy5. Since Cy5 is known as one of the best IR dyes, C_m:Ag_n can potentially be used for IR dyes and biological labeling.

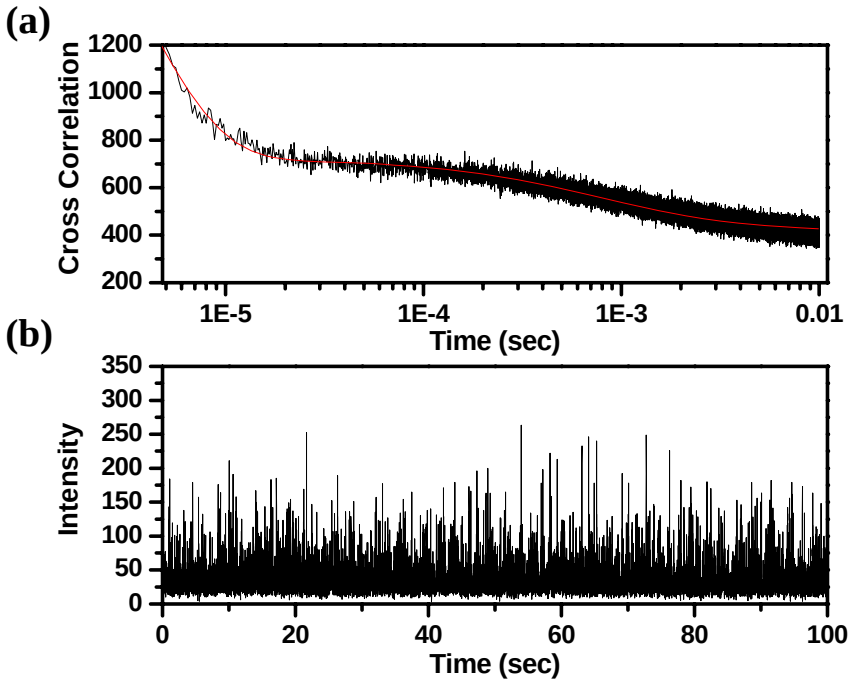

Figure 58. (a) Fluorescence time traces of C_{24}:Ag_2 in PBS solution excited with a 647 nm pulsed laser using 5 ms of bin time. (b) Raw (unnormalized) cross correlation curve of (a). The red line is a fit of the curve.

5.2 Single molecule study of C_m:Ag_n on PVA films.

Under identical imaging conditions, our near IR emitting nanoclusters appear at least twice as bright as Cy5.29 (Figure 59). As the fluorescence quantum yields (0.17 for Ag_2, 0.3 for Cy5.29) and the extinction coefficients ($3.2x10^5M^{-1}cm^{-1}$ for Ag_2, $2.5x10^5M^{-1}cm^{-1}$ for Cy5.29) roughly offset, the increased brightness of C_{12}-Ag_2 under weak excitation (~$5W/cm^2$ incident intensity) likely arises from significant differences in blinking dynamics. While the photophysics and blinking of Cy5 fluorophores are well-known (156, 157) and can be minimized(158) or used to one's advantage,(157, 159) like all organic dyes, O_2-sensitivity, moderate photobleaching quantum yields (~10^{-6}), and intensity-dependent blinking timescales that obscure true dynamics of the system under study, all seriously limit application in single molecule studies. Excited at 647 nm under ambient conditions, single nanocluster emission rates increase sublinearly with excitation intensity (Figure 60.A), presumably due to triplet dynamics. Unlike organic fluorophores, Ag nanoclusters show essentially no blinking on experimentally relevant timescales, while exhibiting excellent photostability. At lower excitation intensities (~$1kW/cm^2$), 10kcps is readily detected for minutes to hours without any observable blinking. Figure 60.B shows an example of a single molecule excited with 633 nm CW excitation ($1.5kW/cm^2$) which had a constant total fluorescence intensity of about 20000 counts per second for 1250 seconds after which the molecule bleached or transitioned into a long off state. Although devoid of intensity fluctuations on normal experimental/binning timescales, autocorrelation traces of both immobilized molecules (Figure 60.C and Table 1) and those free in solution as measured by FCS (Table 1) show fast intensity fluctuations on

the tens of microseconds scale. This correlation decay time is a combination of on and off times (Equation 3.2.1 and 3.2.2), presumably corresponding to the triplet quantum yield and triplet lifetime, respectively. Further suggesting triplet dynamics, the correlation time decreases with increasing excitation intensity (Figure 60.C). As the correlation decay is given by equations 3.2.1 and 3.2.2, this often-observed correlation time shortening with excitation intensity typically arises from a shortened "on" time (i.e. increased rate of intersystem crossing), while not changing τ_{off}. Expected to lengthen the off time, oxygen exclusion (10^{-6} torr) did not alter the correlation decay at any intensity level (data not shown). This fast decay component therefore arises from a heavy atom effect of silver that enhances the rates both into and out of the triplet level, such that the triplet lifetime is faster than quenching by oxygen, yielding the observed oxygen insensitivity, fast triplet decay, and extreme photostability. As molecules detected by FCS sample vastly different intensities as they traverse different regions of the excitation volume, comparing intensity-dependent photophysical parameters with those of immobilized species is problematic. The similar correlation decays to those of immobilized molecules (Table 1), however, indicates that aqueous and immobilized molecule photophysics are very similar, even with the increased range of motion available in solution. Consequently, long time photophysics and parameters are extracted only from immobilized species, with the understanding that these appear similar to those free in solution.

With increased excitation intensity, emission rates continue to increase to levels unattainable with current organic fluorophores in aqueous solutions, and without bleaching. These higher excitation intensities yield upwards of 200,000cps (detected), but

at the expense of blinking with long on and off times that are easily discriminated by a single threshold (Figure 60.E), but the number of events is currently too low to determine consensus time scales. Currently thought to be a multi-photon process based on higher power pulsed data, more extensive intensity dependent long-time blinking dynamics will be reported in a future publication. With cw excitation, the long off times are quite rare and only appear at the very highest excitation intensities, further suggesting multiphoton origins. While emission rates and photostabilities are more reminiscent of much larger semiconductor quantum dots than of organic fluorophores, the single exponential blinking dynamics only on very fast timescales demonstrates that these are molecular species that should improve on the problematic power-law blinking of quantum dots (105) for single molecule tracking studies.

Modeling observed photophysics by a three level system at all intensity levels, one can directly extract τ_{on} and τ_{off}, and consequently the intersystem crossing rate constant, k_{isc}, from fitting the correlation function (C(t), with correlation time τ_c) coupled with independently measured relevant experimental and molecular photophysical parameters (Eq. 3.2.1-4).(160)

$$C(t) = A+Be^{-t/\tau_c} \qquad \text{Equation 3.2.1}$$

$$1/\tau_c = 1/\tau_{on} + 1/\tau_{on} \qquad \text{Equation 3.2.2}$$

$$\tau_{on}/\tau_{off} = A/B \qquad \text{Equation 3.2.3}$$

$$k_{isc}= \Phi_{fl}\Phi_{eff}/\tau_{fl}\tau_{on}I_{on} \qquad \text{Equation 3.2.4}$$

In these equations, Φ_{fl} is the fluorescence quantum yield (0.17), Φ_{eff} is the experimental detection efficiency (0.05), τ_{fl} is the fluorescence lifetime, τ_{on} and τ_{off} are the on and off times, and I_{on} is the intensity/bin while in the "on" state.

Extracted intensity dependent molecular photophysical parameters were similar for both 647-nm and 633-nm cw excitation (Table 1). Interestingly, the shortened correlation decay at high excitation intensities results from not only the expected decreased on time (i.e. more cycles through the excited singlet state/second), but also a decreased off time. Both excitation wavelengths at high enough incident intensity shorten the triplet lifetime, thereby enabling more photons/second to be obtained from individual molecules. Intrinsic triplet lifetimes are ~30 μs, but decrease to below 10 μs for the highest excitation intensities, significantly increasing the duty cycle (rate) of emission. In other words, instead of having to wait for some long time for the triplet to decay, triplet-triplet absorption and back intersystem crossing significantly shortens the off time yielding many more excitation cycles/second to be achieved.

The value of τ_{on} naturally decreases with increasing excitation intensity, yielding an average k_{isc} of 3.3×10^7 s^{-1}. This relatively high intersystem crossing rate indicates a triplet quantum yield of ~0.9% and causes the on time for the highest intensity level to be comparable to or shorter than the off time, thereby demonstrating the importance of shortening of the dark state lifetime with increasing intensity to yield bright emission. Consequently, the actual fluorescence intensity while in the on state is significantly higher than the value one obtains from binning the data in long intervals (e.g. 0.1 or 1 sec). This instantaneous fluorescence intensity is represented in Table 1 as "Burst" intensity while the average intensity is the fluorescence intensity in 0.1 second intervals.

Figure 60.A shows the evolution of the fluorescence intensity versus excitation intensity on a log/log scale. The red connected curve corresponds to 647 nm excitation while the black connected curve corresponds to 633 nm excitation. This average emission seems to become sub-linear at high excitation intensities and tends toward saturation. The black and red scatter points which are not connected to the curves show the "Burst" intensities, which increasingly deviate from the average intensities as excitation intensity increases, further indicating that the triplet limits the overall emission rate. The detected fluorescence at 633 nm is roughly half that of the value detected at 647 nm at the same excitation intensity, reflecting the relative molar extinctions at 633 nm and 647 nm (Figure 59.B).

To demonstrate the remarkable photostability, Figure 60.E shows a typical single nanocluster excited at 647 nm (23 kW/cm^2), that during this 650-sec trace enabled more than 10^8 photons to be collected before it transitioned to a long-lived off state. Assuming 5% detection efficiency, this corresponds to more than $2x10^9$ emitted photons and $> 10^{10}$ excitation cycles. If one uses excitation intensities near $1kW/cm^2$, intensity traces are readily recorded for several hours with virtually no long term blinking. At high excitation intensities, we observe occasional transitions into usually recoverable long-lived dark states, but due to the length of these off periods, it is difficult to say whether or not we observe photobleaching. At low excitation intensities, typically, the only intensity fluctuations on timescales greater than 100μs result from mechanical instability and refocusing.

While blinking is generally accepted evidence of single quantum system observation, the apparent lack of intensity fluctuations at low excitation intensity and

achievable extremely high emission rates seemingly contradict our assertion that these are single molecules. Consequently, using two detectors in a Hanbury Brown-Twiss setup,(161) and introducing a delay between the two APD channels of 4.9 microseconds, we time-stamped the arrival times of all photons detected in both channels and performed a cross correlation, which shows excellent antibunched emission(23) from Ag_2 species at all observed emission rates (Figure 60.D, right panel). Cw antibunching requires extreme photostability and high emission rates, further indicating the promise of these materials, and providing the only conclusive proof of single molecule emission.

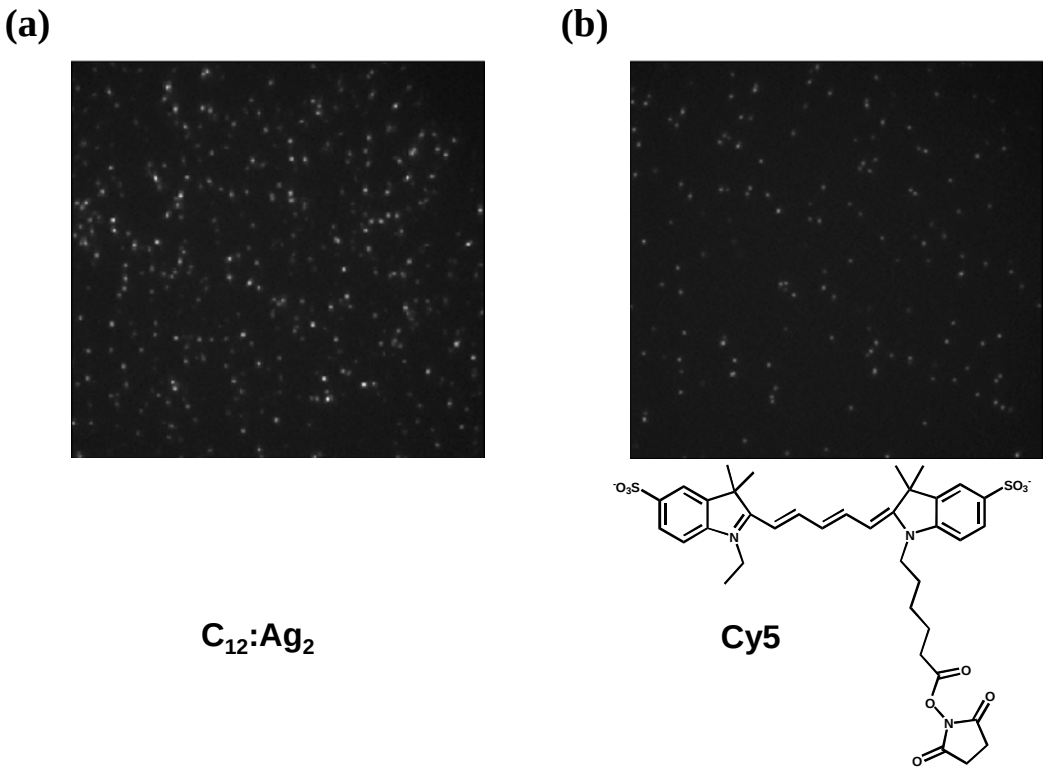

Figure 59. The fluorescence image of (a) C_{12}:Ag_2 and (b) Cy5 on PVA film excited by red Hg lamp. The structure of Cy5 is shown below the image of Cy5.

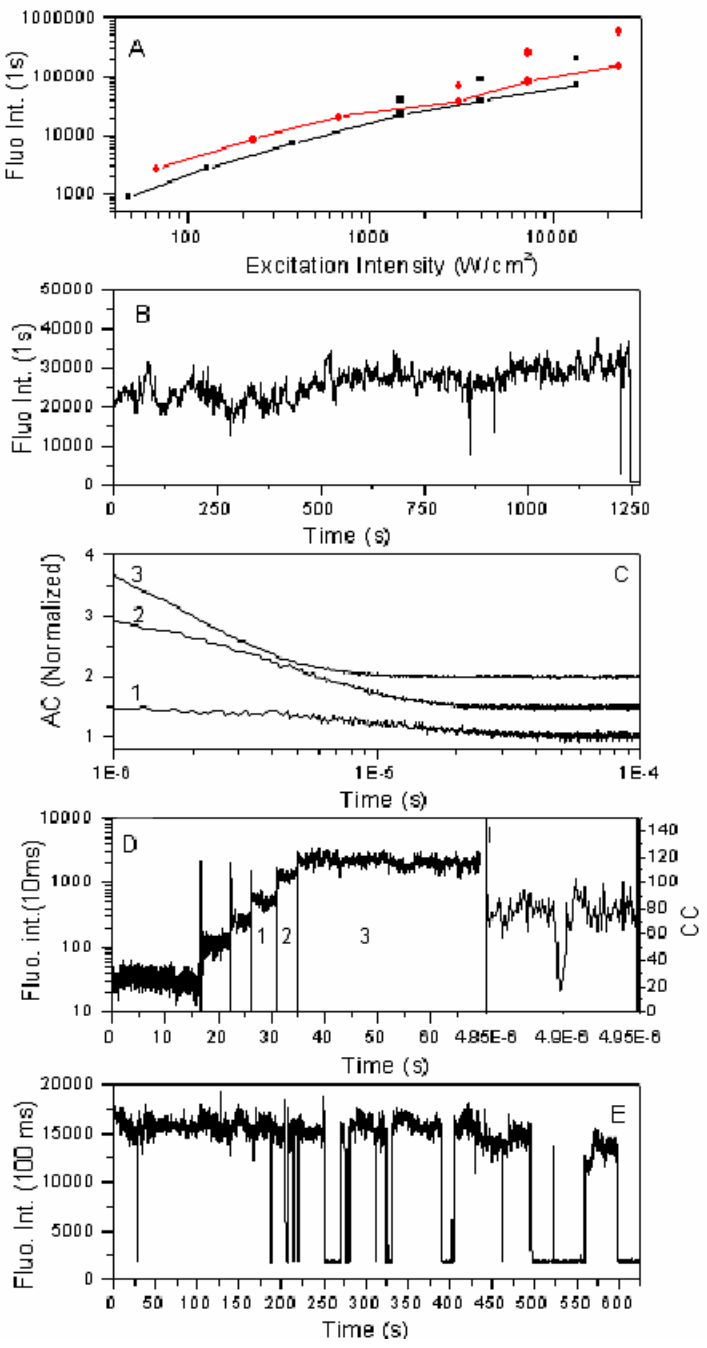

Figure 60. A) Fluorescence intensity versus excitation intensity curves for 647 nm (red) and 633 nm excitation (black). The connected scatter points correspond to the average fluorescence intensity while the unconnected scatter points correspond to the burst fluorescence intensity level in the on period. The latter is only presented for the three highest fluorescence intensities. B) Fluorescence intensity trajectory of a single C_{12}-Ag_2 molecule excited at 633 nm CW excitation and an excitation intensity of 1500 W/cm^2. C) Autocorrelation traces of the three brightest intensity levels from (D). The numbers from 1 to 3 correspond to the levels indicated in figure 2D. The autocorrelation curves were

constructed using bin times of 100 ns and curves 2 and 3 are vertically offset by 0.5 and 1.0, respectively for clarity. D) Fluorescence intensity trajectory of a single molecule excited with cw 647 nm as incident intensity is changed from 67 to 230, 670, 3000, 7200 and 23000 W/cm^2. Vertical lines demarcate intensity changes. The right panel of (D) shows the zero-delay portion (one channel is artificially delayed by ~4.9ms with a Stanford Research Systems DG-535 delay generator to avoid detection dead times) of the photon arrival cross correlation of a molecule excited with 23000 W/cm^2 using a bin time of 1 ns. This region shows the antibunching feature of the fluorescence from the singlet excited state. E) Fluorescence intensity trajectory of a single C_{12}:Ag_2 molecule excited at 647 nm CW excitation using an excitation intensity of 23000 W/cm^2.

Table 1. Experimental and extracted photophysical parameters from C_{12}:Ag_2 emitters. * = Measured by FCS.

λ_{exc} (nm)	Exc. Int. (W/cm^2)	τ_c (μs)	Avg. Int. (counts/sec)	"Burst" Int. (counts/sec)	τ_{off} (μs)	τ_{on} (μs)	k_{ISC} (s^{-1})	Φ_{ISC}
647	6.72E+01		2631					
647	2.28E+02		7700					
647	6.72E+02		17481					
647	1.13E+03	11.67	31386	57348	19.58	28.88	3228000	0.0084
647	3.04E+03	9.41	33030	73256	18.06	19.63	3332000	0.0087
647	7.22E+03	6.39	67169	261257	10.33	16.77	3728000	0.0097
647	2.28E+04	3.09	128106	596231	5.54	7.00	3593000	0.0094
647	2.81E+03	4.88*						
633	4.81E+01		982					
633	1.28E+02		2811					
633	3.73E+02		7918					
633	1.47E+03	20.93	20393	34578	29.32	73.10	2922000	0.0079
633	4.03E+03	14.78	35969	78094	21.65	46.60	2735000	0.0077
633	1.34E+04	8.87	60509	173687	13.54	25.69	3665000	0.0110

5.3 Conclusions.

A new type of fluorescent probe, C_{12}:Ag_2, was introduced. C_{12}:Ag_2 is brighter and more photostable than Cy5 which is known to be one of the best IR dyes. Using low excitation power, molecules can be monitored for hours, giving bright blinking free, stable fluorescence. Fast dynamics in the microsecond range were observed which might be related to inter system crossing to the triplet state that seems to be insensitive to oxygen. Data from single molecule experiments in solution and in PVA polymer films show similar photophysics. The photophysics of this new dye make it a promising candidate for single molecule studies in biological applications.

6 FUTURE WORK AND OUTLOOK

In this document an extensive characterization of silver nanoclusters encapsulated by polycytosine was performed. The influence of the polycytosine length, pH of the solution, buffers, temperature and more on the emission properties was investigated. Also a preliminary study of C_{12}:Ag_2 on the single molecule level was performed. This data showed very promising potential for this molecule as a single molecule dye.

Several things are still to be explored.

1. Investigating the effect of different buffers and pH on the emission of individual molecules in a PVA film. Related to this, the study of the IR emitting C_{12}:Ag_2 anchored to a surface but submerged in a solution would be interesting to compare the performance of the dye versus being immobilized in a polymer film.
2. The study of the single molecule properties of the different emissive species formed in different DNA lengths has to be done to see if there is an influence on emission properties.
3. In order to use this dye for biological applications, uptake studies and toxicity studies on living cell have to be performed. Related to this the stability of the C_n:Ag_m in the presence of DNase I has to be investigated.
4. Mixing in different nucleotides in the DNA like T, G or A or optimizing synthesis conditions of the polycytosine DNA in order to try to create only one emissive species at the time.

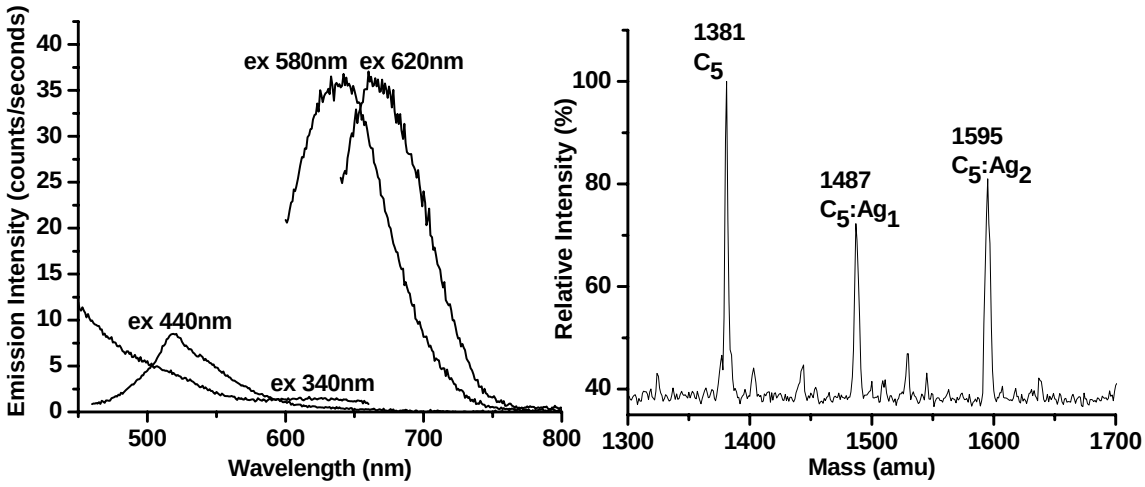

Figure A-1. Emission spectra excited at 340 nm, 440 nm, 580 nm and 620 nm for C_5:Ag_n. This spectrum was taken from fluorometer at Pchem lab in Boggs. (b) The corresponding electrospray ionization mass spectrum in (a). C_5 = 1384g. C_5:Ag_n. Original conditions: [C_5] = 120 μM, [Ag^+] = 300 μM, and [BH_4^-] = 300 μM. Experimental conditions: (18 M Ω deionized water, air saturated, measurement within a day after reduction, stored at room temperature under room light, etc). Mass spectra were obtained by using a Micromass Quattro LC operated in positive ion mode with 2.5 kV needle and 40 V cone voltage. Using a self-made origin program, the raw mass spectra data were deconvoluted.

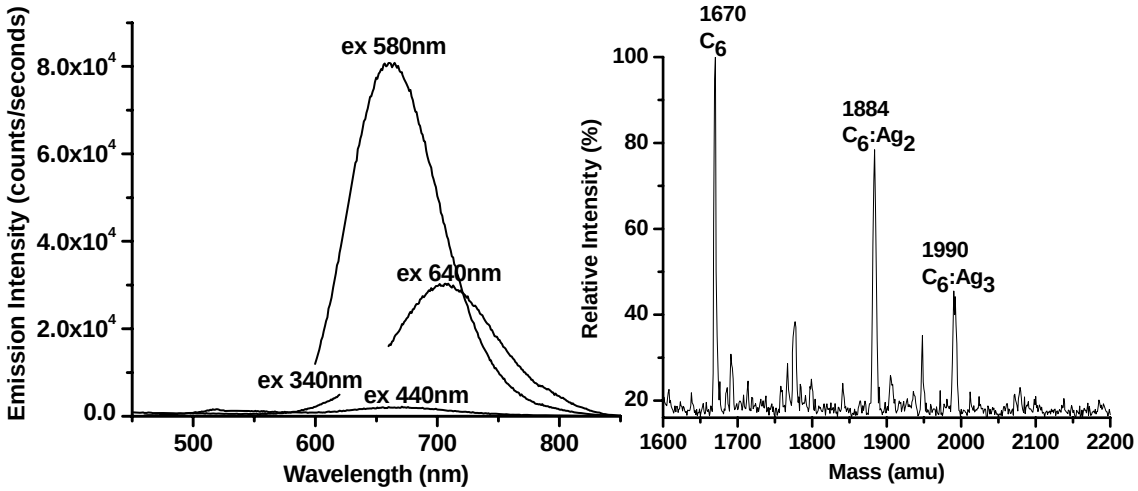

Figure A-2. Emission spectra excited at 340 nm, 440 nm, 580 nm and 620 nm for C_6:Ag_n. This spectrum was taken from PTI fluorometer in our lab. (b) The corresponding electrospray ionization mass spectrum in (a). C_6 = 1673g. C_6:Ag_n. Original conditions: [C_6] = 120 μM, [Ag^+] = 360 μM, and [BH_4^-] = 360 μM. Experimental conditions: (18 M Ω deionized water, air saturated, measurement within a day after reduction, stored at room temperature under room light, etc). Mass spectra were obtained by using a Micromass Quattro LC operated in positive ion mode with 2.5 kV needle and 40 V cone voltage. Using a self-made origin program, the raw mass spectra data were deconvoluted.

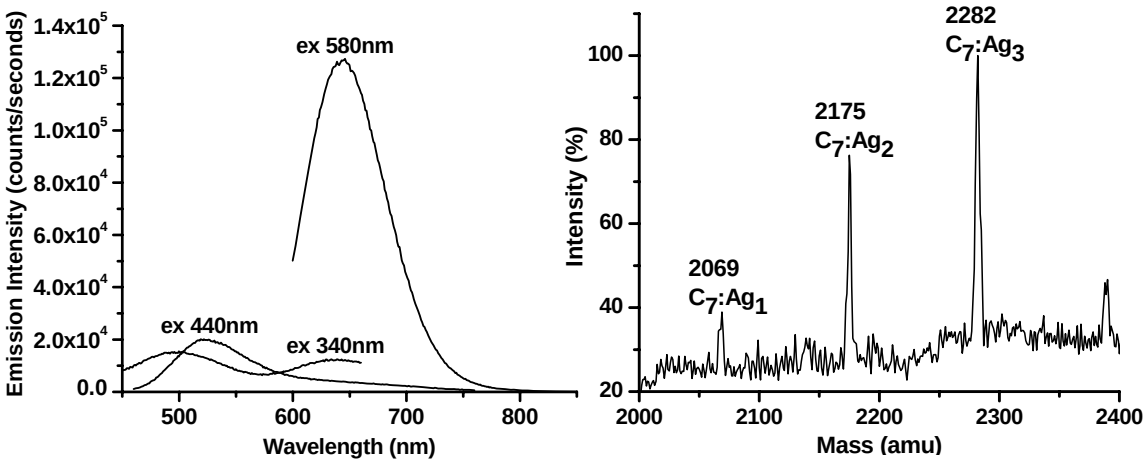

Figure A-3. Emission spectra excited at 340 nm, 440 nm and 580 nm for C_7:Ag_n. This spectrum was taken from PTI fluorometer in our lab. (b) The corresponding electrospray ionization mass spectrum in (a). C_7 = 1962g. C_7:Ag_n. Original conditions: [C_7] = 100 μM, [Ag^+] = 350 μM, and [BH_4^-] = 350 μM. Experimental conditions: (18 M Ω deionized water, air saturated, measurement within a day after reduction, stored at room temperature under room light, etc). Mass spectra were obtained by using a Micromass Quattro LC operated in positive ion mode with 2.5 kV needle and 40 V cone voltage.

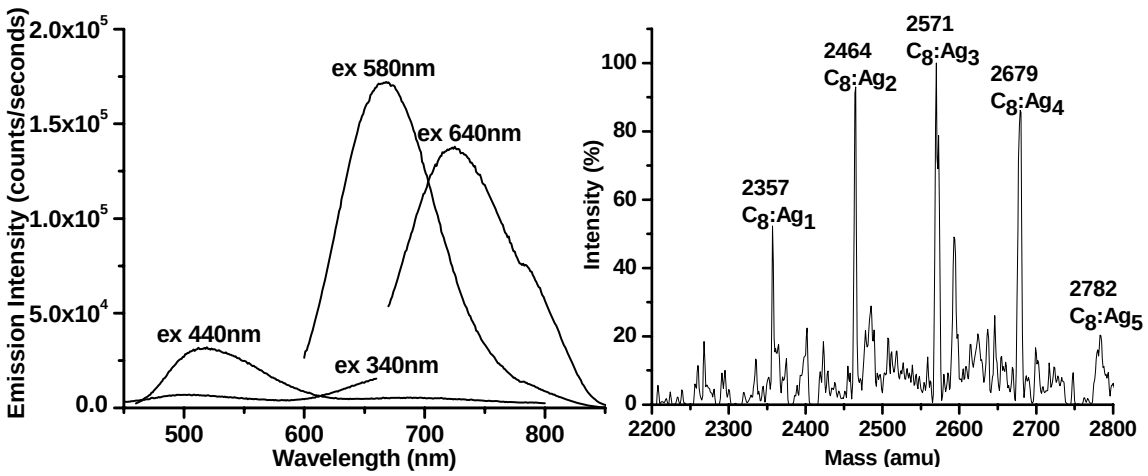

Figure A-4. Emission spectra excited at 340 nm, 440 nm, 580 nm and 640 nm for C_8:Ag_n. This spectrum was taken from PTI fluorometer in our lab. (b) The corresponding electrospray ionization mass spectrum in (a). C_8 = 2251g. C_8:Ag_n. Original conditions: [C_8] = 100 μM, [Ag^+] = 400 μM, and [BH_4^-] = 400 μM. Experimental conditions: (18 M Ω deionized water, air saturated, measurement within a day after reduction, stored at room temperature under room light, etc). Mass spectra were obtained by using a Micromass Quattro LC operated in positive ion mode with 2.5 kV needle and 40 V cone voltage. Using a self-made origin program, the raw mass spectra data were deconvoluted.

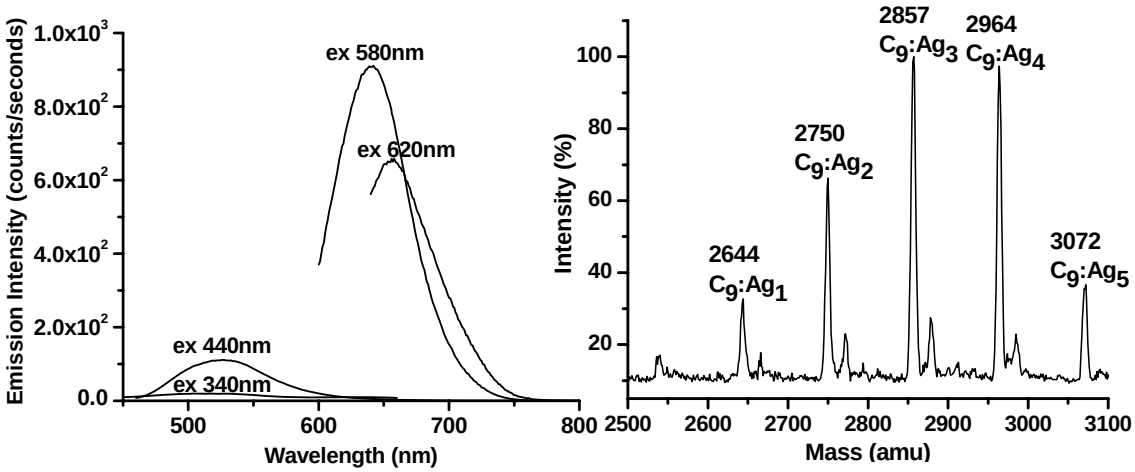

Figure A-5. Emission spectra excited at 340 nm, 440 nm, 580 nm and 640 nm for C_9:Ag_n. This spectrum was taken from PTI fluorometer in our lab. (b) The corresponding electrospray ionization mass spectrum in (a). C_9 = 2540g. C_9:Ag_n. Original conditions: [C_9] = 100 μM, [Ag^+] = 450 μM, and [BH_4^-] = 450 μM. Experimental conditions: (18 M Ω deionized water, air saturated, measurement within a day after reduction, stored at room temperature under room light, etc). Mass spectra were obtained by using a Micromass Quattro LC operated in positive ion mode with 2.5 kV needle and 40 V cone voltage. Using a self-made origin program, the raw mass spectra data were deconvoluted.

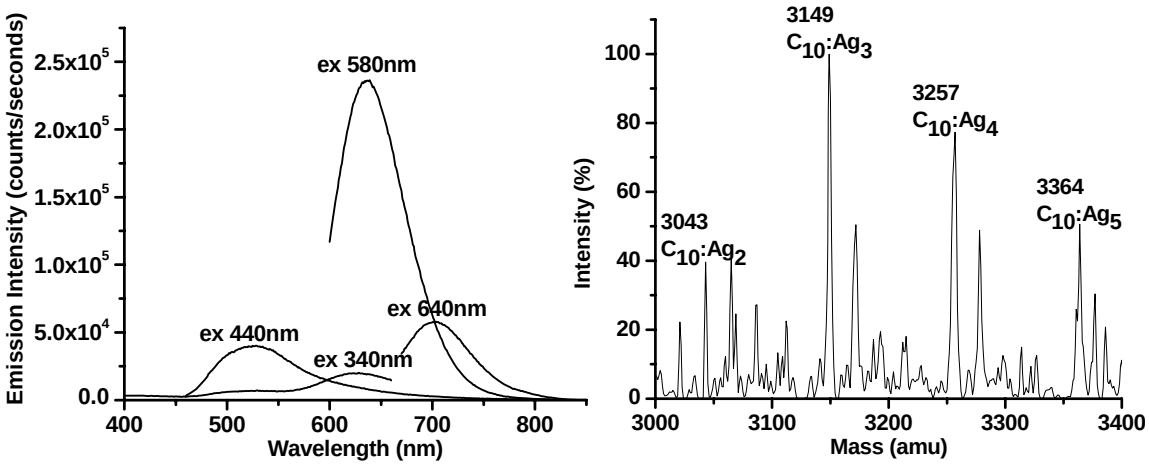

Figure A-6. Emission spectra excited at 340 nm, 440 nm, 580 nm and 640 nm for C_{10}:Ag_n. This spectrum was taken from PTI fluorometer in our lab. (b) The corresponding electrospray ionization mass spectrum in (a). C_{10} = 2829g. C_{10}:Ag_n. Original conditions: [C_{10}] = 100 μM, [Ag^+] = 500 μM, and [BH_4^-] = 500 μM. Experimental conditions: (18 M Ω deionized water, air saturated, measurement within a day after reduction, stored at room temperature under room light, etc). Mass spectra were obtained by using a Micromass Quattro LC operated in positive ion mode with 2.5 kV needle and 40 V cone voltage.

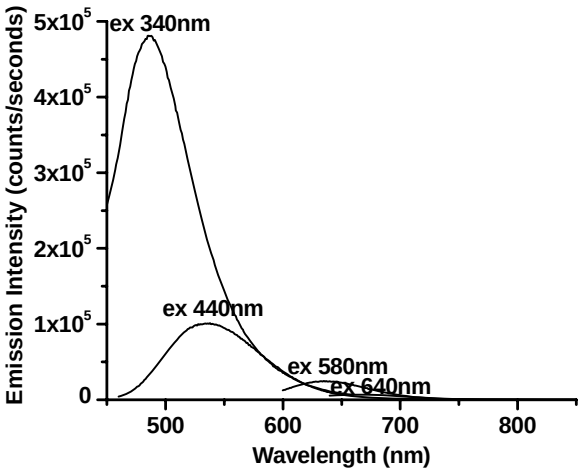

Figure A-7. Emission spectra excited at 340 nm, 440 nm, 580 nm and 640 nm for C_{36}:Ag_n. This spectrum was taken from PTI fluorometer in our lab. C_{36}:Ag_n. Original conditions: [C_{36}] = 60 μM, [Ag^+] = 1080 μM, and [BH_4^-] = 1080 μM. Experimental conditions: (18 M Ω deionized water, air saturated, measurement within a day after reduction, stored at room temperature under room light, etc). Mass spectra could not be obtained from mass spectroscopy facility at GA tech.

REFERENCES

1. Johnston, R. L. (2002) *Atomic and Molecular Clusters* (Taylor & Francis, London and New York).

2. Rabin, I., Schulze, W., Ertl, G., Felix, C., Sieber, C., Harbich, W., & Buttet, J. Absorption and fluorescence spectra of Ar-matrix-isolated Ag-3 clusters (2000) *Chemical Physics Letters* **320,** 59-64.

3. Peyser, L. A., Vinson, A. E., Bartko, A. P., & Dickson, R. M. Photoactivated fluorescence from individual silver nanoclusters (2001) *Science* **291,** 103-106.

4. Lee, T.-H., Gonzalez, J. I., & Dickson, R. M. Strongly enhanced field-dependent single-molecule electroluminescence (2002) *Proc. Natl. Acad. Sci. USA* **99,** 10272-10275.

5. Lee, T. H., Gonzalez, J. I., Zheng, J., & Dickson, R. M. Single-molecule optoelectronics (2005) *Accounts of Chemical Research* **38,** 534-541.

6. Bonacic-Koutecky, V., Mitric, R., Burgel, C., Noack, H., Hartmann, M., & Pittner, J. Tailoring the chemical reactivity and optical properties of clusters by size, structures and lasers (2005) *European Physical Journal D* **34,** 113-118.

7. Lee, T.-H., Hladik, C. R., & Dickson, R. M. Asymmetric photoconductivity within nanoscale break junctions (2003) *Nano Letters* **3,** 1561-1564.

8. Rabin, I., Schulze, W., & Ertl, G. Absorption spectra of small silver clusters Ag-n (n >= 3) (1999) *Chemical Physics Letters* **312,** 394-398.

9. Felix, C., Sieber, C., Harbich, W., Buttet, J., Rabin, I., Schulze, W., & Ertl, G. Fluorescence and excitation spectra of Ag-4 in an argon matrix (1999) *Chemical Physics Letters* **313,** 105-109.

10. Rabin, I., Schulze, W., & Ertl, G. Light emission in matrix assisted cluster-cluster reactions (1998) *Crystal Research and Technology* **33,** 1075-1084.

11. Rabin, I., Schulze, W., & Ertl, G. Light emission during the agglomeration of silver clusters in noble gas matrices (1998) *Journal of Chemical Physics* **108,** 5137-5142.

12. Konig, L., Rabin, I., Schulze, W., & Ertl, G. Chemiluminescence in the agglomeration of metal clusters (1996) *Science* **274,** 1353-1355.

13. Zheng, J. & Dickson, R. M. Individual water-soluble dendrimer-encapsulated silver nanodot fluorescence (2002) *Journal of the American Chemical Society* **124,** 13982-13983.

14. Bonacic´-Koutecky, V., Veyret, V., & Mitric´, R. Ab initio study of the absorption spectra of Ag_n (n=5–8) clusters (2001) *Journal of Chemical Physics* **115,** 10450-10460.

15. Bonacic-Koutecky, V., Pittner, J., Boiron, M., & Fantucci, P. An accurate relativistic effective core potential for excited states of Ag atom: An application for studying the absorption spectra of Agn and Ag+ clusters (1999) *Journal of Chemical Physics* **110,** 3876.

16. Bonacic´-Koutecky, V., Cespiva, L., Fantucci, P., & Koutecky, J. Effective core potential-configuration interaction study of electronic structure and geometry of small neutral and cationic Agn clusters : predictions and interpretation of measured properties (1993) *Journal of Chemical Physics* **98,** 7981-7994.

17. Yoon, J., Kim, K. S., & Baeck, K. K. Ab initio study of the low-lying electronic states of Ag_3^-, Ag_3, and Ag_3^+: a coupled-cluster approach (2000) *Journal of Chemical Physics* **112,** 9335-9342.

18. Fedrigo, S., Harbich, W., & Buttet, J. Optical response of Ag2, Ag3, Au2, and Au3 in argon matrices (1993) *Journal of Chemical Physics* **99,** 5712-5717.

19. Diederich, T., Tiggesbaumker, J., & Meiwes-Broer, K. H. Spectroscopy on rare gas-doped silver clusters in helium droplets (2002) *Journal of Chemical Physics* **116,** 3263-3269.

20. Harbich, W., Fedrigo, S., Meyer, F., Lindsay, D. M., Lignieres, J., Rivoal, J. C., & Kreisle, D. Deposition of mass selected silver clusters in rare gas matrices (1990) *Journal of Chemical Physics* **93,** 8535-8543.

21. Haslett, T. L., Bosnick, K. A., & Moskovits, M. Ag-5 is a planar trapezoidal molecule (1998) *Journal of Chemical Physics* **108,** 3453-3457.

22. Bromann, K., Felix, C., Brune, H., Harbich, W., Monot, R., Buttet, J., & Kern, K. Controlled deposition of size-selected silver nanoclusters (1996) *Science* **274,** 956-958.

23. Peyser-Capadona, L., Zheng, J., Gonzalez, J. I., Lee, T. H., Patel, S. A., & Dickson, R. M. Nanoparticle-free single molecule anti-stokes Raman spectroscopy (2005) *Physical Review Letters* **94,** art. no. 058301.

24. Slocik, J. M., Moore, J. T., & Wright, D. W. Monoclonal antibody recognition of histidine-rich peptide encapsulated nanoclusters (2002) *NanoLetters* **2,** 169-173.

25. Yu, J., Patel, S. A., Dickson, R. M. In vitro and intracellular production of peptide-encapsulated fluorescent silver nanoclusters (2007) *Angewandte Chemie International Edition*.

26. Pulleyblank, D. E. Specific Suppression of Depurination at Deoxyguanylate Residues by Silver Ions - a Useful Reaction for the Identification of Deoxyadenylate Residues in DNA (1982) *Febs Letters* **139,** 276-278.

27. Rossetto, F. E. & Nieboer, E. The Interaction of Metal-Ions with Synthetic DNA - Induction of Conformational and Structural Transitions (1994) *Journal of Inorganic Biochemistry* **54,** 167-186.

28. Berti, L., Alessandrini, A., & Facci, P. DNA-templated photoinduced silver deposition (2005) *Journal of the American Chemical Society* **127,** 11216-11217.

29. Tanaka, K., Yamada, Y., & Shionoya, M. Formation of silver(I)-mediated DNA duplex and triplex through an alternative base pair of pyridine nucleobases (2002) *Journal of the American Chemical Society* **124,** 8802-8803.

30. Albiser, G. P., S. Fibre x-ray and conformational study of the binding of metal ions on DNA (1985) *Journal of Biomolecular structure and Dynamics* **2,** 745-757.

31. KARGOV S. I., K. N. I., STANISLAVSKII O. B., Kuznetsov, I. A. interaction of immobilized DNA with silver ions (1986) *molecular biology* **20,** 1225-1230.

32. Wilhelm, F. X. D., M. Interaction of metallic ions with DNA. III. Stability and configuration of silver-DNA complexes (1969) *Biopolymers* **8,** 121-137.

33. Braun, E., Eichen, Y., Sivan, U., & Ben-Yoseph, G. DNA-templated assembly and electrode attachment of a conducting silver wire (1998) *Nature* **391,** 775-778.

34. Niemeyer, C. Nanoparticles, Proteins, and Nucleic Acids: Biotechnology Meets Material Science (2001) *Angewandte Chemie International Edition* **40,** 4128-4158.

35. Richter, J., Seidel, R., Kirsch, R., Mertig, M., Pompe, W., Plaschke, J., & Schackert, H. K. Nanoscale Palladium Metallization of DNA (2000) *Advanced Materials* **12,** 507-510.

36. Richter, J., Mertig, M., Pompe, W., Monch, I., & Schackert, H. K. Construction of highly conductive nanowires on a DNA template (2001) *Applied Physics Letters* **78,** 536-538.

37. Mertig, M., Ciacchi, L. C., Seidel, R., Pompe, W., & De Vita, A. DNA as a selective metallization template (2002) *Nano Letters* **2,** 841-844.

38. Monson, C. F. & Woolley, A. T. DNA-templated construction of copper nanowires (2003) *Nano Letters* **3,** 359-363.

39. Zhong, X. H., Feng, Y. Y., Knoll, W., & Han, M. Y. Alloyed ZnxCd1-xS nanocrystals with highly narrow luminescence spectral width (2003) *Journal of the American Chemical Society* **125,** 13559-13563.

40. Zhong, X. H., Han, M. Y., Dong, Z. L., White, T. J., & Knoll, W. Composition-tunable ZnxCd1-xSe nanocrystals with high luminescence and stability (2003) *Journal of the American Chemical Society* **125,** 8589-8594.

41. Bailey, R. E. & Nie, S. M. Alloyed semiconductor quantum dots: Tuning the optical properties without changing the particle size (2003) *Journal of the American Chemical Society* **125,** 7100-7106.

42. Kim, S., Fisher, B., Eisler, H. J., & Bawendi, M. Type-II quantum dots: CdTe/CdSe(core/shell) and CdSe/ZinTe(core/shell) heterostructures (2003) *Journal of the American Chemical Society* **125,** 11466-11467.

43. Wehrenberg, B. L., Wang, C. J., & Guyot-Sionnest, P. Interband and intraband optical studies of PbSe colloidal quantum dots (2002) *Journal of Physical Chemistry B* **106,** 10634-10640.

44. Zheng, J., Zhang, C., & Dickson, R. M. Highly Fluorescent, Water-Soluble, Size-Tunable Gold Quantum Dots (2004) *Physical Review Letters* **93,** art. no. 077402.

45. Zheng, J., Petty, J. T., & Dickson, R. M. High quantum yield blue emission from water-soluble Au-8 nanodots (2003) *Journal of the American Chemical Society* **125,** 7780-7781.

46. Lee, T. H., Gonzalez, J. I., & Dickson, R. M. Strongly enhanced field-dependent single-molecule electrolurninescence (2002) *Proceedings of the National Academy of Sciences of the United States of America* **99,** 10272-10275.

47. Peyser, L. A., Lee, T. H., & Dickson, R. M. Mechanism of Ag-n nanocluster photoproduction from silver oxide films (2002) *Journal of Physical Chemistry B* **106,** 7725-7728.

48. Frohlich, H. The specific temperatures of the electrons of small metal particles at low temperatures (1937) *Physica* **4,** 0406-0412.

49. Kubo, R. Electronic Properties of Metallic Fine Particles .1 (1962) *Journal of the Physical Society of Japan* **17,** 975-&.

50. Dupree, R. & Smithard, M. A. Electronic Properties of Small Metal Particles - Electric Polarizability (1972) *Journal of Physics Part C Solid State Physics* **5,** 408-&.

51. Wertheim, G. K. Electronic-Structure of Metal-Clusters (1989) *Zeitschrift Fur Physik D-Atoms Molecules and Clusters* **12,** 319-326.

52. Knight, W. D., Clemenger, K., de Heer, W. A., Saunders, W. A., Chou, M. Y., & Cohen, M. L. Electronic Shell Structure and Abundances of Sodium Clusters (1984) *Physical Review Letters* **52,** 2141-2143.

53. Uchtmann, H., Rademann, K., & Hensel, F. Metal-Nonmetal Transition and Homogeneous Nucleation of Mercury-Vapor (1991) *Annalen Der Physik* **48,** 207-214.

54. Knight, W. D., Clemenger, K., de Heer, W. A., & Saunders, W. A. Polarizability of Alkali Clusters (1985) *Physical Review B* **31,** 2539-2540.

55. Skala, L. Interpolation Formulas for Describing Size Dependence of Properties of Finite Systems and Their Use for Clusters and Biologically Important Molecules (1991) *Theochem-Journal of Molecular Structure* **73,** 103-109.

56. Hoffmann, E. D. C., J.; Stroobant, V. (1996) *Mass spectrometry: principles and applications* (Chichester, New York).

57. Mitchell, S. A. & Ozin, G. A. Silver Clusters in Rare-Gas Matrices - Thermal and Photochemical Silver Atom Aggregation Reactions (1984) *Journal of Physical Chemistry* **88,** 1425-1436.

58. Willey, K. F., Cheng, P. Y., Yeh, C. S., Robbins, D. L., & Duncan, M. A. Electronic spectroscopy of silver dimer rare-gas complexes (1991) *Journal of Chemical Physics* **95,** 6249-6256.

59. Fedrigo, S., Harbich, W., & Buttet, J. Collective Dipole Oscillations in Small Silver Clusters Embedded in Rare-Gas Matrices (1993) *Physical Review B* **47,** 10706-10715.

60. Fedrigo, S., Harbich, W., & Buttet, J. Soft landing and fragmentation of small clusters deposited in noble-gas films (1998) *Physical Review B* **58,** 7428-7433.

61. Ievlev, D., Rabin, L., Schulze, W., & Ertl, G. Fluorescence spectroscopy of silver clusters formed in rare gas droplets (2001) *European Physical Journal D* **16,** 157-160.

62. Robbins, D. L., Willey, K. F., Yeh, C. S., & Duncan, M. A. Electronic Spectroscopy of Ag2-Xe (1992) *Journal of Physical Chemistry* **96,** 4824-4829.

63. Ozin, G. A. & Hugues, F. Silver Atoms and Small Silver Clusters Stabilized in Zeolite-Y - Optical Spectroscopy (1983) *Journal of Physical Chemistry* **87,** 94-97.

64. Felix, C., Sieber, C., Harbich, W., Buttet, J., Rabin, I., Schulze, W., & Ertl, G. Ag_8 Fluorescence in Argon (2001) *Physical Review Letters* **86,** 2992-2995.

65. Stienkemeier, F., Higgins, J., Ernst, W. E., & Scoles, G. Laser Spectroscopy of Alkali-Doped Helium Clusters (1995) *Physical Review Letters* **74,** 3592-3595.

66. Felix, C., Sieber, C., Harbich, W., Buttet, J., Rabin, I., Schulze, W., & Ertl, G. Ag-8 fluorescence in argon (2001) *Physical Review Letters* **86,** 2992-2995.

67. Radcliffe, P., Przystawik, A., Diederich, T., Doppner, T., Tiggesbaumker, J., & Meiwes-Broer, K. H. Excited-state relaxation of Ag-8 clusters embedded in helium droplets (2004) *Physical Review Letters* **92**.

68. Fedrigo, S., Harbich, W., & Buttet, J. Optical-Response of Ag2, Ag3, Au2, and Au3 in Argon Matrices (1993) *Journal of Chemical Physics* **99,** 5712-5717.

69. Schulze, W., Rabin, I., & Ertl, G. Formation of light-emitting Ag-2 and Ag-3 species in the course of condensation of Ag atoms with Ar (2004) *Chemphyschem* **5,** 403-407.

70. Alameddin, G., Hunter, J., Cameron, D., & Kappes, M. M. Electronic and geometric structure in silver clusters (1992) *Chemical Physics Letters* **192,** 122-128.

71. Taylor, K. J., Pettiettehall, C. L., Cheshnovsky, O., & Smalley, R. E. Ultraviolet Photoelectron-Spectra of Coinage Metal-Clusters (1992) *Journal of Chemical Physics* **96,** 3319-3329.

72. Ho, J., Ervin, K., & Lineberger, W. C. Photoelectron spectroscopy of metal cluster anionsL Cun-, Agn- and Aun- (1990) *Journal of Chemical Physics* **93,** 6987-7002.

73. Handschuh, H., Cha, C. Y., Bechthold, P. S., Gantefor, G., & Eberhardt, W. Electronic Shells or Molecular-Orbitals - Photoelectron-Spectra of Ag-N(-) Clusters (1995) *Journal of Chemical Physics* **102,** 6406-6422.

74. Katakuse, I., Ichihara, T., Fujita, Y., Matsuo, T., Sakurai, T., & Matsuda, H. Mass Distributions of Negative Cluster Ions of Copper, Silver, and Gold (1986) *International Journal of Mass Spectrometry and Ion Processes* **74,** 33-41.

75. Zhao, J., Luo, Y., & Wang, G. Tight-binding study of structural and electronic properties of silver clusters (2001) *European Physical Journal D* **14,** 309-316.

76. Bao, X., Muhler, M., Pettinger, B., Schlogl, R., & Ertl, G. On the Nature of the Active State of Silver During Catalytic-Oxidation of Methanol (1993) *Catalysis Letters* **22,** 215-225.

77. Robert P. Nielsen, J. H. L. R. (1976) (Shell Oil Company, U.S.A).

78. Lefferts, L., Vanommen, J. G., & Ross, J. R. H. The Oxidative Dehydrogenation of Methanol to Formaldehyde over Silver Catalysts in Relation to the Oxygen Silver Interaction (1986) *Applied Catalysis* **23,** 385-402.

79. Sun, T. & Seff, K. Silver Clusters and Chemistry in Zeolites (1994) *Chemical Reviews* **94,** 857-870.

80. Zhang, F. X., Guan, N. J., Li, Y. Z., Zhang, X., Chen, J. X., & Zeng, H. S. Control of morphology of silver clusters coated on titanium dioxide during photocatalysis (2003) *Langmuir* **19,** 8230-8234.

81. Henglein, A. Small-Particle Research - Physicochemical Properties of Extremely Small Colloidal Metal and Semiconductor Particles (1989) *Chemical Reviews* **89,** 1861-1873.

82. Linnert, T., Mulvaney, P., Henglein, A., & Weller, H. Long-Lived Nonmetallic Silver Clusters in Aqueous-Solution - Preparation and Photolysis (1990) *Journal of the American Chemical Society* **112,** 4657-4664.

83. Henglein, A., Mulvaney, P., & Linnert, T. Chemistry of Agn Aggregates in Aqueous-Solution - Nonmetallic Oligomeric Clusters and Metallic Particles (1991) *Faraday Discussions,* 31-44.

84. Ershov, B. G., Janata, E., & Henglein, A. Growth of Silver Particles in Aqueous-Solution - Long-Lived Magic Clusters and Ionic-Strength Effects (1993) *Journal of Physical Chemistry* **97,** 339-343.

85. Henglein, A. Physicochemical Properties of Small Metal Particles in Solution - Microelectrode Reactions, Chemisorption, Composite Metal Particles, and the Atom-to-Metal Transition (1993) *Journal of Physical Chemistry* **97,** 5457-5471.

86. Wade, L. G. (1999) *Organic Chemistry* (Prentice hall, New Jersey).

87. Henglein, A. Non-Metallic Silver Clusters in Aqueous-Solution - Stabilization and Chemical-Reactions (1989) *Chemical Physics Letters* **154,** 473-476.

88. Hilpert, K. & Gingerich, K. A. Atomization Enthalpies of the Molecules Cu-3, Ag-3, and Au-3 (1980) *Berichte Der Bunsen-Gesellschaft-Physical Chemistry Chemical Physics* **84,** 739-745.

89. Henglein, A. Remarks on the Electrochemical Potential of Small Silver Clusters in Aqueous-Solution (1990) *Berichte Der Bunsen-Gesellschaft-Physical Chemistry Chemical Physics* **94,** 600-603.

90. Eichhorn, G. L., Butzow, J. J., Clark, P., & Tarien, E. Interaction of Metal Ions with Polynucleotides and Related Compounds .X. Studies on Reaction of Silver(I) with Nucleosides and Polynucleotides and Effect of Silver(1) on Zinc(2) Degradation of Polynucleotides (1967) *Biopolymers* **5,** 283-&.

91. Arya, S. K. & Yang, J. T. Optical-Rotatory Dispersion and Circular-Dichroism of Silver(I)-Polyribonucleotide Complexes (1975) *Biopolymers* **14,** 1847-1861.

92. Yamane, T. & Davidson, N. On Complexing of Deoxyribonucleic Acid by Silver(I) (1962) *Biochimica Et Biophysica Acta* **55,** 609-&.

93. Eichhorn, G. L. (1973) in *Inorganic Biochemistry volume 2*, ed. Eichhorn, G. L. (Elsevier scientific publishing company, Amsterdam-london-new york).

94. Daune, M., Dekker, C. A., & Schachma.Hk Complexes of Silver Ion with Natural and Synthetic Polynucleotides (1966) *Biopolymers* **4,** 51-&.

95. Schmidt, T., Kubitscheck, U., Rohler, D., & Nienhaus, U. Photostability Data for Fluorescent Dyes: An Update. (2002) *Single Molecules* **3,** 327.

96. Vosch, T., Cotlet, M., Hofkens, J., Van der Biest, K., Lor, M., Weston, K., Tinnefeld, P., Sauer, M., Latterini, L., Mullen, K., *et al.* Probing Forster type energy pathways in a first generation rigid dendrimer bearing two perylene imide chromophores (2003) *Journal of Physical Chemistry A* **107,** 6920-6931.

97. Dubertret, B., Skourides, P., Norris, D. J., Noireaux, V., Brivanlou, A. H., & Libchaber, A. In vivo imaging of quantum dots encapsulated in phospholipid micelles (2002) *Science* **298,** 1759-1762.

98. Ballou, B., Lagerholm, B. C., Ernst, L. A., Bruchez, M. P., & Waggoner, A. S. Noninvasive imaging of quantum dots in mice (2004) *Bioconjugate Chemistry* **15,** 79-86.

99. Eggeling, C., Widengren, J., Rigler, R., & Seidel, C. A. M. Photobleaching of fluorescent dyes under conditions used for single-molecule detection: Evidence of two-step photolysis (1998) *Analytical Chemistry* **70,** 2651-2659.

100. Gao, X. H., Yang, L. L., Petros, J. A., Marshal, F. F., Simons, J. W., & Nie, S. M. In vivo molecular and cellular imaging with quantum dots (2005) *Current Opinion in Biotechnology* **16,** 63-72.

101. Lill, Y. & Hecht, B. (2004) *Appl. Phys. Lett.* **84,** 1165-1167.

102. Alivisatos, A. P. Semiconductor clusters, nanocrystals, and quantum dots (1996) *Science* **271,** 933-937.

103. Michalet, X., Pinaud, F. F., Bentolila, L. A., Tsay, J. M., Doose, S., Li, J. J., Sundaresan, G., Wu, A. M., Gambhir, S. S., & Weiss, S. Quantum dots for live cells, in vivo imaging, and diagnostics (2005) *Science* **307,** 538-544.

104. Derfus, A. M., Chan, W. C. W., & Bhatia, S. N. (2004) *Nanoletters* **4,** 11-18.

105. Verberk, R., Van Oijen, A. M., & Orrit, M. (2002) *Phys. Rev. B* **66,** 233202-233201 - 233202-233204.

106. Zhang, K., Chang, H., Fu, A., Alivisatos, P. A., Yang, H. Continuous distribution of emission states from single CdSe/ZnS quantum dots (2006) *nano letters* **6,** 843-847.

107. Kuno, M., Fromm, D. P., Hamann, H. F., Gallagher, A., & Nesbitt, D. J. Nonexponential "blinking" kinetics of single CdSe quantum dots: A universal power law behavior (2000) *Journal of Chemical Physics* **112,** 3117-3120.

108. Yao, J., Larson, D. R., Vishwasrao, H. D., Zipfel, W. R., & Webb, W. W. Blinking and nonradiant dark fraction of water-soluble quantum dots in aqueous solution (2005) *Proceedings of the National Academy of Sciences of the United States of America* **102,** 14284-14289.

109. Bruchez, M., Moronne, M., Gin, P., Weiss, S., & Alivisatos, A. P. Semiconductor nanocrystals as fluorescent biological labels (1998) *Science* **281,** 2013-2016.

110. Chan, W. C. W. & Nie, S. M. Quantum dot bioconjugates for ultrasensitive nonisotopic detection (1998) *Science* **281,** 2016-2018.

111. Howarth, M., Takao, K., Hayashi, Y., & Ting, A. Y. Targeting quantum dots to surface proteins in living cells with biotin ligase (2005) *Proceedings of the National Academy of Sciences of the United States of America* **102,** 7583-7588.

112. Pinaud, F., King, D., Moore, H. P., & Weiss, S. Bioactivation and cell targeting of semiconductor CdSe/ZnS nanocrystals with phytochelatin-related peptides (2004) *Journal of the American Chemical Society* **126,** 6115-6123.

113. Wu, X. Y., Liu, H. J., Liu, J. Q., Haley, K. N., Treadway, J. A., Larson, J. P., Ge, N. F., Peale, F., & Bruchez, M. P. Immunofluorescent labeling of cancer marker Her2 and other cellular targets with semiconductor quantum dots (2003) *Nature Biotechnology* **21,** 41-46.

114. Zollinger, M. (1987) *colour chemistry. Synthesis, properties and applications of organic dyes and pigments* (VCH, Weinheim).

115. Griffiths, J., pender, K. J. APPLICATION OF THE PPP-MO METHOD TO THEPREDICTION OF COLOUR IN DI- AND TRI-ARYLMETHANE DYES (1981) *dyes and pigments* **2**.

116. Tuemmler, W. B. & Wildi, B. S. Polymethine Dyes .1. a Comparison of Several Vinylogous Series in Which the Polymethine Chains Are Terminated by Aryl Groups (1958) *Journal of the American Chemical Society* **80,** 3772-3777.

117. Chu, K. Y., Griffiths, J (1978) *Journal of chemical research. Synopses* **180,** 2319.

118. Bello, K. A. & Griffiths, J. Azo Dyes with Absorption-Bands in the near-Infrared (1986) *Journal of the Chemical Society-Chemical Communications***,** 1639-1640.

119. Mujumdar, R. B., Ernst, L. A., Mujumdar, S. R., Lewis, C. J., & Waggoner, A. S. Cyanine Dye Labeling Reagents - Sulfoindocyanine Succinimidyl Esters (1993) *Bioconjugate Chemistry* **4,** 105-111.

120. Dickson, R. M., Cubitt, A. B., Tsien, R. Y., & Moerner, W. E. On/off blinking and switching behaviour of single molecules of green fluorescent protein (1997) *Nature* **388,** 355-358.

121. Huang, Z. X., Ji, D. M., Wang, S. F., Xia, A. D., Koberling, F., Patting, M., & Erdmann, R. Spectral identification of specific photophysics of Cy5 by means of ensemble and single molecule measurements (2006) *Journal of Physical Chemistry A* **110,** 45-50.

122. Yamane, T. D., N. (1962) *Biochim. Biophys. Acta* **55,** 609-621.

123. Dattagupta, N. C., D. M. (1981) *Nucleic Acids Res.* **9,** 2971-2985.

124. Rodger, A. N., B. (1997) *Circular Dichroism and Linear Dichroism.* (Oxford., New York).

125. Voet, D. V., J. G. second edition. (1995) *Biochemistry* (John Wiley & Sons, Inc., New York).

126. manual, S.-B.-H.

127. Weston, K. D., Dyck, M., Tinnefeld, P., Müller, C., Herten, D. P., & Sauer, M. (2002) *Anal. Chem.* **74, ,** 5342-5349.

128. Paul, H. (1982) *Rev. Mod. Phys.* **54,** 1061-1102.

129. Krichevsky, O. & Bonnet, G. Fluorescence correlation spectroscopy: the technique and its applications (2002) *Reports on Progress in Physics* **65,** 251-297.

130. Petty, J. T., Zheng, J., & Dickson, R. M. DNA templated growth of Ag nanoclusters (2004) *Journal of the American Chemical Society* **126,** 5207-5212.

131. Donald, V. & Judith, V. G. (1994) *Biochemistry Second Edition.* (John Wiley & Sons, Inc., New York).

132. de Heer, W. A. The Physics of Simple Metal-Clusters - Experimental Aspects and Simple-Models (1993) *Reviews of Modern Physics* **65,** 611-676.

133. Skoog, D. A., West, D. M., & Holler, F. J. (1997) (Saunders College Publishing).

134. Manzini, G., Yathindra, N., & Xodo, L. E. Evidence for Intramolecularly Folded I-DNA Structures in Biologically Relevant Ccc-Repeat Sequences (1994) *Nucleic Acids Research* **22,** 4634-4640.

135. Hardin, C. C., Corregan, M.,Brown II, B. A., Frederick, L. N. (1993) *Biochemistry* **32,** 5870-5880.

136. Mergny, J. L. Fluorescence energy transfer as a probe for tetraplex formation: The i-motif (1999) *Biochemistry* **38,** 1573-1581.

137. Phan, T. A. M., J. (2002) *Nuclei Acids Research* **30,** 4618-4625.

138. Gehring, K. L., J.-L..; Gueron, M. (1993) *Nature* **10,** 561-565.

139. Leory, J.-L. G., M.; Mergny, J.-L.; Helene, C. (1994) *Nuclei Acids Research* **22,** 1600-1606.

140. Robinson, R. A., Stokes, R. H. (1968) *Electrolyte solutios, the measurement and interpretation of conductance, and diffusion in solutions of simple electrolytes* (Butterworths, London).

141. Pack, G. R., Wong, L., Lamm, G. PKa of cytosine on the third strand of triplex DNA: Preliminary Poisson-Boltzmann calculations (1998) *International Journal of Quantum Chemistry* **70,** 1177 - 1184.

142. Mills, M. L. L. A., A. B.; Leroy, J.-L.; Francois, J.-C.; Klump, H.; Mergny, J.-L. Unusual DNA Conformations: Implications for Telomeres (2002) *Curr. Med. Chem.-Anti-Cancer Agents.* **2,** 627-644.

143. Empedocles, S. A., Norris, D. J., & Bawendi, M. G. Photoluminescence spectroscopy of single CdSe nanocrystallite quantum dots (1996) *Physical Review Letters* **77,** 3873-3876.

144. Aichele, T., Zwiller, V., & Benson, O. (2004) *New Journal of Physics* **6,** 90-102.

145. Dabbousi, B. O., RodriguezViejo, J., Mikulec, F. V., Heine, J. R., Mattoussi, H., Ober, R., Jensen, K. F., & Bawendi, M. G. (CdSe)ZnS core-shell quantum dots: Synthesis and characterization of a size series of highly luminescent nanocrystallites (1997) *Journal of Physical Chemistry B* **101,** 9463-9475.

146. Norris, D. J. & Bawendi, M. G. Structure in the Lowest Absorption Feature of Cdse Quantum Dots (1995) *Journal of Chemical Physics* **103,** 5260-5268.

147. Zhang, K., Chang, H. Y., Fu, A. H., Alivisatos, A. P., & Yang, H. Continuous distribution of emission states from single CdSe/ZnS quantum dots (2006) *Nano Letters* **6,** 843-847.

148. Klimov, V. I., Mikhailovsky, A. A., McBranch, D. W., Leatherdale, C. A., & Bawendi, M. G. Quantization of multiparticle Auger rates in semiconductor quantum dots (2000) *Science* **287,** 1011-1013.

149. Petty, J. T., Zheng, J., Hud, N. V., & Dickson, R. M. DNA-Templated Ag Nanocluster Formation (2004) *Journal of the American Chemical Society* **126,** 5207-5212.

150. Antoku, Y. t. b. p.

151. Fletcher, A. N. & Bliss, D. E. Laser-Dye Stability .5. Effect of Chemical Substituents of Bicyclic Dyes Upon Photodegradation Parameters (1978) *Applied Physics* **16,** 289-295.

152. Isak, S. J. & Eyring, E. M. Fluorescence Quantum Yield of Cresyl Violet in Methanol and Water as a Function of Concentration (1992) *Journal of Physical Chemistry* **96,** 1738-1742.

153. Schwille, P. & Haustein, H. *Fluorescence Correlation Spectroscopy: An Introduction to its Concepts and Applications.*

154. Maiti, S., Haupts, U., & Webb, W. W. Fluorescence correlation spectroscopy: Diagnostics for sparse molecules (1997) *Proceedings of the National Academy of Sciences of the United States of America* **94,** 11753-11757.

155. Kim, S. A., Heinze, K. G., Waxham, M. N., & Schwille, P. Intracellular calmodulin availability accessed with two-photon cross-correlation (2004) *Proceedings of the National Academy of Sciences of the United States of America* **101,** 105-110.

156. Huang, Z. X., Ji, D. M., & Xia, A. D. Fluorescence intensity and lifetime fluctuations of single Cy5 molecules immobilized on the glass surface (2005) *Colloids and Surfaces a-Physicochemical and Engineering Aspects* **257-58,** 203-209.

157. Heilemann, M., Margeat, E., Kasper, R., Sauer, M., & Tinnefeld, P. Carbocyanine dyes as efficient reversible single-molecule optical switch (2005) *Journal of the American Chemical Society* **127,** 3801-3806.

158. Rasnik, I., McKinney, S. A., & T., H. (2006) *Nature Methods* **3,** 891-893.

159. Bates, M., Blosser, T. R., & Zhuang, X. W. Short-range spectroscopic ruler based on a single-molecule optical switch (2005) *Physical Review Letters* **94,** art. no. 108101.

160. Yip, W. T., Hu, D. H., Yu, J., Vanden Bout, D. A., & Barbara, P. F. Classifying the photophysical dynamics of single- and multiple- chromophoric molecules by single molecule spectroscopy (1998) *Journal of Physical Chemistry A* **102,** 7564-7575.

161. Kumar, P., Lee, T. H., Mehta, A., Sumpter, B. G., Dickson, R. M., & Barnes, M. D. Photon antibunching from oriented semiconducting ploymer nanostructures (2004) *Journal of the American Chemical Society* **126,** 3376-3377.

VITA

Yasuko Antoku was born in 1974 in Yamaguchi, Japan. She received B.S. degree in chemistry from the Fairmont State University, WV in 2002. During her undergraduate period, she conducted summer research under Tim Hanks at Furman University, SC and under John R. Barker at University of Michigan. In 2007, she finished her Ph.D. at the Georgia Institute of Technology under Prof. Robert Dickson.